MULTICARRIER CDMA SYSTEMS WITH MIMO TECHNOLOGY

A thesis submitted to the University of Manchester
for the degree of Doctor of Philosophy
in the Faculty of Engineering and Physical Sciences

2010

By

Antonis Phasouliotis

MACS Research Group
School of Electrical and Electronic Engineering

Contents

List of Figures

List of Abbreviations

1G	First Generation
2G	Second Generation
3G	Third Generation
4G	Fourth Generation
3GPP	Third Generation Partnership Project
ADSL	Asymmetric Digital Subscriber Line
AWGN	Additive White Gaussian Noise
BER	Bit Error Rate
BPSK	Binary Phase Shift Keying
CATV	Cable TV
CDMA	Code Division Multiple Access
CI MC-CDMA	Carrier Interferometry MC-CDMA
CP	Cyclic Prefix
CR	Cognitive Radio
CSI	Channel State Information
DAB	Digital Audio Broadcasting
DVB	Digital Video Broadcasting
DS	Direct Sequence
DSSS	Direct Sequence Spread Spectrum
DS-CDMA	Direct Sequence Code Division Multiple Access
ECC	Error Correcting Coding
EGC	Equal Gain Combining
FDMA	Frequency Division Multiple Access
FH	Frequency Hopping
FER	Frame Error Rate
FFT	Fast Fourier Transform
FT	Fourier Transform
HSPA	High Speed Packet Access
IC	Interference Cancellation
ICI	Inter Carrier Interference
ISI	Inter Symbol Interference
IFFT	Inverse Fast Fourier Transform

LMMSE	Linear Minimum Mean Square Error
LTE	Long Term Evolution
MA	Multiple Access
MC-CDMA	Multi-Carrier Code Division Multiple Access
MIMO	Multiple Input Multiple Output
ML	Maximum Likelihood
MMSE	Minimum Mean Square Error
M-OFDM	Multiuser OFDM
MRC	Maximal Ratio Combining
MUD	Multiuser Detection
NC-OFDM	Non-Contiguous OFDM
NC MC-CDMA	Non-Contiguous MC-CDMA
NLOS	Non Line-of-Sight
OFDM	Orthogonal Frequency Division Multiplexing
OFDMA	Orthogonal Frequency Division Multiple Access
OSIC	Ordered Successive Interference Cancellation
OSSMIC	Ordered Successive Spatial Multiuser Interference Cancellation
pdf	Probability Density Function
PN	Pseudo Random
P/S	Parallel-to-Serial
QAM	Quadrature Amplitude Modulation
QoS	Quality of Service
QPSK	Quadrature Phase Shift Keying
SC	Selection Combining
SINR	Signal-to-Interference and Noise Ratio
SNR	Signal-to-Noise Ratio
SS	Spread Spectrum
S/P	Serial-to-Parallel
STC	Space Time Coding
STBC	Space Time Block Coding
STTC	Space Time Trellis Coding
TDCS	Transform-Domain Communication System
TDMA	Time Division Multiple Access
V-BLAST	Vertical Bell Laboratory Layered Space Time
WCDMA	Wideband Code Division Multiple Access
WLANs	Wireless Local Area Networks
WMAN	Wireless Metropolitan Area Network
ZF	Zero Forcing

List of Notations

$\mathbf{X} \circ \mathbf{Y}$	Element wise matrix multiplication
$\mathbf{X}^T$	Transpose of matrix $\mathbf{X}$
$\mathbf{X}^+$	Moore-Penrose pseudoinverse of matrix $\mathbf{X}$
$\mathbf{X}^H$	Hermitian Transpose of matrix $\mathbf{X}$
$\|\mathbf{X}\|_F^2$	Frobenious norm of matrix $\mathbf{X}$
$[\mathbf{X}]_k$	Row k of matrix $\mathbf{X}$
$(\mathbf{X})_k$	Column k of matrix $\mathbf{X}$
$tr(\mathbf{X})$	Trace of matrix $\mathbf{X}$
$\text{diag}(\mathbf{X})$	Diagonal of matrix $\mathbf{X}$
$\mathbf{I}_k$	Identity matrix of size $k \times k$
$\|x\|$	Magnitude of x
$\|x\|$	Absolute value of x
$(x)^{-1}$	Inverse of x
x^*	Conjugate of complex number x
$\lfloor x \rfloor$	Largest integer that is smaller than x
$p(x)$	Probability density function (pdf) of x
$mod(x)$	Modulo of x
$\text{argmin}_x \{f(x)\}$	Value of x for which $f(x)$ has the minimum value
$\delta(.)$	Unit impulse function
$Q(.)$	Complementary Gaussian distribution function
$\mathcal{Q}(.)$	Quantization function
$E[.]$	Expectation operator
$O(.)$	Complexity order
$\otimes$	Kronecker product

Abstract

The rapid demand for broadband wireless access with fast multimedia services initiated a vast research on the development of new wireless systems that will provide high spectral efficiencies and data rates. A potential candidate for future generation wireless systems is multi-carrier code division multiple access (MC-CDMA). To achieve higher user capacities and increase the system data rate, various multiple-input multiple-output (MIMO) technologies such as spatial multiplexing and spatial diversity techniques have been proposed recently and combined with MC-CDMA.

This research proposes a chip level coded ordered successive spatial and multiuser interference cancellation (OSSMIC) receiver for downlink MIMO MC-CDMA systems. As the conventional chip level OSIC receiver [1] is unable to overcome multiple access interference (MAI) and performs poorly in multiuser scenarios, the proposed receiver cancels both spatial and multiuser interference by requiring only the knowledge of the desired user's spreading sequence. Simulation results show that the proposed receiver not only performs better than the existing linear detectors [2] but also outperforms both the chip and symbol level OSIC receivers. In this work we also compare the error rate performance between our proposed system and MIMO orthogonal frequency division multiple access (MIMO OFDMA) system and we justify the comparisons with a pairwise error probability (PEP) analysis. MIMO MC-CDMA demonstrates a better performance over MIMO OFDMA under low system loads whereas in high system loads, MIMO OFDMA outperforms MIMO MC-CDMA. However if all users' spreading sequences are used at the desired user receiver, MIMO MC-CDMA performs better than MIMO OFDMA at all system loads.

In the second part of this work, user grouping algorithms are proposed to provide power minimisation in grouped MC-CDMA and space-time block code (STBC) MC-CDMA systems. When the allocation is performed without a fair data rate requirement, the optimal solution to the minimisation problem is provided. However when some fairness is considered, the optimal solution requires high computational complexity and hence we solve this problem by proposing two suboptimal algorithms. Simulation results illustrate a significantly reduced power consumption in comparison with other techniques.

Declaration

No portion of the work referred to in this thesis has been submitted in support of an application for another degree or qualification of this or any other university or other institute of learning.

Copyright

i. The author of this thesis (including any appendices and/or schedules to this thesis) owns any copyright in it (the "Copyright") and s/he has given The University of Manchester the right to use such Copyright for any administrative, promotional, educational and/or teaching purposes.

ii. Copies of this thesis, either in full or in extracts, may be made only in accordance with the regulations of the John Rylands University Library of Manchester. Details of these regulations may be obtained from the Librarian. This page must form part of any such copies made.

iii. The ownership of any patents, designs, trade marks and any and all other intellectual property rights except for the Copyright (the "Intellectual Property Rights") and any reproductions of copyright works, for example graphs and tables ("Reproductions"), which may be described in this thesis, may not be owned by the author and may be owned by third parties. Such Intellectual Property Rights and Reproductions cannot and must not be made available for use without the prior written permission of the owner(s) of the relevant Intellectual Property Rights and/or Reproductions.

iv. Further information on the conditions under which disclosure, publication and exploitation of this thesis, the Copyright and any Intellectual Property Rights and/or Reproductions described in it may take place is available

from the Head of School of School of Electrical and Electronic Engineering (or the Vice-President).

Αφιερώνεται στους γονείς

μου Αντρέα και Λουκία

και στον αδερφό

μου Νικόλα

Acknowledgements

First I would like to express my deep appreciation to my respectful supervisor, Dr. Daniel Ka Chun So for his excellent supervision and continuous guidance throughout my research. His professional attitude and useful advice have inspired and motivated me towards the completion of my research.

My sincere thanks to Dr. Emad Alsusa and Dr. Khairi Hamdi for their advice during the first and second end year examinations of my PhD. Their recommended corrections of some parts in my previous reports are greatly acknowledged.

I would also like to thank my colleague and very good friend Christos Masouros for his invaluable support and guidance during the time of my PhD. Also, many thanks to all my colleagues and friends in the Microwave and Communications Group and the IEEE student branch in the University of Manchester for the endless discussions and the social and research events that we organised together.

Last but not least I would like to thank my beloved parents Antreas and Loukia and the rest of my family for their endless love and support and for believing in me throughout all these years.

Chapter 1

Introduction

1.1 Wireless Communication & Cellular Systems Background

The third generation partnership project (3GPP) wireless communication technologies for mobile networks have progressed rapidly over the past decade. Evolving from wideband code division multiple access (WCDMA) and high speed packet access (HSPA) to long term evolution (LTE), the ultimate goal of these standards has been to significantly increase data transfer rates in order to meet the demand of latest wireless services such as mobile internet, video telephony, and high quality multimedia streaming. The aforementioned goal remains the same for the future technologies.

The recent invention of multiple input multiple output (MIMO) [3–6] system that uses multiple transmit and receive antennas showed that capacity of MIMO systems can grow linearly with the number of transmit antennas as long as the number of receive antennas is greater than or equal to the number of transmit

antennas [7]. This discovery ensured a linear increase of data rate with the number of transmit antennas without increasing the transmission bandwidth or the total transmitted power. In the past years a lot of research has been performed on exploiting the available capacity of MIMO systems. In particular, the vertical Bell laboratories layered space-time (V-BLAST) [8–10] architecture (also known as ordered successive interference cancellation (OSIC)) can realize very high data transfer rates by using spatial multiplexing to exploit the multiple spatial channels. In addition, laboratory experiments for V-BLAST have demonstrated an enormous capacity of $20 - 40$ bit/s/Hz in indoor conditions with realistic SNR and error rates. Hence, V-BLAST is considered as a strong candidate for future wireless communication systems.

A major problem in wireless communications which prohibits high data rate transmission is the effect of multipath fading. Fading is caused by constructive or destructive interference produced when different versions of the transmitted signal arrive at the receiver through different paths having different time delays, attenuations and phases. Frequency selective fading is one type of channel where inter symbol interference (ISI) is created due to time dispersion of the transmitted symbols within the channel. ISI causes significant performance degradation and for this reason in order to achieve high data rates, technologies that perform well under fading channels have to be used.

Multicarrier code division multiple access (MC-CDMA), a technology first proposed in [11–13] and thoroughly overviewed in [14–16], performs well under frequency selective channels. It permits multiple users to access the wireless channel simultaneously by modulating and spreading their input data signals across the frequency domain using different spreading sequences. MC-CDMA combines the robustness to multipath fading accomplished by orthogonal frequency division multiplexing (OFDM) [17–19], with the enhanced frequency diversity that

can be achieved by code division multiple access (CDMA) [17, 20, 21]. When integrated with MIMO techniques such as the V-BLAST architecture, MC-CDMA can realise very high data transfer rates in rich multipath scattering environments without increasing the transmission bandwidth of the system [22–28].

1.2 Motivation

The chip level OSIC (V-BLAST) receiver was originally proposed for MIMO MC-CDMA systems in [1] where it demonstrated good performance for single user case. However, its performance is severely degraded in multiuser case and high error floor appears in medium SNR range due to multiple access interference (MAI) and significant error propagation. As a result, it performs even worse than the linear zero forcing (ZF) or minimum mean square error (MMSE) receivers. Chip level and symbol level MMSE linear receivers are presented in [2]. Although the symbol level detector has better performance over the chip level detector, it needs higher computational complexity and also requires the knowledge of all other users spreading sequence to avoid MAI. In [25], a partial MMSE-OSIC receiver based on multiuser detection performs similarly to the symbol level MMSE-OSIC in full system load scenario, but also the partial receiver uses all other users spreading sequence.

As explained before, existing work on MIMO MC-CDMA has shown that the combination of MC-CDMA systems with MIMO technology for multiuser communications is not a straight forward procedure especially because of the presence of interference arising from multiple antenna transmission as well as interference caused by multiple users. Therefore, a major objective of this research has been to propose ways to develop downlink MIMO MC-CDMA systems that can overcome multi-user and multi-antenna interference, and outperform existing techniques in

terms of system performance and complexity.

Another major goal of next generation wireless communication systems is the need for more energy efficient technologies. Saving energy will not only reduce operating cost but also reduces greenhouse gas emissions which is important for combating climate change. For this reason, reducing the power consumption to a minimum level is vital for the future wireless systems. In the past years, resource allocation has been used to minimise the total transmitted power in MC-CDMA systems [29, 30]. This significantly improves the energy efficiency of the system. Although some research has been done for power minimisation in MC-CDMA systems, resource allocation with user grouping has not been considered for power minimisation in grouped MC-CDMA systems.

The idea of user and subcarrier grouping [31] allows different users in a group to share the same set of subcarriers while using their distinct spreading codes. In this way multiuser interference in each group is small and does not affect users in the rest of the groups. Hence multiuser detectors for different groups are practically feasible.

Hence, another important aim of this work has been to provide user grouping algorithms to minimise the total transmitted power in grouped MC-CDMA and space-time block code (STBC) MC-CDMA systems.

The final objective in this work is to investigate MC-CDMA for underlay cognitive radio (CR) networks [32]. CR is a new emerging technique that can significantly improve spectrum efficiency in future mobile networks. Underlay CR is a spectrum sharing technique where the CR user (secondary user in the CR network) is allowed to share the same frequency bands (gray spectral regions) for transmission with the licensed users (primary users in the primary radio (PR) network) as long as their transmit power is regarded as noise by the licensed users [33]. MC-CDMA could be a potential candidate for underlay CR networks.

In this way the signal of the cognitive user can be spread over a wider bandwidth which will cause low interference to the primary users. Furthermore, MC-CDMA has good interference rejection from primary users.

1.3 Achievements & Contributions

The main contributions of this work are presented below:

- The chip level ordered successive spatial and multiuser interference cancellation (OSSMIC) receiver is proposed for open loop downlink MIMO MC-CDMA systems. The OSSMIC receiver performs layered space-time processing with both spatial and multiuser interference cancellation. Unlike [25, 26] & [2], the proposed receiver does not require the knowledge of other users' spreading sequence in the system and this reduces the computational complexity of the system. Also, unlike the OSIC receiver in [1], OSSMIC is capable for multiuser scenarios. Furthermore, the proposed scheme invalidates the perception that linear MMSE detector performs better than iterative detectors for MIMO MC-CDMA systems [1].

- In order to justify the use of chip level detection for OSSMIC, comparison is made to a modified symbol level with OSIC detector. Furthermore, performance comparison is made between MIMO MC-CDMA & MIMO OFDMA. In order to provide an analytical comparison between these systems, their pairwise error probabilities (PEP) are derived.

- The minimisation of the total transmitted power in downlink MC-CDMA and space-time block code (STBC) MC-CDMA under a bit error rate (BER) constraint for each user is studied by performing power control according to an efficient user grouping algorithm. The optimal allocation algorithm for

the minimisation problem is presented when there is no fairness requirement on the data rate. On the other hand when fairness is considered, two complexity reduced suboptimal allocation algorithms are proposed.

- The performance of MC-CDMA and OFDM is investigated in underlay CR networks. MC-CDMA causes lower interference to the primary user network compared to OFDM. Furthermore, MC-CDMA is capable of good interference rejection coming from the primary user.

1.4 List of publications

Accepted & Published

1. A. Phasouliotis and D.K.C. So, "User Grouping for Power Minimization in STBC MC-CDMA systems," *in Proc. IEEE PIMRC 2010 accepted*, Sep. 2010.

2. A. Phasouliotis and D.K.C. So, "User Grouping for Power Minimization in MC-CDMA systems," *in Proc. IEEE VTC fall accepted*, Sep. 2010.

3. A. Phasouliotis and D.K.C. So, "Performance Analysis and Comparison of Downlink MIMO MC-CDMA and MIMO OFDMA Systems," *in Proc. IEEE VTC spring*, Apr 2009, pp. 1-6.

4. A. Phasouliotis and D.K.C. So, "A novel OSSMIC receiver for downlink MIMO MC-CDMA systems," *in Proc. IEEE VTC spring*, vol. 3, May 2008, pp. 1271-1275.

Submitted & In preparation

1. A. Phasouliotis and D.K.C. So, "Layered Space-Time Receiver for Downlink MIMO MC-CDMA Systems," *submitted in IET Transactions in Communications.*

2. A. Phasouliotis and D.K.C. So, "Power Minimization in STBC MC-CDMA systems," *journal paper currently under preparation.*

1.5 Thesis Outline

The thesis is divided into seven chapters. The first chapter presents the motivation for conducting this research and lists the main objectives and contributions of this work.

Chapter 2 provides the basic theory behind radio wave propagation for wireless channels by exploring the large-scale and small-scale wave propagations such as path loss, shadowing multipath and fading. Multipath propagation and the main fading channel conditions are further illustrated and various diversity techniques are described. Furthermore the principles behind existing wireless communication systems, important to this work, are analysed and their system models are also presented. These systems include the OFDM, CDMA, MC-CDMA, OFDMA and MIMO schemes. The performance of each system is also evaluated.

Chapter 3 introduces the transmitted and the received signal models for the downlink MIMO MC-CDMA system. In addition, existing receiver architectures for MIMO MC-CDMA systems are presented.

In Chapter 4, the novel chip-level OSSMIC receiver is proposed. The explanation of co-antenna interference (CAI) and multiple access interference (MAI) cancellation procedure and the optimum detection ordering are also described. Finally the performance of the proposed OSSMIC receiver is evaluated through

simulations and compared with the performance of the existing chip and symbol level linear and OSIC MIMO MC-CDMA detectors.

PEP expressions for the chip and symbol level MIMO MC-CDMA and MIMO OFDMA are presented in Chapter 5. The frame error rate (FER) and PEP performance of these systems is also compared.

In Chapter 6, we propose user grouping algorithms to provide power minimisation in grouped MC-CDMA and STBC MC-CDMA systems. The total transmitted power is minimised under a BER constraint.

Chapter 7 compares the performance of MC-CDMA and OFDM in underlay cognitive radio networks.

Chapter 8 concludes and summarises the significance of this research. Furthermore a number of ideas are suggested for future research and to enhance the performance of the proposed system.

Chapter 2

Theoretical Background

This chapter introduces the basic concepts of wireless channels and presents the background theories of the wireless systems used in this research. In particular, the sections for multipath propagation, fading channels and different diversity techniques are described first. Next, various multicarrier and multiple access schemes are presented and these include OFDM, OFDMA, CDMA and MC-CDMA wireless technologies. Finally, spatial multiplexing and spatial diversity techniques for MIMO systems are detailed in the last section.

2.1 Wireless Communication Channels

In urban areas, a typical wireless channel between the transmitter and the receiver contains various objects and obstacles that cause signals to be reflected, diffracted or scattered into many directions during transmission. These effects result in multiple versions of the transmitted signal to arrive at the receiver through different paths at different time delays and different phases. The received signal is the constructive or destructive combination of all these signal versions. The interaction between these waves can cause significant attenuation to the received

signal. Various statistical models have been proposed to describe the effects of the wireless channel on the transmitted signals and to predict the variability of the received signal strength. These are called radio wave propagation models [34] and are categorised as follows:

- Large-scale models which are based on path loss (PL) and shadowing.
- Small-scale models which are based on multipath fading.

2.1.1 Large-scale Path Loss and Shadowing

Large scale propagation models are useful in estimating radio coverage area by modelling the signal attenuation over a large transmitter-receiver (Tx-Rx) separation distance. Extensive studies have shown that signal power attenuates exponentially with the increase of Tx-Rx separation distance [34]. PL is a large scale propagation model which represents the difference (in dB) between the effective transmitted power and the received power. Shadowing effect is another large-scale propagation model which predicts the variation of the average signal power at different locations of a fixed Tx-Rx separation. Shadowing is caused by the change of environment in different locations.

Extensive studies revealed that the PL at a Tx-Rx separation distance d can be modelled by a log-normal (normal in dB) distribution [35] expressed as

$$PL(d) = \overline{PL}(d_0) + 10n\log\left(\frac{d}{d_0}\right) + X_\sigma \tag{2.1}$$

where d_0 denotes a reference distance, $\overline{PL}(d_0)$ signifies the mean path loss at d_0 and n indicates the path loss exponent. It should be noted that different path loss exponents correspond to different types of environments. Also, if $\overline{PL}(d_0)$ is not specified, it is usually taken as free-space path loss at a distance of 1m [34]. X_σ

represents the log-normal shadowing effect with zero mean and standard deviation σ. Hence the path loss at distance d is considered to be a random variable with $\overline{PL}$ mean and standard deviation σ.

2.1.2 Small-scale Multipath Fading

Contrary to large-scale, small-scale propagation models characterise the rapid variations of the received signal power over short distances (in the order of a few wavelengths) or short time periods (in the order of seconds). Multipath fading is caused by interference between multiple versions of the transmitted signal that arrive at the receiver through different propagation paths and at different times. In urban areas, multipath fading occurs because the mobile antennas are lower

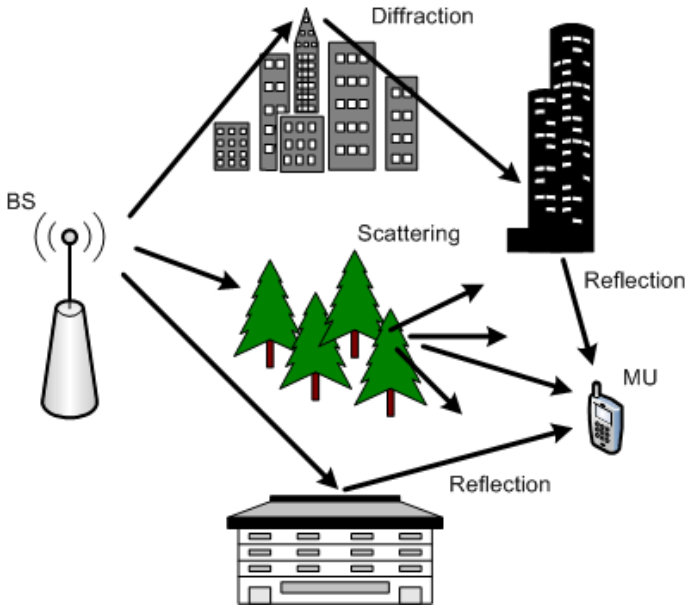

Figure 2.1: Multipath propagation.

than the height of the surrrounding structures, and so there are a lot of obstacles between the transmitter and the receiver. In such cases the transmitted signal is reflected, diffracted or scattered at different directions and these radio signals arrive at the receiver at different times as shown in Figure 2.1. Also, these distinct

multiple paths have random amplitudes, phases and angle of arrivals which cause rapid variations in signal strength when combined at the receiver. Hence it is important to study and establish the multipath channel model.

2.1.2.1 Multipath Channel Model

A general multipath channel model is presented in [36]. In this model the impulse response of the time varying multipath channel $h(t,\tau)$ is a function of t and τ. The variable t represents the time that the channel changes when the receiver travels with a constant velocity over a short distance. The variable τ denotes the channel multipath delay. The multipath channel delay axis is divided into equally spaced segments, called the excess delay bins, and the excess delay bin width is $\Delta\tau = \tau_l - \tau_{l-1}$. The first signal that arrives at the receiver is denoted as τ_0. It should be noted that the signals received within the *l-th* bin are represented by a single multipath component with time delay width τ_{l-1}. The baseband impulse response of the multipath channel is modelled by the summation of all multipath components that arrive at the receiver with different attenuations, phase shifts and time delays. It can be expressed as

$$h(t,\tau) = \sum_{l=0}^{L-1} a_l(t,\tau) exp\left[j\theta_l(t,\tau)\right] \delta\left(\tau - \tau_l(t)\right) \tag{2.2}$$

where $a_l(t,\tau)$, $\tau_l(t)$ and $\theta_l(t,\tau)$ denote the attenuation factor, the excess time delay and the phase shift of the *l-th* multipath component at time t respectively. It should be noted that if an excess delay bin has no arrival path at a given time t and delay τ, that $a_l(t,\tau)$ is zero. The total number of multipath components is represented by L and $\delta(.)$ is the unit impulse function.

Assuming pulse shaping and matched filtering at the receiver, the multipath channel could be described using the time-invariant tap delay line model shown

in Figure 2.2. In this model, each multipath component arrives at the receiver

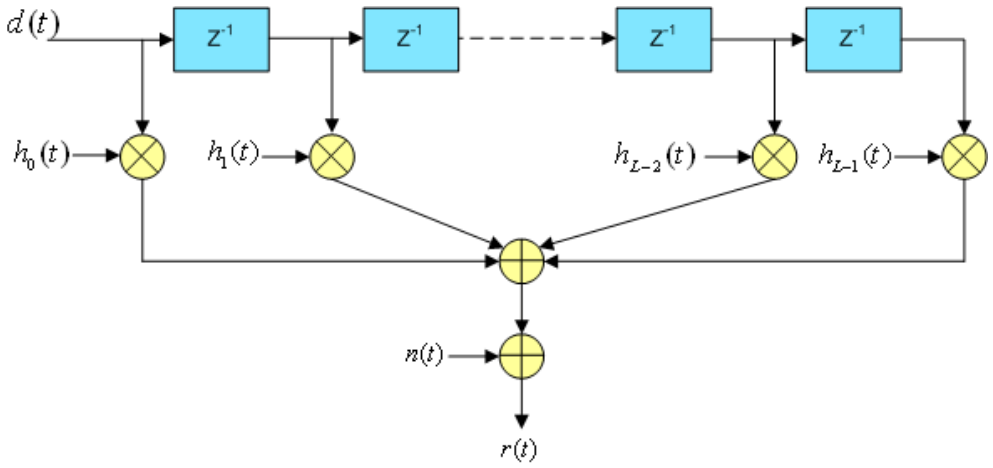

Figure 2.2: Tap delay line model.

after one tap delay of Z^{-1} and it has different amplitude and phase. Z denotes the Z-transformation of the wideband signal. It is assumed that each tap delay equals to one symbol period. Thus if signal $d(t)$ is transmitted over the multipath channel, the received signal can be expressed as

$$r(t) = \sum_{l=0}^{L-1} h_l(t) d(t - lT_d) + n(t) \tag{2.3}$$

where $h_l(t)$ denotes the channel gain for the $l\text{-}th$ tap at time t and T_d represents the symbol period. This type of channel represents a frequency selective fading which will be explained in a later section.

In mobile radio channels with non line-of-sight (NLOS), the Rayleigh distribution is usually used to model the received envelope of individual multipath components at specific time instants. Considering a NLOS multipath channel, the channel gain at the $l\text{-}th$ bin with N_l arriving paths is given by

$$\overline{a}_l = a_l e^{j\theta_l} = \sum_{k=0}^{N_l-1} a_{l,k} e^{j\theta_{l,k}} = \sum_{k=0}^{N_l-1} a_{l,k}^I + j a_{l,k}^Q = a_l^I + j a_l^Q \tag{2.4}$$

where a_l^I and a_l^Q denote the in-phase and quadrature Gaussian distributed $N(0, \sigma^2)$ components of the *l-th* bin. The Rayleigh distribution is formed by the magnitude of the channel gain $a_l = \sqrt{a_l^{I^2} + a_l^{Q^2}}$ where the average channel power is represented by $E[a_l^2] = 2\sigma^2$. In order to compare different multipath channels, the main parameters that quantify a multipath channel have to be analysed.

2.1.2.2 Multipath Channel Characteristics

The multipath channel is mainly characterised by the following four parameters:

- RMS delay spread (σ_τ) and mean excess delay ($\overline{\tau}$) quantify the time dispersive properties of the multipath channel. These parameters can be determined from a power delay profile [34]. Such profiles are produced by averaging instantaneous power delay measurements over a given area. $\overline{\tau}$ represents the first moment of the power delay profile and σ_τ is the square root of the second central moment of the power delay profile.

- Coherence bandwidth (B_c) provides a statistical measure of the range of frequencies over which the multipath channel is considered to be flat. In general, a flat channel lets all the multipath spectral components to pass with equal gain and linear phase.

- Doppler spread (B_D) indicates an estimation of the spectral increase due to the temporal rate of change of the mobile radio channel. Doppler spread provides the range of frequencies over which the Doppler spectrum is not zero.

- Coherence time (T_c) gives a statistical measure of the time duration over which the multipath channel impulse response stays constant.

2.1.3 Fading Channels

Fading is caused by constructive or destructive interference between different versions of the transmitted signal which arrive at the receiver at different times. There are different types of fading which are defined according to the relationship between the transmitted signal parameters (such as bandwidth, symbol period, etc.) with respect to the channel parameters (such as rms delay spread, doppler spread). Time dispersion due to multipath delay spread causes the transmitted signal to experience either flat or frequency selective fading.

2.1.3.1 Flat Fading

The received signal undergoes flat fading channel conditions when the wireless channel contains constant gain and linear phase response within a bandwidth which is much greater than the signal bandwidth (i.e. $B_c >> B_s$). In other words, if a change in the channel gain occurs, this will cause a constant amplitude and linear phase change of the transmitted signal bandwidth. In the time domain, flat fading describes a channel where the symbol period of the transmitted signal is much larger than the multipath delay spread of the channel ($T_d >> \sigma_\tau$). This approximates the fact that multipath channel impulse response has no excess delay.

The flat fading channel response is represented by

$$h(t) = a(t)exp\left[j\theta(t)\right] \tag{2.5}$$

where the phase $\theta(t)$ is uniformly distributed and $a(t)$ denotes the amplitude.

2.1.3.2 Frequency Selective Fading

On the other hand, a signal propagates through a frequency selective fading channel only when the channel keeps a constant gain and linear phase response over a bandwidth which is smaller than the signal bandwidth (i.e. $B_c < B_s$). In other words, the spectrum of the transmitted signal has a larger bandwidth than the coherence bandwidth of the channel. In the time domain, the channel impulse response has a multipath delay spread larger than the symbol period ($\sigma_\tau > T_d$) and this causes multiple versions of the transmitted signal to appear at the receiver. These versions have different gains and phase hence the detected signal is distorted. Frequency selective fading channels induce inter symbol interference (ISI) due to time dispersion of the transmitted symbols by the channel.

Frequency selective fading channel can be modelled with the tap delay line filter shown in Figure 2.2. Hence the channel response is given by

$$h(t,\tau) = \sum_{l=0}^{L-1} h_l(t,\tau)\delta\left(\tau - lT_d\right) \tag{2.6}$$

where $h_l(t,\tau)$ denotes the channel gain for the $l\text{-}th$ tap at time t and delay τ.

Fading effects cause deep fades to the received symbols (the channel for that symbol period has small value). These symbols cannot be detected correctly and this significantly degrades the system performance. For this reason, techniques to overcome fading are very important.

2.1.4 Diversity Techniques

Diversity techniques are used to combat the multipath fading effects and to improve the overall system performance. Diversity is implemented by transmitting multiple versions of the same signal at different times, frequencies or spatial

location. In this way, the same information data can be received multiple times under different channel gains and hence the probability for receiving signals in deep fades gets smaller. Furthermore, diversity techniques can improve the quality of wireless link.

The most well known diversity techniques are categorised as follows:

- *Spatial diversity* is achieved with the use of multiple antennas at the transmitter and/or the receiver to create multiple signal observations. Spatial diversity is classified into receive and transmit diversity techniques. In the former, multiple receive antennas with sufficient spatial separation are used to take multiple signal observations. To achieve transmit diversity, multiple transmit antennas are considered. According to that, one antenna at a time can be used to transmit the coded symbols of a time diversity code successively over the different antennas.

- *Time diversity* is employed by transmitting data symbols in different timeslots separated in time intervals which are more than the channel's coherence time so that multiple repetitions of the signal will be received with different fading conditions.

- On the other hand in *frequency diversity*, the same data are transmitted using more than one carrier frequencies separated by more than the coherence bandwidth of the channel. As a result, the same signal experiences different channel gains.

When multiple observations of the same signal are obtained at the receiver, diversity combining schemes are needed to combine the different fading paths (branches) of these received signals. The three main combining schemes are:

- Selection combining (SC) scheme which selects the branch with the highest

SNR for detection.

- Equal gain combining (EGC) technique in which all the received signals are multiplied by the conjugate of the channel phase before combining them.
- Maximal ratio combining (MRC) where the SNRs of all the signals from all branches are summed before detection.

A detailed discussion on diversity combining techniques falls out of the scope of this research and thus it will not be covered in this thesis.

2.2 Multicarrier and Multiple Access Systems

Multicarrier systems [37] convert a serial high-rate data stream into multiple parallel low-rate substreams, each modulated on a different subcarrier. Since the symbol rate on each subcarrier is much less than the serial data stream symbol rate, the effects of multipath delay spread, i.e. ISI, are significantly decreased. This research is mainly focused on two multicarrier technologies and these are OFDM and MC-CDMA.

Multiple access (MA) [38, 39] systems allow multiple users to access the wireless radio spectrum simultaneously. The wireless spectrum is a scarce resource therefore a wireless system has to allocate simultaneously the available amount of channels to multiple users in order to achieve higher system capacity. There are various techniques available for attaining multiple access and these include frequency division multiple access (FDMA), time division multiple access (TDMA), CDMA and OFDMA. For the purpose of this work, CDMA and OFDMA are discussed in more details later on.

2.2.1 Orthogonal Frequency Division Multiplexing (OFDM)

OFDM was first introduced five decades ago. The patent for OFDM was first clarified in the mid 1960s [40] but it was only until 1985 [41] that OFDM was suggested for wireless communications. Currently, OFDM is used for several wireless applications including digital audio broadcasting (DAB) [42], digital video broadcasting (DVB) [43], asymmetric digital subscriber line (ADSL) [44] and wireless local area networks (WLANs) [45]. OFDM is a multicarrier modulation technique employed for high data rate wireless applications suitable for combating ISI that arises in frequency selective channels. It divides an input high rate serial datastream into multiple low rate substreams which are transmitted over different orthogonal narrowband channels centred at different subcarrier frequencies. In this way, the bandwidth of the substreams becomes less than the coherence bandwidth of the channel. In other words, the symbol period of the substreams is longer than the delay spread of the time dispersive radio channel. This ensures that each individual subcarrier experiences flat fading conditions hence the low rate substreams can avoid ISI [17].

2.2.1.1 Principle of OFDM

OFDM splits the input data into N_s parallel streams and each symbol is modulated using a separate carrier frequency. The carrier spacing is selected so that each subcarrier is located on all the other subcarriers' spectra zero crossing points as shown in Figure 2.3. Although there are spectral overlaps among subcarriers, they do not interfere with each other if each subcarrier is sampled at the time when the main lobe occurs [46]. In other words, spectral orthogonality between the subcarriers is maintained. Figure 2.3 illustrates the OFDM spectrum [47] in

the frequency domain, where the subcarrier spacing is $1/T_d$.

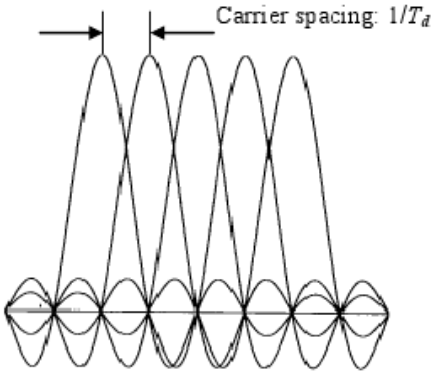

Figure 2.3: OFDM spectrum.

It must be said that for large number of subcarriers, OFDM requires very accurate frequency synchronisation between the receiver and the transmitter. This is because with frequency deviation (offsets), the subcarriers lose their orthogonality and this causes inter-carrier interference (ICI). Frequency offsets are typically caused by transmitter-receiver mismatch, or by Doppler shift due to rapid Tx-Rx movement.

2.2.1.2 OFDM System Model

Figure 2.4 depicts the transceiver block diagram for the OFDM system. In the transmitter, the information bits are modulated into P symbols. Thus the symbol vector can be represented as, $\mathbf{d} = \begin{bmatrix} d_1 & d_2 & \cdots & d_P \end{bmatrix}^T \in \mathbb{C}^{P\times 1}$. where $\mathbb{C}$ denotes a set of complex numbers. The symbols are serial-to-parallel (S/P) converted and then mapped onto N_s parallel orthogonal subcarriers and transformed into the time domain by the inverse Fast Fourier transform (IFFT). Next the output samples of the IFFT are parallel-to-serial (P/S) converted to form the baseband signal which is added with cyclic prefix (CP) before transmission over the multipath radio channel.

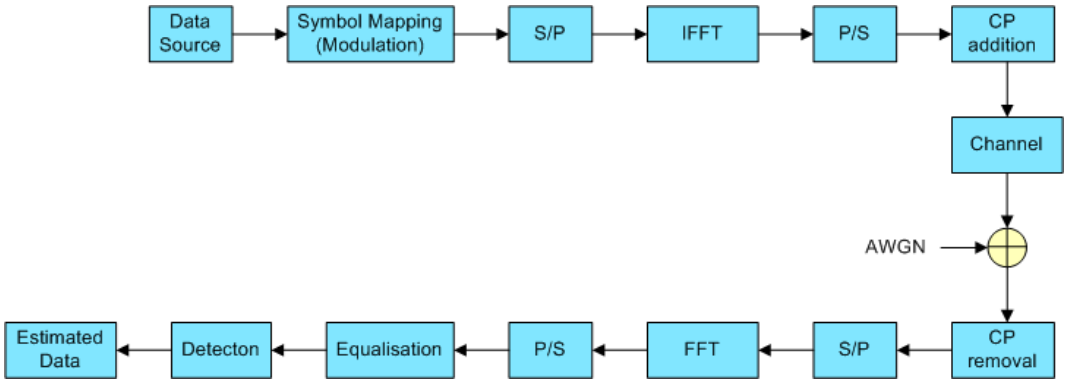

Figure 2.4: OFDM system block diagram.

CP is introduced on the transmitted signal in order to combat ISI which arises between OFDM symbols from large multipath delay spreads. CP is a cyclically extended guard interval, where each OFDM symbol is preceded by a periodic extension. The total symbol duration is $T_{total} = T_g + T_d$, where T_g is the guard interval and T_d is the symbol duration. When the guard interval is longer than the multipath delay, ISI can be avoided. CP converts the linear convolution of the transmitted signal with the channel impulse response into a cyclic convolution. This means that the multipath fading effect on the transmitted symbols is simplified to an element-wise multiplication between the transmitted data constellations $\mathbf{d}$ with the channel frequency response $\mathbf{H}$.

The frequency response of the channel is given by the Fourier Transform (FT) of the channel impulse response $\mathbf{h}$. As a result, the orthogonality of the subcarriers is recovered. The channel is considered to be quasi-static frequency selective fading corrupted by additive white Gaussian noise (AWGN).

Upon receiving the signal, the CP is removed and the Fast Fourier transform (FFT) of size N_s is performed. The received signal model after the FFT at the *i-th* subcarrier, can be characterised as

$$r_i = H_i d_i + n_i \tag{2.7}$$

where H_i and n_i denote the channel and the AWGN signal at the *i-th* subcarrier. According to [48], the subchannel frequency response at the *i-th* subcarrier ($i = 1, 2, ..., N_s$) is calculated by

$$H_i = \sum_{l=0}^{L-1} h(l) exp(-j2\pi i \overline{\tau}_l / N_s) \tag{2.8}$$

where $\overline{\tau}_l$ is the path arrival time normalised to the OFDM subcarrier spacing, such that $\overline{\tau}_l T_d$ is the delay and $1/T_d$ is the OFDM subcarrier spacing. The significance of (2.8) is that the path arrival time can be any positive real number. This can be used to represent realistic channel environments.

The estimates of the transmitted symbol at the *i-th* subcarrier are obtained by performing zero forcing (ZF) equalisation on each subcarrier and it is given by

$$y_i = H_i^{-1} r_i = H_i^{-1} H_i d_i + H_i^{-1} n_i = d_i + \widetilde{n}_i \tag{2.9}$$

where H_i^{-1} denotes the inverse of H_i. Finally the detection of the estimated symbols is performed. In general, equalisation techniques are used to compensate for ISI created in frequency selective channels. For convenience of presentation and because of it's simplicity, ZF is considered for equalisation in this chapter. However it has to be said that ZF causes poor system performance because of noise amplification. For this reason equalisers that can provide improved performance will be introduced later on.

2.2.1.3 Performance of OFDM

The bit error rate (BER) performance with respect to different E_b/N_0 for the coded and uncoded OFDM system is evaluated through Monte Carlo simulations and presented in Figure 2.5. The transmitted frame is assumed to comprise 128

QPSK modulated symbols (P=128). The coded OFDM system makes use of rate 1/2 convolutional codes with constraint length 3 and generators {5,7}, and Viterbi decoder in the receiver. The size of the FFT is considered to be the same as the number of subcarriers, and is thus N_s=128. The radio channel for coded

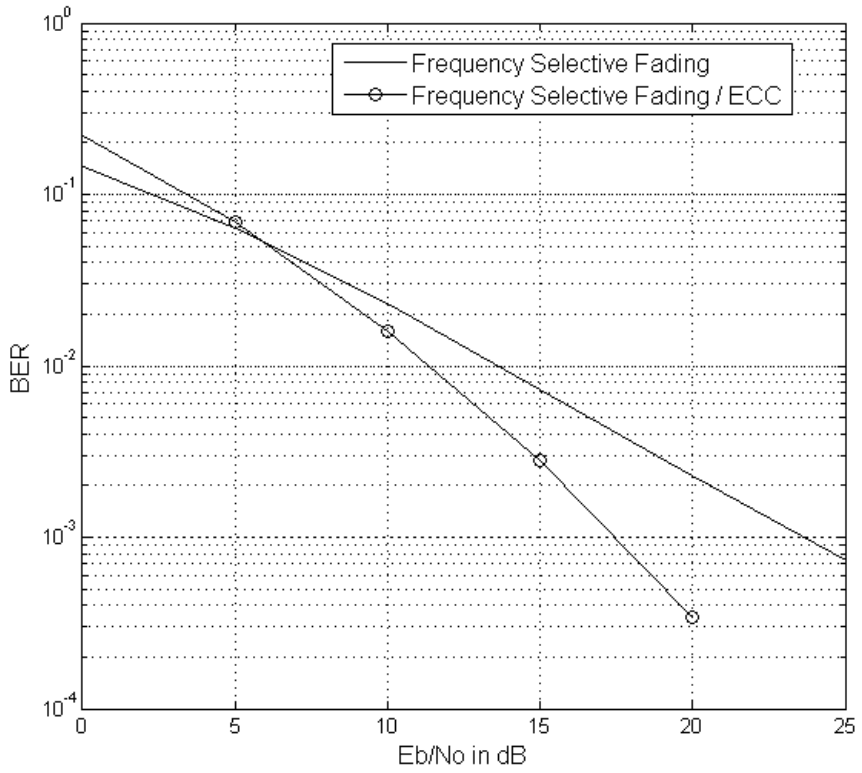

Figure 2.5: Performance of OFDM in Rayleigh fading channels.

and uncoded OFDM is assumed to experience Rayleigh frequency selective fading with two taps at normalised arrival times {0,1}. The maximum delay spread is assumed to be shorter than the duration of the CP. Hence ISI is avoided and each subcarrier experiences flat fading.

The results show 6 dB improvement at BER = 10^{-3} for coded OFDM over uncoded OFDM system. Observations on the asymptotic slope of coded OFDM show that with error correcting coding (ECC), diversity is exploited to correct

errors.

2.2.2 Code Division Multiple Access (CDMA)

As mentioned earlier, the major MA technologies include the FDMA, TDMA, CDMA and OFDMA systems. In FDMA, distinct frequencies are assigned to different users so as to access the channel concurrently. TDMA allocates different timeslots to different users in order to access the spectrum together on the same frequency band. FDMA and TDMA technologies have mostly used in first and second generation (1G & 2G) cellular systems as well as WLANs. On the other hand, CDMA techniques are currently used in third generation (3G) cellular systems. In CDMA, each user is assigned a distinct spreading sequence that spreads the incoming data over a large bandwidth. In this way, different users can access the available spectrum at the same frequency band and time slot. The two main CDMA techniques for providing multiple access are frequency hopping (FH) and direct sequence (DS). This thesis focuses on the latter.

2.2.2.1 Direct Sequence Code Division Multiple Access (DS-CDMA)

Direct sequence code division multiple access (DS-CDMA) [49–51] employs the direct sequence spread spectrum (DSSS) technique to allow multiple users sharing the same bandwidth at the same time. DSSS spreads the incoming data stream with a pseudo-random (PN) code over a bandwidth much larger than the data bandwidth. This supplies the transmitted signal with the same large bandwidth as the spreading signal. Thus, while the transmit power remains constant and the bandwidth of the spreading signal is large, the power spectral density of the transmitted signal is kept below the noise power spectral density. This allows each user to detect his own transmitted data which also ensures secure

communications.

The transceiver of a DS-CDMA system for a single user is demonstrated in Figure 2.6. Consider P BPSK modulated symbols with a symbol rate of $R_d =$

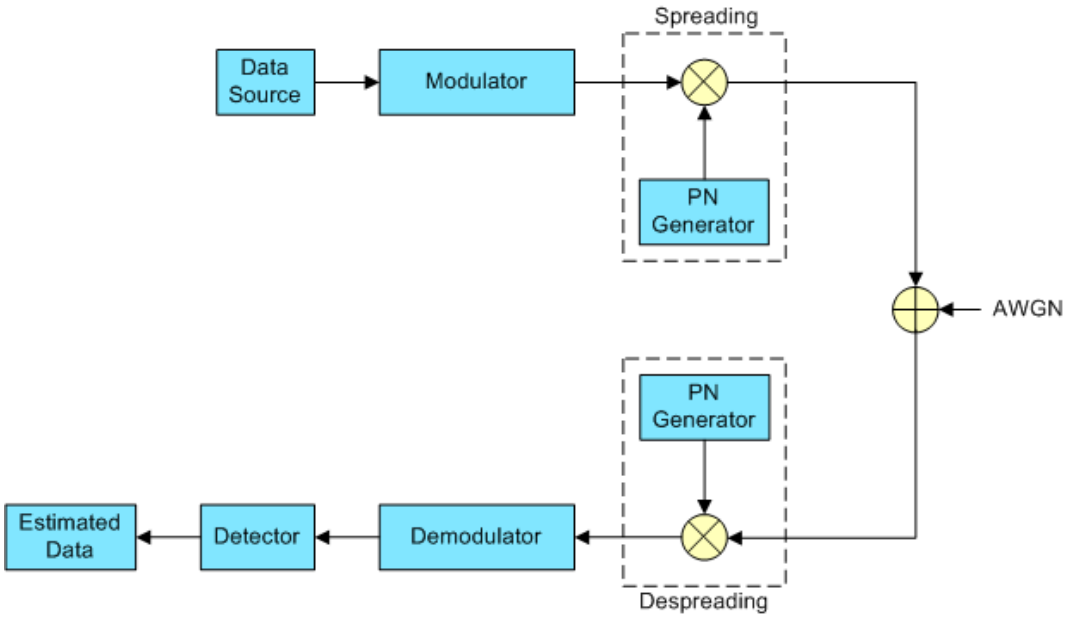

Figure 2.6: Block diagram of DS-CDMA system.

$1/T_d$ represented by $\mathbf{d} = \begin{bmatrix} d_1 & d_2 & \cdots & d_P \end{bmatrix}^T \in \mathbb{C}^{P\times 1}$. In the transmitter, the symbols are spread by the wideband PN spreading code to form the transmitted baseband signal

$$\mathbf{x} = \mathbf{dc} \tag{2.10}$$

where $\mathbf{c} = \begin{bmatrix} c_1 & c_2 & \cdots & c_G \end{bmatrix} \in \mathbb{C}^{1\times G}$ is the PN spreading sequence with chip rate $R_c = 1/T_c$ and G refers to the length of the spreading code. The bandwidth of the spreading sequence, $B_c \approx 1/T_c$, is approximately T_d/T_c times larger than the bandwidth of the input symbols B_d. The spreading factor of the system is equal to the number of chips per bit indicated by SF=$B_c/B_d = T_d/T_c$ which is equal to G. The baseband signal is next transmitted over the AWGN channel

and the received baseband signal after demodulation can be characterized by

$$\mathbf{r} = \mathbf{dc} + \mathbf{n} \tag{2.11}$$

where $\mathbf{n}$ denotes the AWGN vector. The symbol decision statistic is obtained by despreading the received signal with the PN spreading sequence. This can be represented by

$$\widehat{\mathbf{d}} = \mathbf{rc}^T \tag{2.12}$$

2.2.2.2 Performance of DS-CDMA

The performance for a three user (N_u=3) DS-CDMA system is evaluated through Monte Carlo simulation. The transmitted frame of each user is assumed to comprise of 1000 BPSK modulated symbols (P=1000) and the spreading sequence length G contains 32 chips. The channel is assumed to be corrupted by AWGN. The BER performance of DS-CDMA system with three different spreading sequences is tested and compared in Figure 2.7. These include the PN, Gold and Walsh-Hadamard spreading sequences [12].

It can be clearly observed that when the DS-CDMA system uses Walsh-Hadamard spreading codes, it achieves the best performance. This is because Walsh-Hadamard sequences possess better crosscorrelation properties (equal to 0) when compared with the crosscorrelation of PN and Gold sequences. This means that if no multipath exists, multiple access interference (MAI) arising from different users is avoided. However in a multipath environment, the orthogonality of Walsh-Hadamard sequences is lost and hence the performance is degraded. The performance of DS-CDMA with Gold sequences is better when compared to the one with PN codes. This is because Gold sequences have better cross correlation properties than PN codes.

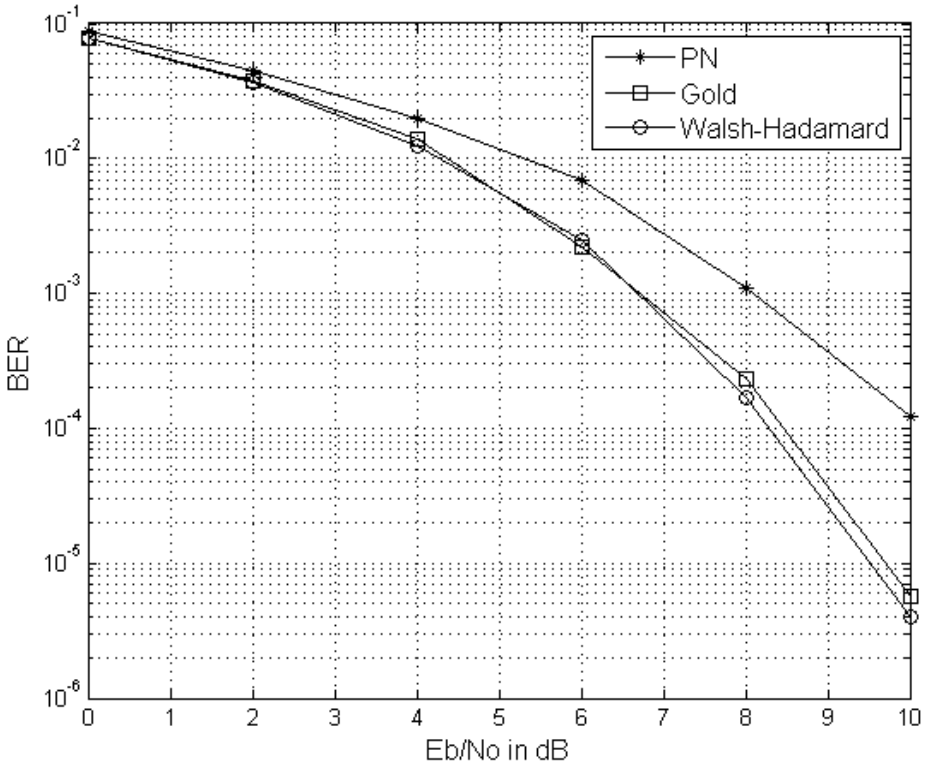

Figure 2.7: Performance of DS-CDMA in AWGN channel.

2.2.3 Multi Carrier Code Division Multiple Access (MC-CDMA)

MC-CDMA signifies the combined system of OFDM and CDMA technologies. MC-CDMA was first proposed in [11, 13, 52] and thoroughly reviewed in [14–16]. This technique permits multiple users to access the wireless channel simultaneously by modulating and spreading their input data signals across the frequency domain using different spreading sequences. MC-CDMA combines the robustness to multipath fading of OFDM with the multi-user spectrum access of CDMA [53].

2.2.3.1 System Model

The MC-CDMA system model for N_u users is illustrated in Figure 2.8 [54]. The information data are grouped into N_u frames and then each frame is modulated to P symbols. Therefore the symbol matrix for user n_u ($n_u = 1, 2, ..., N_u$) can be indicated as $\mathbf{d}_{n_u} = \begin{bmatrix} d_{n_u,1} & d_{n_u,2} & \cdots & d_{n_u,P} \end{bmatrix}^T \in \mathbb{C}^{P\times 1}$. The symbols of each user are first serial-to-parallel converted and then spread with the corresponding user specific spreading sequence in order to form the chip-level transmit matrix

$$\mathbf{s}_{n_u} = \begin{bmatrix} \mathbf{s}_{n_u,1} & \mathbf{s}_{n_u,2} & \cdots & \mathbf{s}_{n_u,PG} \end{bmatrix} = \mathbf{d}_{n_u} \otimes \mathbf{c}_{n_u} \in \mathbb{C}^{1\times PG} \tag{2.13}$$

where $\otimes$ denotes the Kronecker product and the signature sequence of user n_u is expressed as

$$\mathbf{c}_{n_u} = \begin{bmatrix} c_{n_u,1} & c_{n_u,2} & \cdots & c_{n_u,G} \end{bmatrix} \in C^{1\times G} \tag{2.14}$$

in which C refers to the spreading code chip alphabet and G is the length of the spreading sequence. Each user is allocated a distinct spreading code to ensure orthogonality between the different users. The chips of the frames of all users are then combined and all the $P \times G$ parallel data sequences are mapped onto $N_s = P \times G$ subcarriers and transformed into the time domain by the IFFT. The subcarrier is indexed by i, and is related to the *p-th* symbol ($p = 1, 2, \ldots, P$) and the *g-th* chip (g = 1,2,...,G) by

$$i(p, g) = (p - 1)G + g. \tag{2.15}$$

It must be noted that throughout Chapters 2, 3, 4 and 5, the subcarrier index i, symbol index p, and chip index g are inter-connected together by (2.15). Hence the corresponding symbol and chip indexes are represented with respect to the

i-th subcarrier by

$$p(i) = (i-1) mod G + 1 \tag{2.16}$$

and

$$g(i) = \left\lfloor \frac{i-1}{G} \right\rfloor + 1 \tag{2.17}$$

respectively where $\lfloor a \rfloor$ denotes the largest integer that is smaller than a. The transmitted *i-th* multiplexed chip of all users can be indicated as

$$x_i = \sum_{n_u=1}^{N_u} s_{n_u,i} = \sum_{n_u=1}^{N_u} c_{n_u,g(i)} d_{n_u,p(i)}. \tag{2.18}$$

The output signal from the IFFT is added with CP before transmission over the wireless multipath channel. The channel is considered to be quasi-static frequency selective fading corrupted by AWGN with power spectral density N_0. The duration of CP is assumed to be longer than the maximum delay spread of the channel in order to avoid ISI.

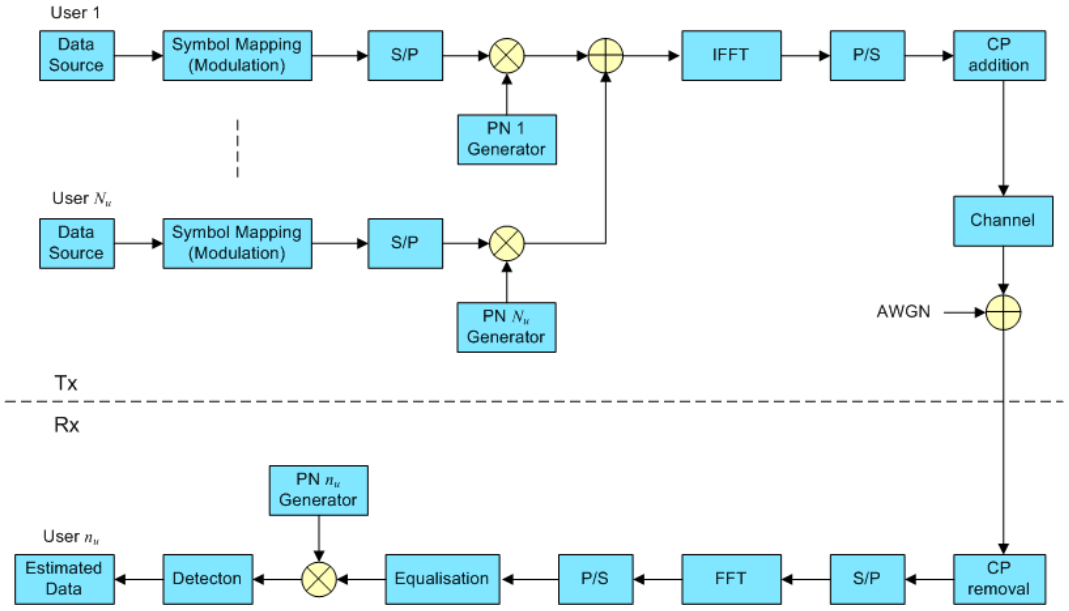

Figure 2.8: Multiuser MC-CDMA system.

Upon receiving the signal, CP is removed and the FFT of size N_s is performed. The received signal model at the *i-th* multiplexed chip after FFT can be characterised as

$$r_i = H_i x_i + n_i. \tag{2.19}$$

The estimates of the transmitted chips at the *i-th* subcarrier can be obtained by performing ZF equalization on each subcarrier as shown by

$$y_i = H_i^{-1} r_i = H_i^{-1} H_i x_i + H_i^{-1} n_i = x_i + \tilde{n}_i. \tag{2.20}$$

The symbol decision statistics is acquired when the chip estimates are despread by the desired user's spreading sequence expressed as

$$z_{n_u,p} = \sum_{g=1}^{G} c_{n_u,g} y_i = d_{n_u,p} + \sum_{g=1}^{G} c_{n_u,g} \tilde{n}_i. \tag{2.21}$$

The estimated *p-th* symbol detection for the n_u-*th* user is performed by slicing $z_{n_u,p}$ using the quantization operation $\mathcal{Q}(.)$ with respect to the type of constellation in use

$$\hat{d}_{n_u,p} = \mathcal{Q}\left(z_{n_u,p}\right). \tag{2.22}$$

It is well known that the ZF technique amplifies the noise and this degrades the system performance. For this reason, the ZF equalisation in (2.20) can be easily extended to the minimum mean square error (MMSE) equaliser. The MMSE filter aims to minimise the MSE between the transmitted symbol and the filtered received signal. This is formed by

$$H_i^{MMSE} = \underset{\widetilde{H}_i}{\operatorname{argmin}} \left\{ E\left[\left| \mathbf{d} - \widetilde{H}_i \mathbf{r} \right|^2 \right] \right\} = (H_i^* H_i + \sigma_n^2)^{-1} H_i^* \tag{2.23}$$

where H_i^* gives the complex conjugate of H_i and $E[.]$ denotes the expectation

operator. The MMSE equalisation is used to evaluate the performance of MC-CDMA in the next section.

2.2.3.2 Performance of MC-CDMA

The performance of the coded and uncoded MMSE MC-CDMA system with chip level block interleaving and eight users ($N_u = 8$) is evaluated under Rayleigh frequency selective fading channels and is demonstrated in Figure 2.9. The transmitted frame is assumed to consist 64 QPSK modulated symbols ($P = 64$) and each spreading sequence contains eight chips ($G = 8$). Walsh-Hadamard spreading sequences are used for each user. The coded MC-CDMA system uses rate 1/2 convolutional codes with constraint length 3 and generators {5,7}, and Viterbi decoder at the receiver. Hence the number of chips for the encoded frame is 1024 and 512 for the uncoded frame. The FFT size is considered to be the same as the number of subcarriers i.e. $N_s = 1024$ and 512 respectively. The block interleaver has a size of 32×32 for the coded and 16×32 for the uncoded MC-CDMA. The

Delay(μs)	0.0	0.2	0.6	1.6	2.4	5.0
Rel. Power (dB)	-3.0	0.0	-2.0	-6.0	-8.0	-10.0

Table 2.1: Relative powers of delay profile [55].

radio channel is assumed to be a typical urban area propagation model specified in [55], with 6 taps and the parameters are listed in Table 2.1. It is also assumed that the excess delay bin width is equal to 0.2 μs and the maximum delay spread is shorter than the duration of the cyclic prefix. Hence, ISI is avoided and each chip experiences flat fading.

The results illustrate that the coded MC-CDMA outperforms the uncoded case by 16 dB at BER = 10^{-4}. The reason is because when block interleaving is applied, consecutive chips will be transmitted at interleaved subcarriers, which

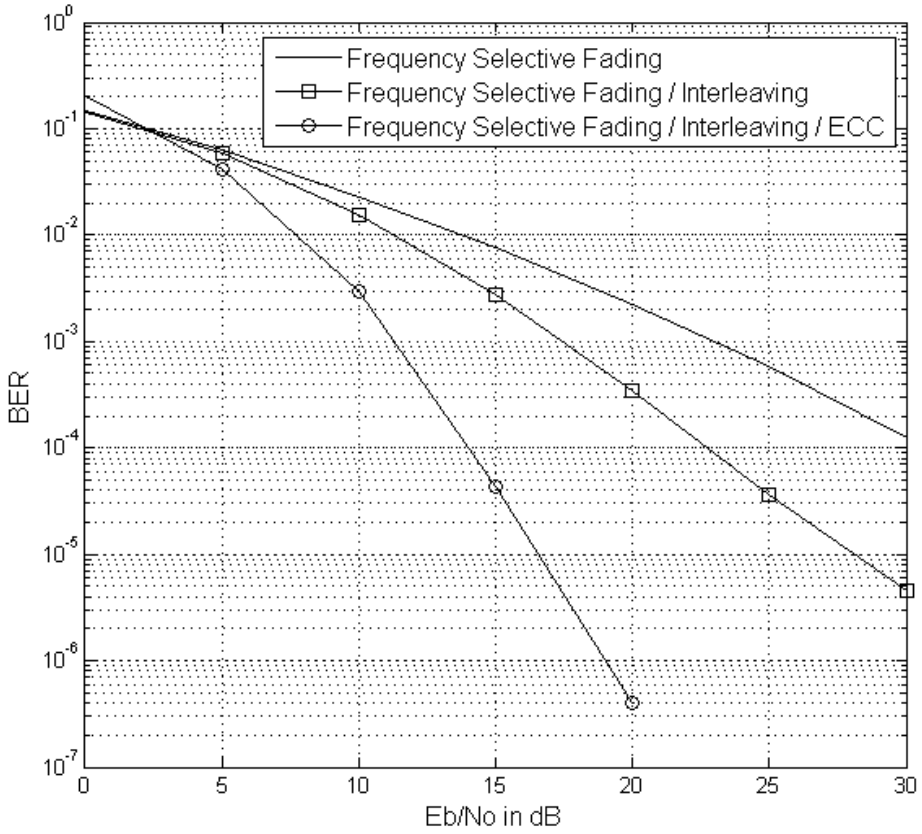

Figure 2.9: Performance of coded and uncoded MC-CDMA in fading channels.

have more diverse channel gains. With ECC, this diversity can be exploited to correct errors and produce significant performance advantage.

2.2.4 Orthogonal Frequency Division Multiple Access (OFDMA)

Multiuser OFDM or OFDMA [56, 57], a scheme originally proposed for cable TV (CATV) networks in Europe [58] and recently adopted in the IEEE 802.16 wireless MAN (WMAN) system [59], is the technology which combines OFDM with FDMA. In this way OFDMA allows multiple users to transmit information simultaneously by allocating different subcarriers to each user.

2.2.4.1 System Model

Consider an OFDMA system with N_u users. The information data are grouped into N_u frames and then each frame is modulated into P symbols. In OFDMA system, each user is allocated P subcarriers so that one subcarrier is used for one symbol transmission. The combined signals of all users have an index i and relate to the p-th symbol ($p = 1, 2, \ldots, P$) and the n_u-th user ($n_u = 1, 2, ..., N_u$) by $i = (n_u - 1)P + p$. Thus the symbol vector at the i-th subcarrier can be represented as $\mathbf{d}_i = \begin{bmatrix} d_1 & d_2 & \cdots & d_{PN_u} \end{bmatrix}^T \in \mathbb{C}^{PN_u \times 1}$. The symbols are then mapped onto $N_s = P \times N_u$ subcarriers and transformed into time domain by IFFT. Upon receiving the signal, the CP is removed and FFT of size $P \times N_u$ is performed. The received signal of OFDMA for the i-th subcarrier, after the FFT can be written as

$$r_i = H_i d_i + n_i. \tag{2.24}$$

The estimates of the transmitted symbols at the i-th subcarrier can be obtained by performing ZF equalisation on each subcarrier as shown by

$$y_i = H_i^{-1} r_i = d_i + \tilde{n}_i. \tag{2.25}$$

The i-th symbol detection is performed by slicing y_i and it is represented by

$$\hat{d}_i = \mathcal{Q}\left(y_i\right). \tag{2.26}$$

2.2.4.2 Performance of OFDMA

The BER performance for coded and uncoded OFDMA system with 4 users ($N_u = 4$) is illustrated in Figure 2.10. The transmitted frame for the n_u-th user is assumed to comprise 32 QPSK modulated symbols ($P = 32$) which are mapped

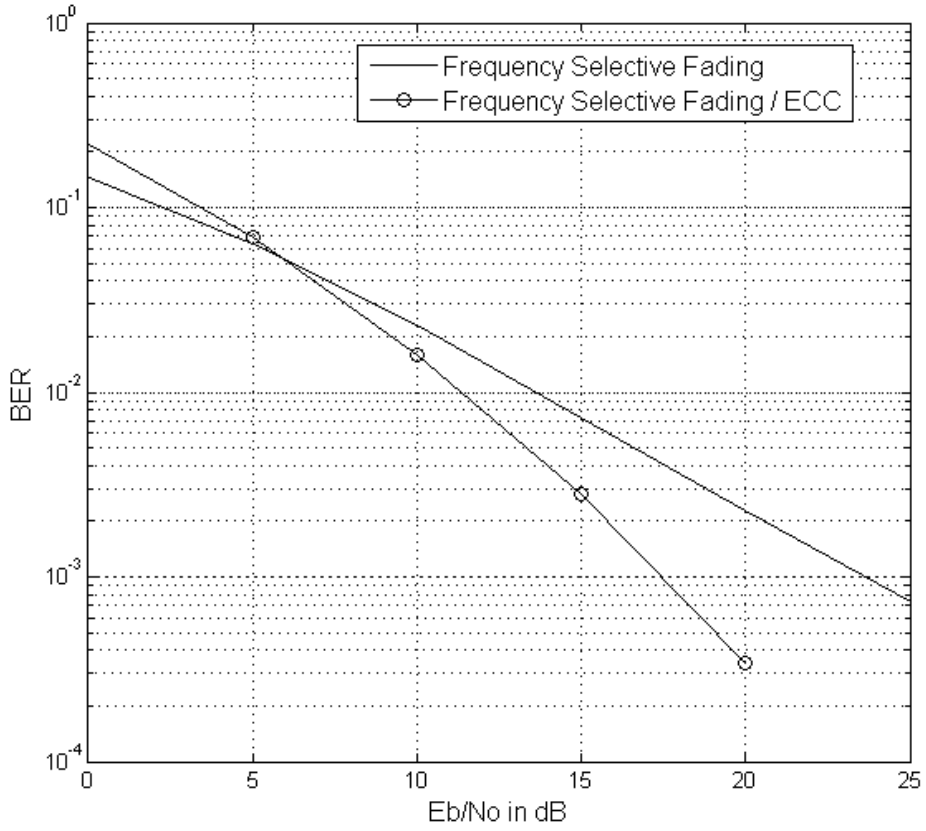

Figure 2.10: Performance of OFDMA in Rayleigh fading channels.

onto the same number of subcarriers. The FFT size is considered to be the same as the total number of subcarriers for all users, i.e. $N_s = 128$. The encoded frames for OFDMA system make use of the same codes as with the OFDM system discussed in Section 2.2.1.3. Also the radio channel used here is assumed to be the same as for OFDM in section 2.2.1.3. As expected, it is clear that the results for OFDMA have shown the same performance with the OFDM system.

2.3 Multiple Input Multiple Output (MIMO)

MIMO system [7, 60, 61] is a scheme based on multiple transmitting and multiple receiving antennas which can achieve very high data rates in rich multipath

scattering environments without increasing the transmission bandwidth or the total transmitted power of the system. The point-to-point MIMO channel of four transmit ($N_t = 4$) and four receive ($N_r = 4$) antennas is depicted in Figure 2.11.

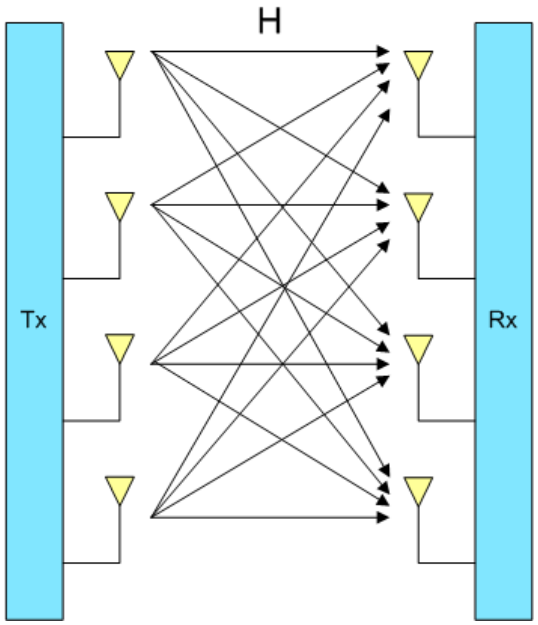

Figure 2.11: 4x4 MIMO channel.

MIMO techniques realise high data rates through spatial multiplexing and increase the spectral efficiency of the system in rich scattering environments by providing spatial diversity. In addition, the MIMO system capacity increases linearly with the number of transmit-receive antenna pairs. This explains the reason why a great interest has risen for spatial multiplexing architectures. The received signal for the MIMO system is characterised by

$$\begin{bmatrix} r^1 \\ \vdots \\ r^{N_r} \end{bmatrix} = \begin{bmatrix} h^{1,1} & \dots & h^{1,N_t} \\ \vdots & \ddots & \vdots \\ h^{N_r,1} & \dots & h^{N_r,N_t} \end{bmatrix} \begin{bmatrix} d^1 \\ \vdots \\ d^{N_t} \end{bmatrix} + \begin{bmatrix} n^1 \\ \vdots \\ n^{N_r} \end{bmatrix} \in \mathbb{C}^{N_r \times N_t} \tag{2.27}$$

The channel model in (2.27) can be simplified to a matrix equation indicated as

$$\mathbf{r} = \mathbf{Hd} + \mathbf{n} \tag{2.28}$$

where $\mathbf{d}$ denotes the N_t dimensional transmitted symbol, $\mathbf{n}$ is the N_r dimensional noise vector with zero mean and variance σ_n^2 and $\mathbf{H}$ indicates the $N_r \times N_t$ complex matrix of channel gains $h^{i,j}$ from transmit antenna j to receive antenna i.

2.3.1 Spatial Multiplexing

Figure 2.12 depicts the block diagram for a spatial multiplexing (SM) [54, 62] technique with parallel symbol mapping. Spatial multiplexing divides a single bit stream into N_t substreams which are next mapped into symbol streams by the appropriate constellation before simultaneous transmission over the wireless channel. The collection of the N_t substreams forms the vertical vector

$$\mathbf{d} = \begin{bmatrix} d^1 & d^2 & \cdots & d^{N_t} \end{bmatrix}^T \in \mathbb{C}^{N_t \times 1} \tag{2.29}$$

which contains the mapped symbols. This process illustrates the encoding of the input serial data into a vertical vector and is referred to as vertical encoding [5]. As N_t parallel transmit antennas are used for spatial multiplexing, the transmission rate is N_t times higher than systems with a single transmit antenna.

2.3.1.1 Linear Detection (Nulling)

Linear filtering (or nulling) suppresses the spatial interference which arises when multiple antennas transmit multiple substreams simultaneously. This interference is called co-antenna interference (CAI). With nulling, one of the received

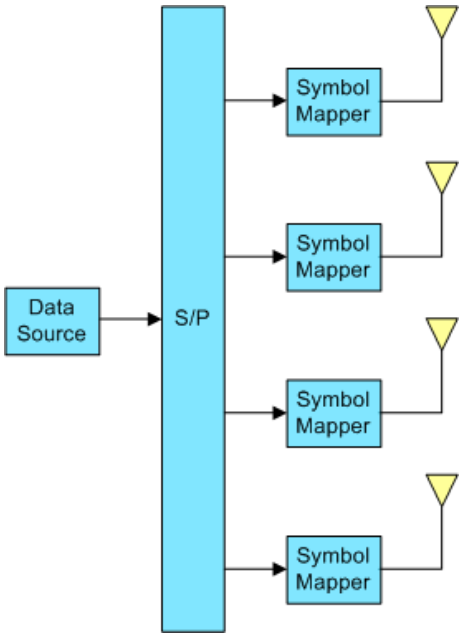

Figure 2.12: Spatial multiplexing architecture.

substreams is considered to be the desired signal while the remaining substreams are suppressed. This is repeated for each of the received substreams. Two different linear filters are used for the purpose of this research and these include the ZF and the minimum mean square error (MMSE) filters. Provided that the number of transmit antenna is not greater than the number of receive antenna ($N_t \leq N_r$), their corresponding spatial transform matrices are given by [1]

$$\mathbf{G}_{ZF} = \mathbf{H}^{+} = (\mathbf{H}^{H}\mathbf{H})^{-1}\mathbf{H}^{H} \tag{2.30}$$

$$\mathbf{G}_{MMSE} = \left[\mathbf{H}^{H}\mathbf{H} + N_0\mathbf{I}_{N_t}\right]^{-1}\mathbf{H}^{H} \tag{2.31}$$

respectively, where $\mathbf{H}^{+}$ and $\mathbf{H}^{H}$ represent the pseudoinverse and Hermitian matrices of $\mathbf{H}$ respectively, and $\mathbf{I}_{N_t}$ signifies the $N_t \times N_t$ identity matrix. After nulling, the decision statistics of the transmitted symbols can be represented as

$$\mathbf{y} = \mathbf{Gr} = \mathbf{Gd} + \mathbf{Gn} \tag{2.32}$$

where **G** denotes the ZF or MMSE spatial suppression matrix given by (2.30) or (2.31) respectively.

2.3.1.2 OSIC Detection (V-BLAST)

The V-BLAST architecture [9] is a MIMO technique that employs a layered detection architecture with interference suppression, symbol detection, and interference cancellation. V-BLAST has recently gained major research interest because it can realize very high data transfer rates by using spatial multiplexing to exploit the multiple spatial channels. The block diagram for the V-BLAST scheme is illustrated in Figure 2.13. At the receiver, the received substreams with

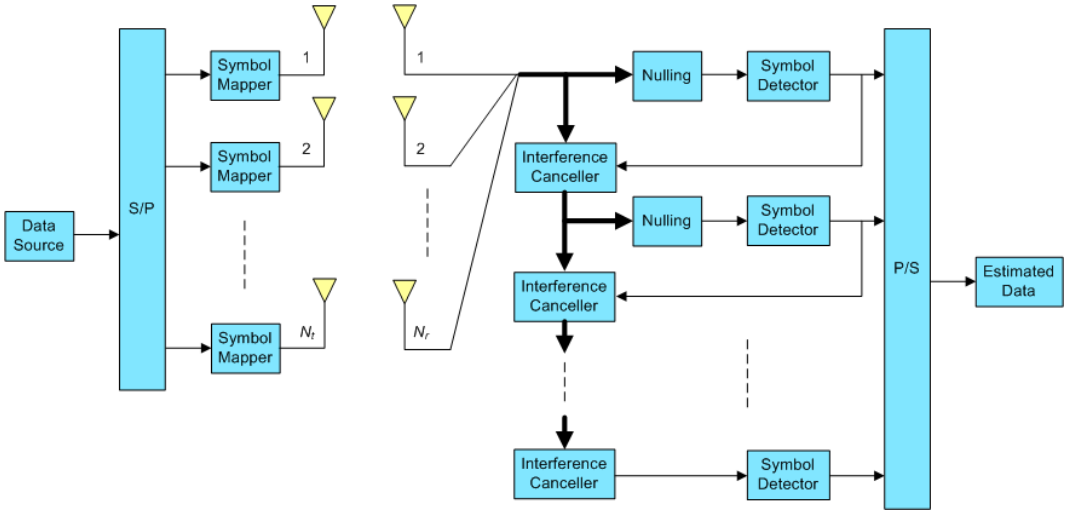

Figure 2.13: V-BLAST architecture.

the highest post detection SNR is considered first to be the desired signal for detection while the remaining substreams are suppressed. Next, the interference from the detected substream is subtracted from the received signal and the result is a modified received vector with less interferers. The layered detection process is performed using an optimum selection ordering. This ordering is given by the set $S \in \{k_1, k_2, ..., k_{N_t}\}$ where k signifies the row of the linear transform matrix **G** with the highest post detection SNR. The general detection procedure can be

described in the following three steps:

- The nulling vector $\mathbf{w}_{k_1}$ represents the k_1-th column of $\mathbf{G}$ and is used to form the decision statistic of the desired substream expressed as

$$y_{k_1} = \mathbf{w}_{k_1}^T \mathbf{r}_1 \tag{2.33}$$

- An estimated value of the detected symbol is obtained by slicing y_{k_1} using the quantization operation $\mathcal{Q}(.)$ with respect to the type of constellation in use

$$\hat{d}_{k_1} = \mathcal{Q}(y_{k_1}) \tag{2.34}$$

- The interference from the detected symbol is cancelled from the received signal resulting in the modified vector

$$\mathbf{r}_2 = \mathbf{r}_1 - \hat{d}_{k_1} (\mathbf{H})_{k_1} \tag{2.35}$$

  where $(\mathbf{A})_{k_1}$ indicates the k_1-th column of matrix $\mathbf{A}$.

The previous steps are repeated for the remaining components of the set S and each time a new modified version of the received vector is used. The full V-BLAST detection algorithm with ZF nulling can be expressed as a recursive procedure, which also includes the computational of optimal ordering as follows:

Initialisation:

$$i \leftarrow 1 \tag{2.36}$$

$$\mathbf{G}_1 = \mathbf{H}^+ \tag{2.37}$$

$$k_1 = \arg\min \left\| (\mathbf{G}_1)_j \right\|^2 \tag{2.38}$$

Recursion:

$$\mathbf{w}_{k_1}^T = (\mathbf{G}_i)_{k_i} \tag{2.39}$$

$$y_{k_i} = \mathbf{w}_{k_i}^T \mathbf{r}_i \tag{2.40}$$

$$\hat{d}_{k_i} = \mathcal{Q}(y_{k_i}) \tag{2.41}$$

$$\mathbf{r}_{i+1} = \mathbf{r}_i - \hat{d}_{k_i} (\mathbf{H})_{k_i} \tag{2.42}$$

$$\mathbf{G}_{i+1} = \left(\mathbf{H}^+\right)_{\bar{k}_i} \tag{2.43}$$

$$k_{i+1} = \arg\min \left\| (\mathbf{G}_{i+1})_j \right\|^2 \tag{2.44}$$

$$i \leftarrow i + 1 \tag{2.45}$$

where $(\mathbf{A})_j$ denotes the *j-th* column of matrix $\mathbf{A}$, $\mathbf{H}_{\bar{k}_i}$ represents the matrix obtained when zeroing columns $(k_1, k_2, ..., k_i)$ of $\mathbf{H}$. Also, $\|\mathbf{a}\|$ stands for the magnitude of the vector $\mathbf{a}$. To summarise the recursive algorithm, (2.38) and (2.44) determine the elements of the ordered set $S \in \{k_1, k_2, ..., k_{N_t}\}$, (2.39), (2.40) and (2.41) resolve the ZF nulling vector, the decision statistic and the estimated component of $\mathbf{d}$ respectively. Furthermore, (2.42) is responsible for the cancellation of the detected signal from the received vector. Lastly, (2.43) computes the new pseudoinverse value of the channel response for the next iteration. It must be noted that the above procedure can be easily extended to use the MMSE filter where the spatial transform matrix is calculated by (2.31).

The performance of ZF OSIC receiver with 2×2 and 4×4 antenna configurations is evaluated through Monte Carlo simulation. Each transmitted frame consists of 100 uncoded QPSK modulated symbols. The MIMO channel is assumed to experience quasi-static flat fading. Figure 2.14 depicts the BER performance for different E_b/N_0 for the ZF OSIC detector. It is evident that the ZF OSIC

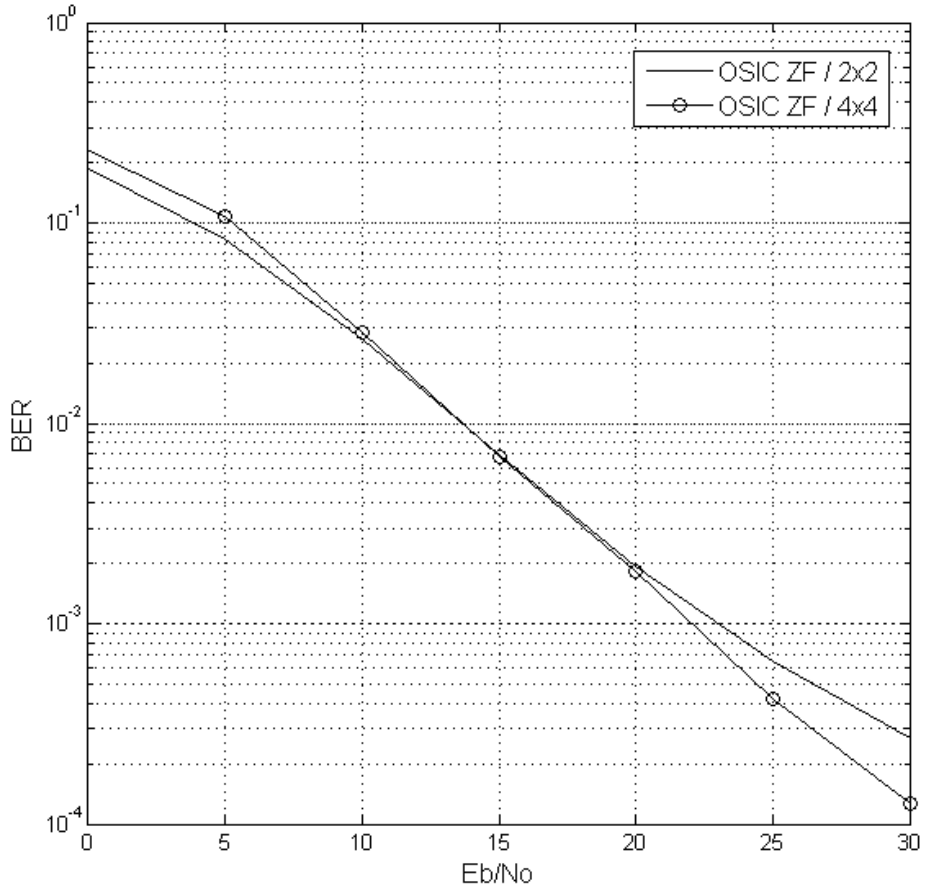

Figure 2.14: Performance of ZF/MMSE OSIC detectors in Rayleigh flat fading channel.

detector performs very similar in 2×2 and 4×4 MIMO channels until 20 dB. In the higher SNR region the performance of 4×4 ZF OSIC detector becomes better than the 2×2 case.

2.3.2 Spatial Diversity

An alternative approach to spatial multiplexing is to achieve transmit and/or receive diversity by transmiting and receiving multiple copies of the same data streams under independent fading paths using multiple transmit and multiple

receive antennas. In this way detection of signals in deep fades is avoided and hence spatial diversity increases the system performance. This method is called space-time coding (STC) [63] and it is illustrated in Figure 2.15. There are two

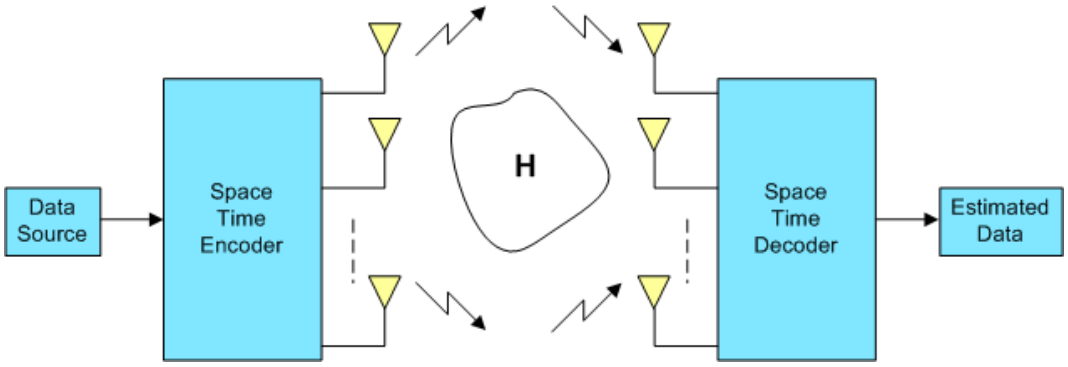

Figure 2.15: Space-time coding (STC).

main STC schemes that provide spatial diversity and these are: (i) space-time trellis code (STTC) [64–67] and (ii) space-time block code (STBC) [68]. STTC introduces spatial correlation into the signals transmitted from different antennas, in order to provide spatial diversity and coding gain without sacrificing extra bandwidth. However, STTC requires trellis decoding which is a high complexity detection process that grows exponentially as a function of the transmit antennas and the transmission rate. However, this work is focused on the STBC, which is explained in the following.

2.3.2.1 Space-Time Block Code (STBC)

Instead of the complex STTC, a low complexity system that achieves transmit diversity was proposed by Alamouti for 2 transmit antennas in [69]. This scheme is the well known STBC and is later generalised to an arbitary number of antennas [70].

In the Alamouti's transmission scheme, consider two symbols d^0 and d^1 in two consecutive symbol periods transmitted over two consecutive transmissions.

During the first transmission, d^0 and d^1 are transmitted simultaneously at time t from the two transmit antennas. During the second transmission, $-d^{1*}$ and d^{0*} are transmitted at time $t + T_d$ where T_d denotes the symbol period. Hence, the transmission matrix is represented by

$$\mathbf{D} = \begin{bmatrix} d^0 & d^1 \\ -d^{1*} & d^{0*} \end{bmatrix}. \tag{2.46}$$

It has to be noted that the transmission matrix is orthogonal and this means that

$$\begin{aligned} \mathbf{D}\mathbf{D}^H &= \begin{bmatrix} d^0 & d^1 \\ -d^{1*} & d^{0*} \end{bmatrix} \begin{bmatrix} d^{0*} & -d^1 \\ d^{1*} & d^0 \end{bmatrix} = \begin{bmatrix} |d^0|^2 + |d^1|^2 & 0 \\ 0 & |d^0|^2 + |d^1|^2 \end{bmatrix} \\ &= \left(\left|d^0\right|^2 + \left|d^1\right|^2 \right) \mathbf{I} \end{aligned} \tag{2.47}$$

The received signals at the first and second symbol periods are given by

$$r(1) = h_1 d^0 + h_2 d^1 + n(1) \tag{2.48}$$

$$r(2) = -h_1 d^{1*} + h_2 d^{0*} + n(2) \tag{2.49}$$

where h_1 and h_2 denote the channel gains from transmit antenna 1 and 2 to receive antennas respectively and it is assumed that h_1 and h_2 are constant over two consecutive symbol periods. Furthermore, $n(1)$ and $n(2)$ represent the AWGN components with zero mean and variance N_0. The received signal matrix can be represented as follows

$$\mathbf{r} = \begin{bmatrix} r(1) \\ r^*(2) \end{bmatrix} = \begin{bmatrix} h_1 & h_2 \\ h_2^* & -h_1^* \end{bmatrix} \begin{bmatrix} d^0 \\ d^1 \end{bmatrix} + \begin{bmatrix} n(1) \\ n^*(2) \end{bmatrix} = \mathbf{H}\mathbf{d} + \mathbf{n}. \tag{2.50}$$

Similar to (2.47), the channel matrix $\mathbf{H}$ is orthogonal such that

$$\mathbf{H}^H\mathbf{H} = \begin{bmatrix} |h_1|^2 + |h_2|^2 & 0 \\ 0 & |h_1|^2 + |h_2|^2 \end{bmatrix}. \tag{2.51}$$

The transmitted signal could be separated by pre-multiplying the received signal in (2.50) with $\mathbf{H}^H$ as shown by

$$\mathbf{y} = \mathbf{H}^H\mathbf{r} = \begin{bmatrix} |h_1|^2 + |h_2|^2 & 0 \\ 0 & |h_1|^2 + |h_2|^2 \end{bmatrix} \mathbf{d} + \mathbf{H}^H\mathbf{n} = \left(|h_1|^2 + |h_2|^2\right)\mathbf{d} + \tilde{\mathbf{n}}. \tag{2.52}$$

The modified noise $\tilde{\mathbf{n}}$ is still AWGN with zero mean but with power equal to

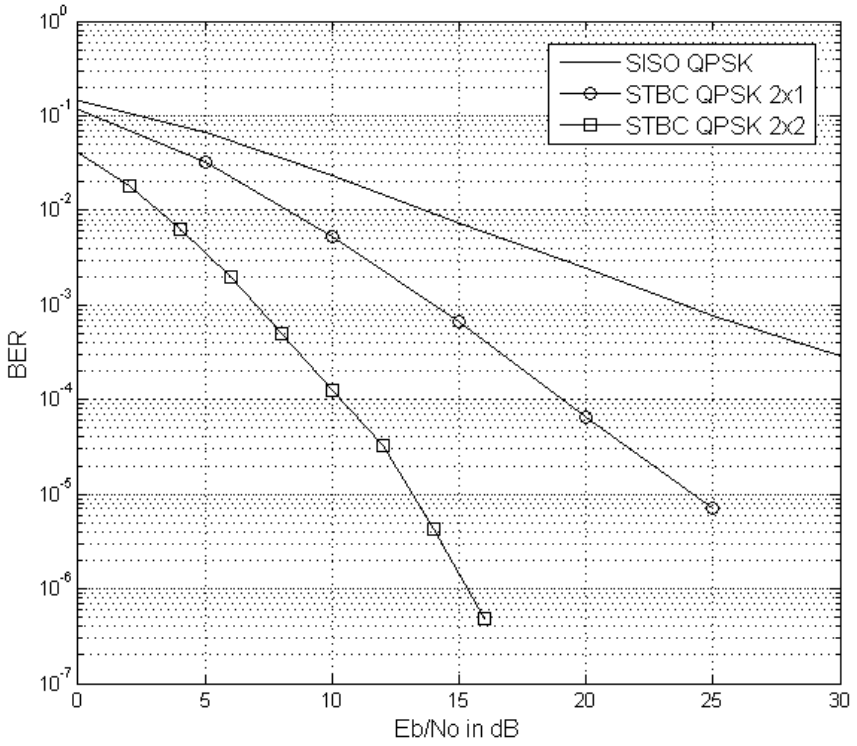

Figure 2.16: Performance of STBC in Rayleigh flat fading channel.

$\left(|h_1|^2 + |h_2|^2\right) N_0\mathbf{I}$. Next, maximum likelihood (ML) symbol-by-symbol detection can be used to derive the estimated data. The above analyis has shown that the Alamuti's STBC scheme achieves a rate of 1 ($\mathcal{R}$=1) as it transmits two symbols in two symbol periods.

The performance of STBC system with 2×1 and 2×2 antenna configurations is evaluated through Monte Carlo simulation. Each transmitted frame consists of 100 uncoded QPSK modulated symbols. The MIMO channel is assumed to experience quasi-static flat fading. Figure 2.16 depicts the BER performance for different E_b/N_0 for the STBC system. It is evident that the 2×2 STBC system significantly outperforms the SISO QPSK system by 10 dB at BER = 10^{-3}. As the number of transmit and receive antennas increases to 4, a further 4 dB improvement is observed for the STBC system at the same BER. This is because as the number of antennas increases, spatial diversity is better exploited to improve performance.

Chapter 3

Downlink MIMO MC-CDMA

In this chapter we introduce the basic signal model for the downlink MIMO MC-CDMA system, and existing receiver architectures. These include the chip and symbol level linear and OSIC receivers.

3.1 Transmit Signal Model

Consider the single cell downlink MIMO MC-CDMA transmitter model with N_u users depicted in Figure 3.1. The information data are grouped into N_t substreams and then each substream is encoded and modulated to P symbols. The uncoded symbol matrix for user n_u (n_u = 1,2,...,N_u) is defined as

$$\mathbf{D}_{n_u} = \left[\begin{array}{cccc} \mathbf{d}_{n_u}^1 & \mathbf{d}_{n_u}^2 & \cdots & \mathbf{d}_{n_u}^{N_t} \end{array} \right]^T \in \mathbb{C}^{N_t \times P} \tag{3.1}$$

where the column vector $\mathbf{d}_{n_u}^{n_t}$ denotes the data stream that is transmitted by the n_t-th antenna ($n_t = 1, 2, ..., N_t$), represented as

$$\mathbf{d}_{n_u}^{n_t} = \left[\begin{array}{cccc} d_{n_u,1}^{n_t} & d_{n_u,2}^{n_t} & \cdots & d_{n_u,P}^{n_t} \end{array} \right]^T \in \mathbb{C}^{P \times 1}. \tag{3.2}$$

Each user is allocated a distinct spreading code. The spreading sequence of user n_u is indicated as

$$\mathbf{c}_{n_u} = \begin{bmatrix} c_{n_u,1} & c_{n_u,2} & \cdots & c_{n_u,G} \end{bmatrix} \in C^{1\times G} \tag{3.3}$$

where C refers to the spreading code chip alphabet and G is the spreading code length. The spreading sequence is used to spread the symbols of the n_u-th user

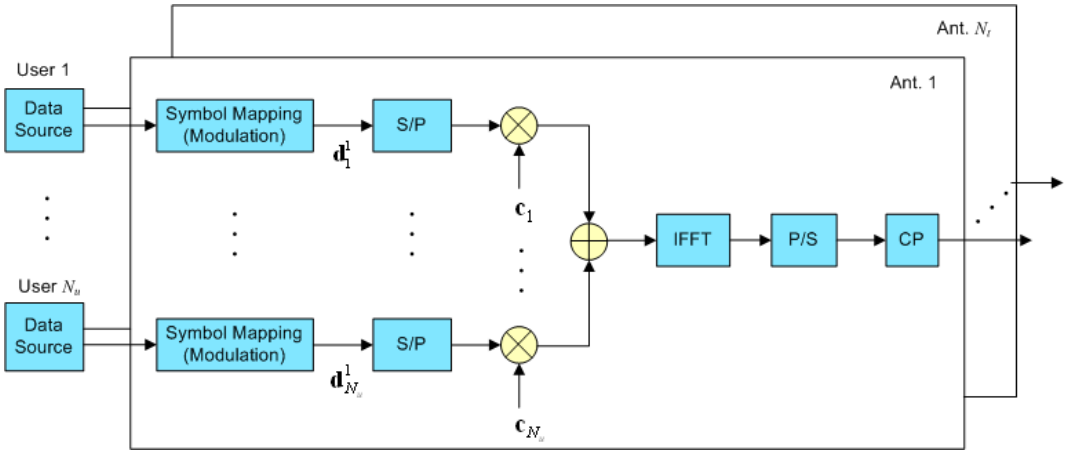

Figure 3.1: MIMO MC-CDMA transmitter.

in order to form the chip-level transmit matrix

$$\mathbf{S}_{n_u} = \begin{bmatrix} \mathbf{s}_{n_u,1} & \mathbf{s}_{n_u,2} & \cdots & \mathbf{s}_{n_u,N_s} \end{bmatrix} = \mathbf{D}_{n_u} \otimes \mathbf{c}_{n_u} \in \mathbb{C}^{N_t\times N_s} \tag{3.4}$$

where $N_s = P \times G$ represents the total number of subcarriers. The combined CDMA chip of all users at the i-th subcarrier is defined as

$$\mathbf{x}_i = \begin{bmatrix} x_i^1 & x_i^2 & \cdots & x_i^{N_t} \end{bmatrix}^T = \sum_{n_u=1}^{N_u} \mathbf{s}_{n_u,i} \in \mathbb{C}^{N_t\times 1} \tag{3.5}$$

where $x_i^{n_t}$ is the combined chip transmitted by the n_t-th antenna, and can be expressed as

$$x_i^{n_t} = \sum_{n_u=1}^{N_u} s_{n_u,i}^{n_t} = \sum_{n_u=1}^{N_u} c_{n_u,g(i)} d_{n_u,p(i)}^{n_t} \tag{3.6}$$

in which $s_{n_u,i}^{n_t}$ denotes the n_u-th user transmitted chip by the n_t-th antenna at the i-th subcarrier. The combined chip sequence for each transmit antenna is transformed into time domain by the IFFT. The output signal from the IFFT follows the same procedure as with the MC-CDMA system in Chapter 2. Furthermore, the channel is considered to be the same with the MC-CDMA system. Other assumptions made include no channel state information (CSI) at the transmitter and perfect CSI at the receiver. It must be noted that if an interleaver is used for MIMO MC-CDMA the performance will become better. This is because consecutive chips will be transmitted at interleaved subcarriers, which have more diverse channel gains. However for brevity of presentation, the following analysis considers a system with no interleaving. It can easily be extended to an interleaved system, which is also used in the simulations.

3.2 Receive Signal Model

Consider the receiver of the desired user with N_r receive antennas. Upon receiving the signal, CP is removed and FFT of size N_s is performed. The received signal model at the i-th subcarrier after FFT is expressed as

$$\mathbf{r}_i = \mathbf{H}_i \mathbf{x}_i + \mathbf{n}_i \tag{3.7}$$

where the received signal is characterised by

$$\mathbf{r}_i = \begin{bmatrix} r_i^1 & r_i^2 & \cdots & r_i^{N_r} \end{bmatrix}^T \in \mathbb{C}^{N_r \times 1}. \tag{3.8}$$

The channel and the AWGN vector with σ_n^2 power are represented respectively as

$$\mathbf{H}_i = \begin{bmatrix} \mathbf{h}_i^1 & \mathbf{h}_i^2 & \cdots & \mathbf{h}_i^{N_t} \end{bmatrix} = \begin{bmatrix} h_i^{(1,1)} & \cdots & h_i^{(1,N_t)} \\ \vdots & \ddots & \vdots \\ h_i^{(N_r,1)} & \cdots & h_i^{(N_r,N_t)} \end{bmatrix} \in \mathbb{C}^{N_r \times N_t} \tag{3.9}$$

$$\mathbf{n}_i = \begin{bmatrix} n_i^1 & n_i^2 & \cdots & n_i^{N_r} \end{bmatrix}^T \in \mathbb{C}^{N_r \times 1} \tag{3.10}$$

where $h_i^{(n_r,n_t)}$ denotes the channel response at the i-th subcarrier between transmit antenna n_t and receive antenna n_r (n_r = 1,2,...,N_r), and $\mathbf{n}_i$ signifies the $N_r \times 1$ AWGN noise vector at the i-th subcarrier. The received signal in (3.7) can be further expanded to

$$\mathbf{r}_i = \overbrace{\mathbf{h}_i^{n_t} s_{n_u,i}^{n_t}}^{\text{desired}} + \overbrace{\sum_{n_t' \neq n_t}^{N_t} \mathbf{h}_i^{n_t'} s_{n_u,i}^{n_t'}}^{\text{CAI}} + \overbrace{\sum_{n_u' \neq n_u}^{N_u} \mathbf{h}_i^{n_t} s_{n_u',i}^{n_t}}^{\text{MAI 1}} + \overbrace{\sum_{n_u' \neq n_u}^{N_u} \sum_{n_t' \neq n_t}^{N_t} \mathbf{h}_i^{n_t'} s_{n_u',i}^{n_t'}}^{\text{MAI 2}} + \mathbf{n}_i. \tag{3.11}$$

Considering the right hand side of (3.11), the first term corresponds to the transmitted chips from the desired substream n_t of the desired user n_u. The second term represents the CAI arising from other substreams of the desired user. The third (MAI 1) and the fourth term (MAI 2) express MAI coming from other users' n_t-th substream and all other substreams respectively. The visual representation of the terms in (3.11) that arrive at the the receiver of the n_u-th user are illustrated in Figure 3.2.

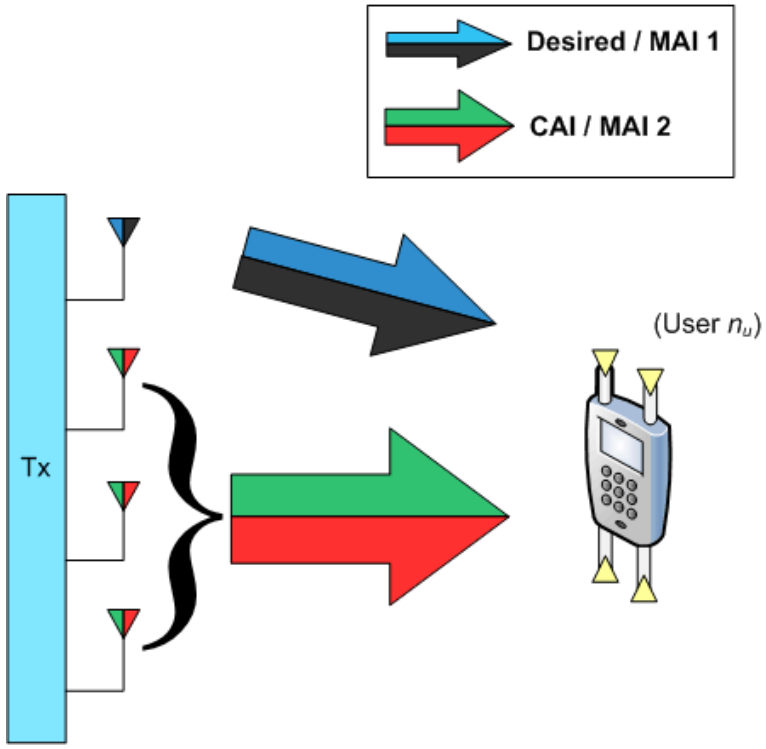

Figure 3.2: Illustration of the desired / CAI / MAI 1 / MAI 2 signals.

3.3 Existing receiver architectures

3.3.1 Chip level Linear & OSIC Receivers

In [1] and [2], chip level linear detectors are presented for downlink MIMO MC-CDMA system. Linear filtering suppresses CAI arising from multi-antenna transmission. It is performed by considering in turn each of the received sub-streams to be the desired signal while suppressing the remaining substreams. The receiver with linear ZF / MMSE filters is depicted in Figure 3.3. Their corresponding spatial transform matrices at the *i-th* subcarrier can be represented by [1]

$$\mathbf{H}_i^{ZF} = \mathbf{H}_i^{+} = (\mathbf{H}_i^H \mathbf{H}_i)^{-1} \mathbf{H}_i^H \tag{3.12}$$

$$\mathbf{H}_i^{MMSE} = \left[\mathbf{H}_i^H \mathbf{H}_i + (G/N_u)\sigma_n^2 \mathbf{I}_{N_t}\right]^{-1} \mathbf{H}_i^H \tag{3.13}$$

respectively. Considering the ZF case, the filtered received signal at the *i-th* subcarrier for the n_u-*th* user can be expressed as

$$\mathbf{y}_{n_u,i} = \mathbf{H}_i^{ZF}\mathbf{r}_i = \mathbf{H}_i^{+}\mathbf{H}_i\mathbf{x}_i + \mathbf{H}_i^{+}\mathbf{n}_i = \mathbf{x}_i + \tilde{\mathbf{n}}_i. \tag{3.14}$$

Next, the chip estimates in (3.14) are despread by the desired user's spreading sequence to obtain the symbol decision statistic,

$$\mathbf{z}_{n_u,p} = \sum_{g=1}^{G} c_{n_u,g}\mathbf{y}_{n_u,i(p,g)}. \tag{3.15}$$

Detection is then performed to obtain the symbol estimates.

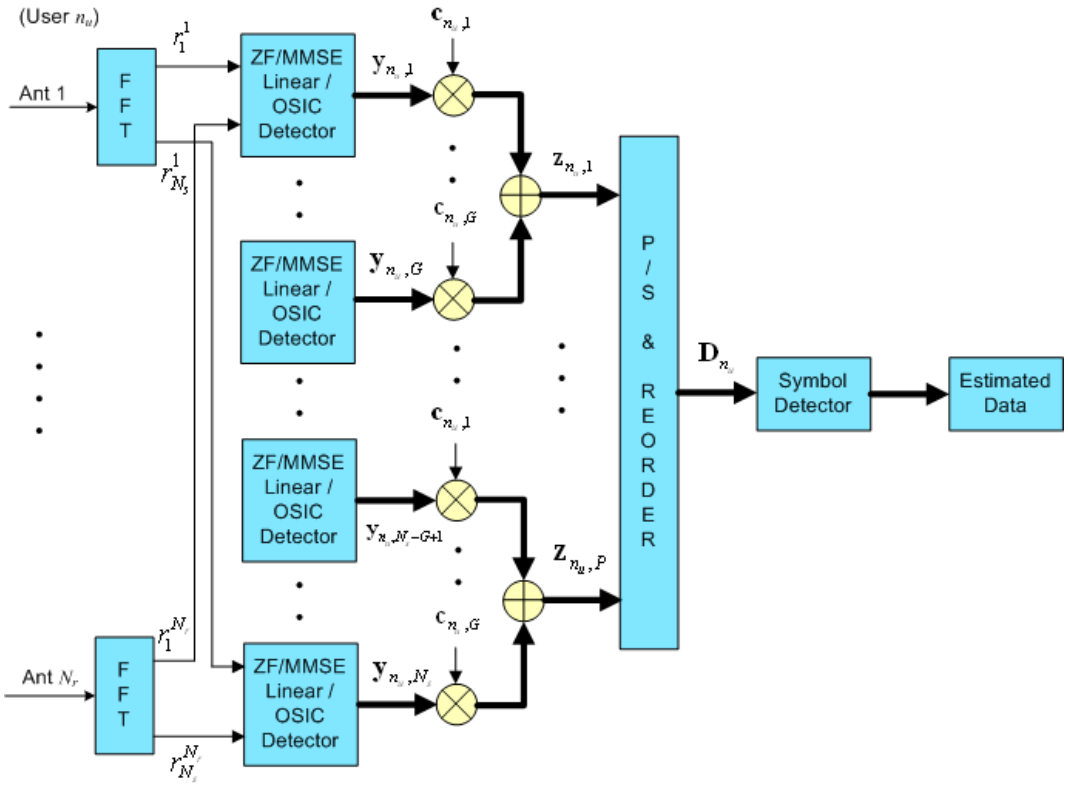

Figure 3.3: Linear & OSIC receivers for MIMO MC-CDMA.

The chip level OSIC (V-BLAST) receiver was originally proposed for MIMO MC-CDMA systems in [1] and studied further in [26–28]. The receiver in [1]

combines the OSIC detector with chip level despreading and symbol detection as shown in Figure 3.3. This receiver demonstrated good performance for single user case. However, its performance is severely degraded in multiuser case as shown next.

Figure 3.4 demonstrates the BER performance with respect to different E_b/N_0 for the linear chip level ZF and MMSE detectors [2] and the chip level OSIC detectors [1] for the half loaded four user ($N_u = 4$) case. As multiple antennas

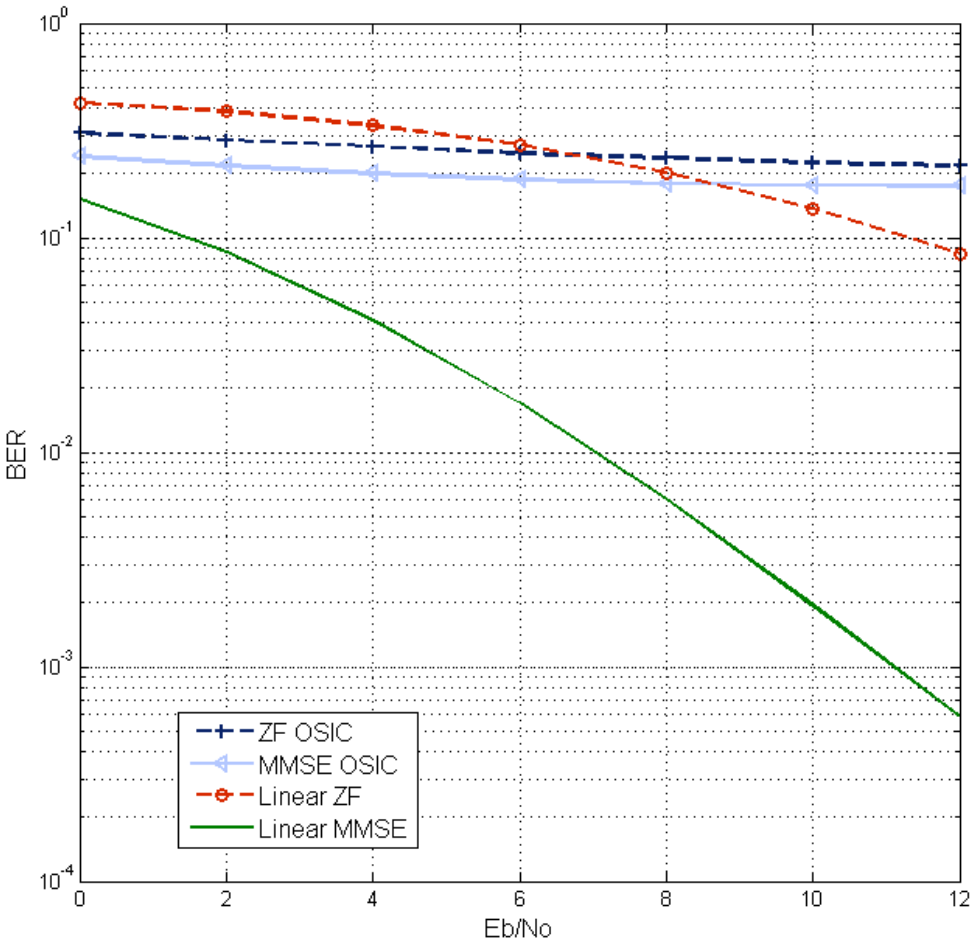

Figure 3.4: BER performance of linear and non linear detectors at half load for downlink MIMO MC-CDMA system.

are used by all systems, the word "MIMO" is omitted to ease the comparative discussion in Chapters 3 - 5. Consider a downlink communication system with 4×4 antenna configuration. Each transmitted frame comprises eight 1/2 rate convolutional coded QPSK modulated symbols ($P = 8$) with generators {5,7}. Each spreading sequence in the MC-CDMA system consists of eight chips ($G = 8$) and Walsh-Hadamard spreading sequences are used for each user. The FFT size is considered to be the same as the number of the subcarriers, i.e. N_s= 128 subcarriers are available per frame in which one subcarrier per one encoded symbol is used. The block interleaver has a size of $G \times P$. Each of the MIMO channels experiences frequency selective Rayleigh fading with two taps at arrival times $\{0, 1\}$ normalized to the chip period of the MC-CDMA system. It is assumed that the maximum delay spread is shorter than the duration of the cyclic prefix. Hence, ISI is avoided and each chip experiences flat fading.

The performance of ZF and MMSE OSIC detectors illustrate significant error floors in the higher SNR region due to MAI and error propagation. As a result, it performs even worse than the linear ZF and MMSE receivers. It can also be observed that the MMSE significantly outperforms the ZF counterpart. This is because the MMSE filter will not amplify the noise as in ZF filter, and hence a reduced error rate occurs.

3.3.2 Symbol level Linear & SIC Receivers

In this subsection we present the symbol level MMSE with SIC detector [2]. The *p-th* received symbol after the IFFT operation is

$$\mathbf{r}_p = \mathbf{W}_p \mathbf{d}_p + \mathbf{n}_p \tag{3.16}$$

where the received symbols, transmitted symbols and noise vector of the *p-th* symbol are represented respectively as

$$\mathbf{r}_p = \left[\begin{array}{cccc} r_1^1 \cdots r_G^1 & \cdots & r_1^{N_r} \cdots r_G^{N_r} \end{array} \right]^T \in \mathbb{C}^{N_r G \times 1} \tag{3.17}$$

$$\mathbf{d}_p = \left[\begin{array}{cccc} d_1^1 \cdots d_1^{N_t} & \cdots & d_K^1 \cdots d_K^{N_t} \end{array} \right]^T \in \mathbb{C}^{N_t K \times 1} \tag{3.18}$$

$$\mathbf{n}_p = \left[\begin{array}{cccc} n_1^1 \cdots n_G^1 & \cdots & n_1^{N_r} \cdots n_G^{N_r} \end{array} \right]^T \in \mathbb{C}^{N_r G \times 1}. \tag{3.19}$$

The combined channel-spreading matrix can be expressed as

$$\begin{aligned} \mathbf{W}_p &= \left[\begin{array}{cccc} \mathbf{w}_{1,p}^1 \cdots \mathbf{w}_{1,p}^{N_t} & \cdots & \mathbf{w}_{N_u,p}^1 \cdots \mathbf{w}_{N_u,p}^{N_t} \end{array} \right] = \\ &= \left[\begin{array}{ccc} h_{i(p,1)}^{(1,1)} c_{1,1} \cdots h_{i(p,1)}^{(1,N_t)} c_{1,1} & \cdots & h_{i(p,1)}^{(1,1)} c_{N_u,1} \cdots h_{i(p,1)}^{(1,N_t)} c_{N_u,1} \\ \vdots & \vdots & \vdots \\ h_{i(p,G)}^{(1,1)} c_{1,G} \cdots h_{i(p,G)}^{(1,N_t)} c_{1,G} & \cdots & h_{i(p,G)}^{(1,1)} c_{N_u,G} \cdots h_{i(p,G)}^{(1,N_t)} c_{N_u,G} \\ \vdots & \vdots & \vdots \\ h_{i(p,1)}^{(N_r,1)} c_{1,1} \cdots h_{i(p,1)}^{(N_r,N_t)} c_{1,1} & \cdots & h_{i(p,1)}^{(N_r,1)} c_{N_u,1} \cdots h_{i(p,1)}^{(N_r,N_t)} c_{N_u,1} \\ \vdots & \vdots & \vdots \\ h_{i(p,G)}^{(N_r,1)} c_{1,G} \cdots h_{i(p,G)}^{(N_r,N_t)} c_{1,G} & \cdots & h_{i(p,G)}^{(N_r,1)} c_{N_u,G} \cdots h_{i(p,G)}^{(N_r,N_t)} c_{N_u,G} \end{array} \right]. \end{aligned} \tag{3.20}$$

Next, the received signal passes through the symbol level MMSE filter and the estimate of the *p-th* transmitted symbol for the n_t*-th* substream can be represented

by

$$\begin{aligned} y_p^{n_t} &= \left[\mathbf{W}_p^{MMSE}\right]_{n_t} \mathbf{r}_p = \overbrace{\left[\mathbf{W}_p^{MMSE}\right]_{n_t} \mathbf{w}_{n_u,p}^{n_t} d_p^{n_t}}^{\text{desired}} + \overbrace{\sum_{n_t' \neq n_t}^{N_t} \left[\mathbf{W}_p^{MMSE}\right]_{n_t} \mathbf{w}_{n_u,p}^{n_t'} d_p^{n_t'}}^{\text{CAI}} \\ &+ \overbrace{\sum_{n_u' \neq n_u}^{N_u} \left[\mathbf{W}_p^{MMSE}\right]_{n_t} \mathbf{w}_{n_u',p}^{n_t} d_p^{n_t}}^{\text{MAI 1}} + \overbrace{\sum_{n_u' \neq n_u}^{N_u} \sum_{n_t' \neq n_t}^{N_t} \left[\mathbf{W}_p^{MMSE}\right]_{n_t} \mathbf{w}_{n_u',p}^{n_t'} d_p^{n_t'}}^{\text{MAI 2}} \\ &+ \left[\mathbf{W}_p^{MMSE}\right]_{n_t} \mathbf{n}_p \end{aligned} \tag{3.21}$$

where the spatial suppression matrix is given by [2]

$$\mathbf{W}_p^{MMSE} = \left[\mathbf{W}_p \mathbf{R}_{dd} \mathbf{W}_p^H + \sigma_n^2 \mathbf{I}_{N_r G}\right]^{-1} \mathbf{W}_p \mathbf{R}_{dd} \tag{3.22}$$

in which $\mathbf{R}_{dd} = E_d I_{N_t}$ and E_d denotes the symbol energy. Detection is then performed to obtain the symbol estimate $\hat{d}_p^{n_t}$. The modified received signal for the next detection layer can be obtained by

$$\mathbf{r}_p' = \mathbf{r}_p - \left(\mathbf{w}_{n_u,p}^{n_t} \hat{d}_p^{n_t}\right) \tag{3.23}$$

where $\mathbf{r}_p'$ contains the CAI and noise terms and some form of residual CAI and MAI for the next detection layer. The above stated steps are repeated until all remaining substreams are detected.

In Figure 3.5 we consider the BER performance for the linear chip level MMSE detector, the chip level OSIC detector and the symbol level MMSE with OSIC for the half loaded case. It must be noted that the symbol level MMSE with SIC detector is modified with a novel detection ordering. Consider the same system parameters and assumptions as in the previous subsection. From the results, it is evident that the symbol level OSIC detector performs 2 dB better than the

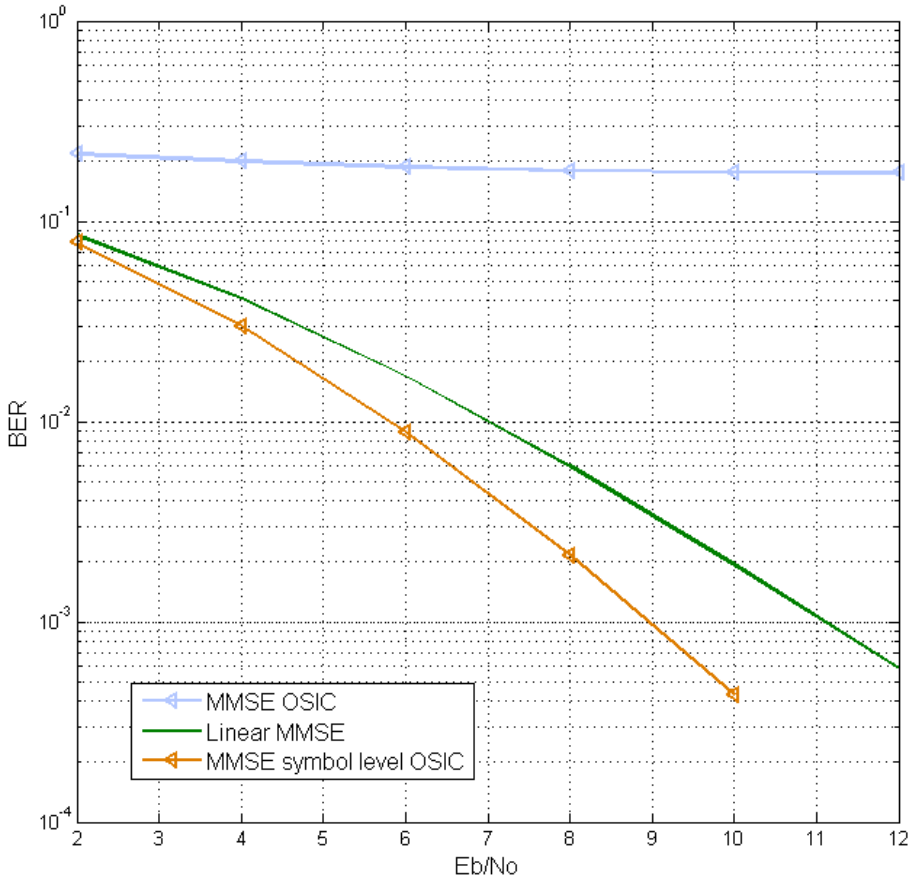

Figure 3.5: BER performance of chip and symbol level MIMO MC-CDMA at half load.

linear detector at BER = 10^{-3}.

Although the symbol level detector performs better than the chip level detectors, it requires higher computational complexity and also it requires the knowledge of all other users' spreading sequence to avoid MAI. For these reasons, the symbol detector is not so practical for downlink MC-CDMA systems.

Chapter 4

OSSMIC Receiver

This chapter first proposes the ordered successive spatial and multiuser interference cancellation (OSSMIC) receiver for the downlink MIMO MC-CDMA system. Next, the performance of the OSSMIC receiver is evaluated and compared to that of existing MIMO MC-CDMA receivers.

In the OSIC receiver for MIMO MC-CDMA systems shown in Figure 3.3 [1], the chip level nulling filter removes CAI and MAI 2 in (3.11). The next step in the OSIC algorithm is chip level hard detection of the selected substream. Then, interference from the detected symbols is cancelled from the received signal and this process comes before the despreading operation. For this reason, the MAI 1 in (3.11) is not suppressed before detection which leads to significant error propagation and severe performance degradation with a high error floor. Alternatively, we propose the novel OSSMIC receiver that can remove this MAI 1 term and avoid the severe degradation in performance. This receiver structure is capable of removing both the spatial and multiuser interference. The three major procedures of this receiver are detailed in the following three sections.

4.1 Spatial Interference Suppression & Cancellation

Without loss of generality, we consider first the n_t-th substream. For ease of presentation, the analysis of OSSMIC receiver with ZF filtering is discussed first and it is extended to the MMSE case later on. Figure 4.1 depicts the block diagram of the novel receiver architecture for the desired user n_u-th user. For ease of presentation, the received signal model in (3.11) is revisited here

$$\mathbf{r}_i = \overbrace{\mathbf{h}_i^{n_t} s_{n_u,i}^{n_t}}^{\text{desired}} + \overbrace{\sum_{n'_t \neq n_t}^{N_t} \mathbf{h}_i^{n'_t} s_{n_u,i}^{n'_t}}^{\text{CAI}} + \overbrace{\sum_{n'_u \neq n_u}^{N_u} \mathbf{h}_i^{n_t} s_{n'_u,i}^{n_t}}^{\text{MAI 1}} + \overbrace{\sum_{n'_u \neq n_u}^{N_u} \sum_{n'_t}^{N_t} \mathbf{h}_i^{n'_t} s_{n'_u,i}^{n'_t}}^{\text{MAI 2}} + \mathbf{n}_i. \tag{4.1}$$

Considering this received signal passing through a linear ZF filter, the estimates of the i-th subcarrier for the n_u-th user's n_t-th substream can be expressed as

$$y_{n_u,i}^{n_t} = \left[\mathbf{H}_i^{+}\right]_{n_t} \mathbf{r}_i = \left[\mathbf{H}_i^{+}\right]_{n_t} \mathbf{H}_i \mathbf{x}_i + \left[\mathbf{H}_i^{+}\right]_{n_t} \mathbf{n}_i = s_{n_u,i}^{n_t} + \sum_{n'_u \neq n_u}^{N_u} s_{n'_u,i}^{n_t} + \tilde{n}_i \tag{4.2}$$

where $[\mathbf{A}]_n$ denotes the n-th row of matrix $\mathbf{A}$. The p-th symbol decision statistic is obtained when the chip estimates in (4.2) are despread by the desired user's spreading sequence represented by

$$\begin{aligned} z_{n_u,p}^{n_t} &= \sum_{g=1}^{G} c_{n_u,g} y_{n_u,i(p,g)}^{n_t} = \sum_{g=1}^{G} c_{n_u,g} s_{n_u,i(p,g)}^{n_t} + \sum_{n'_u \neq n_u}^{N_u} \sum_{g=1}^{G} c_{n_u,g} s_{n'_u,i(p,g)}^{n_t} \\ &+ \sum_{g=1}^{G} c_{n_u,g} \tilde{n}_{i(p,g)} = d_{n_u,p}^{n_t} + \eta_{n_u,p}. \end{aligned} \tag{4.3}$$

where $\eta_{n_u,p} = \sum_{g=1}^{G} c_{n_u,g} \tilde{n}_{i(p,g)}$. As the spatial & multiple access interferences (CAI, MAI1 & MAI2) are removed, detection is then performed to obtain the symbol estimate $\hat{d}_{n_u,p}^{n_t}$.

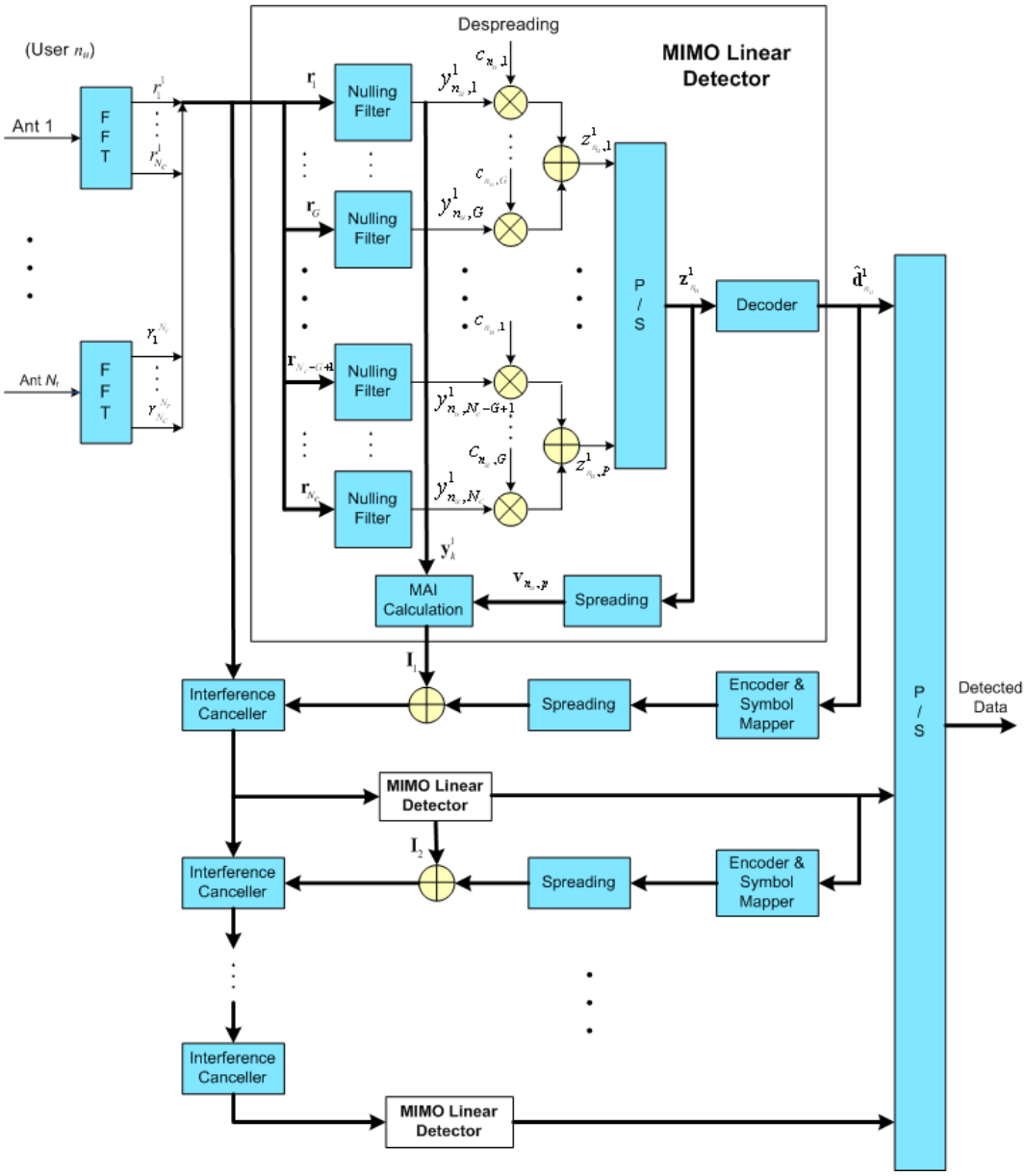

Figure 4.1: Block diagram of OSSMIC receiver for downlink MIMO MC-CDMA.

The next step in the conventional OSIC receiver, is to remove the contribution of the n_t-th detected substream (i.e. the "desired" term in (4.1)) from the received signal. Then, the modified channel matrix is formed by setting the detected substream's channel response to zero, i.e. the n_t-th column of $\mathbf{H}_i$ is zeroed [9]. This modified channel matrix is used to compute the nulling filter for

the subsequent stage. However, the multiuser interference from this n_t-th transmit antenna (i.e MAI 1 in (4.1)) is not removed from the received signal and it will not be suppressed by the subsequent nulling processes. For this reason, error propagation is produced and it significantly deteriorates the system performance. Therefore, the MAI 1 term must be eliminated from the received signal. The proposed OSSMIC receiver removes this interference term with only the knowledge of the desired user's spreading sequence as explained next.

4.2 Multiple Access Interference Calculation & Cancellation

For downlink communications, receivers are usually assumed to know only the desired user's spreading sequence and not all the other users' sequences. Thus, without knowing the spreading sequence of other users, it is difficult to perfectly remove the MAI 1 term in (4.1). Nonetheless, we propose a novel approach that can perfectly compute this MAI term at the expense of noise enhancement.

First, the symbol decision statistic $z^{n_t}_{n_u,p}$ in (4.3) is respread with the desired user's spreading sequence to obtain

$$\mathbf{v}^{n_t}_{n_u,p} = \begin{bmatrix} v^{n_t}_{n_u,i(p,1)} & v^{n_t}_{n_u,i(p,2)} & \cdots & v^{n_t}_{n_u,i(p,G)} \end{bmatrix}^T = \mathbf{c}_{n_u} z^{n_t}_{n_u,p} \in \mathbb{C}^{G\times 1}. \tag{4.4}$$

The respread signal at the i-th subcarrier $v^{n_t}_{n_u,i}$ (where i relates to p and g according to (2.15)) contains the desired user's signal $s^{n_t}_{n_u,i}$ and the modified noise term $c_{n_u,g(i)}\eta_{n_u,p(i)}$. The respread signal is then subtracted from the chip estimate $y^{n_t}_{n_u,i}$ in (4.2) so as to obtain the signal contribution in the MAI 1 term and a second

term which contains the enhanced noise as shown by

$$I_{n_u,i} = y^{n_t}_{n_u,i} - v^{n_t}_{n_u,i} = \sum_{n'_u \neq n_u}^{N_u} s^{n_t}_{n'_u,i} + \left(\tilde{n}_i - c_{n_u,g(i)}\eta_{n_u,p(i)}\right). \tag{4.5}$$

The whole cancellation procedure for the n_t-th substream from the received signal at the i-th subcarrier can be characterized by

$$\mathbf{r}'_i = \mathbf{r}_i - \mathbf{h}^{n_t}_i \left(c_{n_u,g(i)}\hat{d}^{n_t}_{n_u,p(i)} + I_{n_u,i}\right) \tag{4.6}$$

where $\mathbf{r}'_i$ is the modified received signal containing the CAI, MAI 2 and noise terms for the next detection layer. The above stated steps are repeated until all the remaining substreams are detected.

To ease the derivation of error bound for chip level MIMO MC-CDMA in Chapter 5, the above derivation is extended to use the MMSE filter. Hence, the MMSE filtered received signal is presented as

$$\begin{aligned} y^{n_t}_{n_u,i} &= \left[\mathbf{H}^{MMSE}_i\right]_{n_t}\mathbf{r}_i = \overbrace{\left[\mathbf{H}^{MMSE}_i\right]_{n_t}\mathbf{h}^{n_t}_i s^{n_t}_{n_u,i}}^{\text{desired}} + \overbrace{\sum_{n'_t \neq n_t}^{N_t}\left[\mathbf{H}^{MMSE}_i\right]_{n_t}\mathbf{h}^{n'_t}_i s^{n'_t}_{n_u,i}}^{\text{CAI}} \\ &+ \overbrace{\sum_{n'_u \neq n_u}^{N_u}\left[\mathbf{H}^{MMSE}_i\right]_{n_t}\mathbf{h}^{n_t}_i s^{n_t}_{n'_u,i}}^{\text{MAI 1}} + \overbrace{\sum_{n'_u \neq n_u}^{N_u}\sum_{n'_t \neq n_t}^{N_t}\left[\mathbf{H}^{MMSE}_i\right]_{n_t}\mathbf{h}^{n'_t}_i s^{n'_t}_{n'_u,i}}^{\text{MAI 2}} \\ &+ \left[\mathbf{H}^{MMSE}_i\right]_{n_t}\mathbf{n}_i \end{aligned} \tag{4.7}$$

where the MMSE spatial suppression matrix at the i-th subcarrier is $\mathbf{H}^{MMSE}_i = [\mathbf{H}^H_i\mathbf{H}_i + (G/K)\sigma^2_n\mathbf{I}_{N_t}]^{-1}\mathbf{H}^H_i$. It must be noted that when the MMSE filter is used, the interference calculated in (4.5) (i.e. $I_{n_u,i}$) contains not only the MAI 1 and the noise terms, but also some form of residual CAI and MAI. This happens because when the received signal is filtered using MMSE, the CAI and MAI 2 in

(4.1) are not completely removed.

Despite the presence of residual interference, the additional noise and interference power after (4.6) can be included to the MMSE filter for the next detection stage. From (4.5) and (4.6) the additional noise is given by

$$\widehat{n}_i = \mathbf{h}_i^{n_t} \left(\tilde{n}_i - c_{n_u,g(i)} \eta_{n_u,p(i)} \right) \tag{4.8}$$

and its variance is derived as follows,

$$\begin{aligned} \sigma^2_{\widehat{n}_i} &= E\left[\left\| \mathbf{h}_i^{n_t} \left(\tilde{n}_i - c_{n_u,g(i)} \eta_{n_u,p(i)} \right) \right\|^2 \right] \\ &= \|\mathbf{h}_i^{n_t}\|_F^2 \, E\left[\underbrace{\|\tilde{n}_i\|^2}_{\Phi} + \underbrace{\left\| c_{n_u,g(i)} \eta_{n_u,p(i)} \right\|^2}_{\Xi} - \underbrace{2\tilde{n}_i c_{n_u,g(i)} \eta^*_{n_u,p(i)}}_{\Psi} \right] \end{aligned} \tag{4.9}$$

where $\tilde{n}_i = \left[\mathbf{H}_i^{MMSE} \right]_{n_t} \mathbf{n}_i$, $E[.]$ refers to the expectation operator and $\|.\|_F^2$ denotes the Frobenious norm. The conditional expectations of the three terms in (4.9) are evaluated independently as

$$E[\Phi] = N_0 \left\| \left[\mathbf{H}_i^{MMSE} \right]_{n_t} \right\|_F^2 \tag{4.10}$$

$$\begin{aligned} E[\Xi] &= E\left[\left\| c_{n_u,g(i)} \left(c_{n_u,1} \tilde{n}_{i(p(i),1)} + ... + c_{n_u,G} \tilde{n}_{i(p(i),G)} \right) \right\|^2 \right] \\ &= E\left[c^2_{n_u,g(i)} \sum_{g=1}^{G} c^2_{n_u,g} \tilde{n}_{i(p(i),g)} \tilde{n}^*_{i(p(i),g)} \right] \\ &= \frac{N_0}{G^2} \sum_{g=1}^{G} \left\| \left[\mathbf{H}^{MMSE}_{i(p(i),g)} \right]_{n_t} \right\|_F^2 \end{aligned} \tag{4.11}$$

$$\begin{aligned} E\left[\Psi\right] &= E\left[2\tilde{n}_i c_{n_u,g(i)}\left(c_{n_u,1}\tilde{n}^*_{i(p(i),1)} + ... + c_{n_u,G}\tilde{n}^*_{i(p(i),G)}\right)\right] \\ &= E\left[2c_{n_u,g(i)}c_{n_u,g(i)}\tilde{n}_i\tilde{n}^*_i\right] = \frac{2N_0}{G}\left\|\left[\mathbf{H}_i^{MMSE}\right]_{n_t}\right\|_F^2. \end{aligned} \tag{4.12}$$

where $c_i^2 = \frac{1}{G}$ and

$$E\left[\tilde{n}_i\tilde{n}^*_j\right] = \begin{cases} N_0, & \text{if} \quad i = j, \\ 0, & \text{if} \quad i \neq j \end{cases} \tag{4.13}$$

assuming $\tilde{n}_i$ and $\tilde{n}_j$ are independent and the AWGN noise term has zero mean and N_0 power spectral density. By substituting (4.10), (4.11) and (4.12) in (4.9), the variance of the enhanced noise is simplified to

$$\sigma^2_{\widehat{n}_i} = N_0\left\|\mathbf{h}_i^{n_t}\right\|_F^2\left(\left\|\left[\mathbf{H}_i^{MMSE}\right]_{n_t}\right\|_F^2\left(1 - \frac{2}{G}\right) + \frac{1}{G^2}\sum_{g=1}^{G}\left\|\left[\mathbf{H}_{i(p(i),g)}^{MMSE}\right]_{n_t}\right\|_F^2\right). \tag{4.14}$$

Hence the new MMSE filter for the next detection stage can be computed by

$$\widehat{\mathbf{H}}_i^{MMSE} = \left[\overline{\mathbf{H}}_i^H\overline{\mathbf{H}}_i + (G/K)\left(\mathbf{I}_{N_t}\sigma_n^2 + \mathbf{I}_{N_t}\sigma^2_{\widehat{n}_i}\right)\right]^{-1}\overline{\mathbf{H}}_i^H \tag{4.15}$$

where $\overline{\mathbf{H}}_i$ represents the modified channel matrix where the detected substream's channel response is set to zero.

4.3 OSSMIC with all users' spreading sequences

The OSSMIC receiver is also investigated when all the other users' spreading sequences are available at the desired user receiver. This approach is also used in [26] and [25]. Although knowing all the other users' spreading sequences increases the computational complexity of the system as shown in Section 4.5, it helps to remove the MAI 1 term without noise enhancement. This improves the system

performance as shown in Section 4.6. The symbol decision statistics for each user form the decision statistic vector

$$\mathbf{z}_p^{n_t} = \left[\begin{array}{cccc} z_{1,p}^{n_t} & z_{2,p}^{n_t} & \cdots & z_{N_u,p}^{n_t} \end{array} \right] \in \mathbb{C}^{1\times N_u}. \tag{4.16}$$

The *p-th* symbol detection for the n_t*-th* substream for all the users is then performed to obtain the detected symbol vector

$$\hat{\mathbf{d}}_p^{n_t} = \left[\begin{array}{cccc} \hat{d}_{1,p}^{n_t} & \hat{d}_{2,p}^{n_t} & \cdots & \hat{d}_{N_u,p}^{n_t} \end{array} \right] \in \mathbb{C}^{1\times N_u}. \tag{4.17}$$

The cancellation procedure for the n_t*-th* substream from the received signal at the *i-th* subcarrier can then characterized by

$$\mathbf{r}_i' = \mathbf{r}_i - \mathbf{h}_i^{n_t} \sum_{n_u=1}^{N_u} c_{n_u,g} \hat{d}_{n_u,p}^{n_t}. \tag{4.18}$$

The same procedure is followed until all the remaining substreams are detected. It must be noted that if the other users' detected symbols are in error, the MAI 1 term cannot be perfectly computed. However without the noise enhancement in (4.5) and if all other users' spreading sequences are known, the performance of OSSMIC can be improved as it will be shown in Section 4.6.

4.4 Detection Ordering

The optimal detection order for the novel OSSMIC receiver is determined according to the substream which produces the smallest total mean square error (MSE). The MSE matrix for the MMSE receiver with respect to the *i-th*

subcarrier is given by

$$\mathbf{J}_i = \begin{bmatrix} \mathbf{J}_i(1) & \mathbf{J}_i(2) & \cdots & \mathbf{J}_i(N_t) \end{bmatrix}^T = \text{diag}\left(\mathbf{H}_i^H \mathbf{H}_i + \mathbf{R}_{xx}^{-1} N_0 \mathbf{I}_{N_t}\right)^{-1} \quad (4.19)$$

where $\mathbf{R}_{xx} = E_x(N_u/G)\mathbf{I}_{N_t}$ with E_x being the chip energy. The total MSE of the n_t-th substream is represented by

$$\text{MSE}_{TOTAL}(n_t) = \sum_{i=1}^{N_s} \mathbf{J}_i(n_t). \quad (4.20)$$

The substream with the smallest total MSE will be detected at that stage.

4.5 Complexity Evaluation

The computational complexity of the proposed chip level OSSMIC and symbol level OSIC receivers are compared in this section. In addition, the complexity of the OSSMIC when all other users' spreading sequences are known is also considered for comparison. The complexity evaluation is based on the total number of additions and multiplications in the receivers. As shown in [2], a $(N_r \times L)$ and $(L \times N_t)$ matrix multiplication requires $N_r L N_t$ additions and $N_r L N_t$ multiplications whereas a $(N_r \times N_r)$ matrix inversion requires ${N_r}^3/6 - {N_r}^2 + N_r/6$ additions, ${N_r}^3/6 - 5N_r/6$ multiplications and ${N_r}^2$ divisions.

Table 4.1 lists the number of linear algebraic operations per frame for each procedure. A practical example to evaluate the number of computations for these systems is discussed in the following section. From Table 4.1, it is evident that the complexity for symbol level OSIC detector is much higher than the complexity of the chip level OSSMIC receiver. This is because in symbol level receiver, the complexity is significantly affected by the channel-spreading matrix inversion which draws a complexity order of $O((N_r G)^3)$. Alternatively in the chip level

MMSE Filtering	
Operations	**Additions**
Symbol level OSIC	$P(5(N_rG)^3/6-(N_rG)^2+13N_rG/6+N_rN_t{}^2GN_u^2+N_tN_r{}^2N_uG^2)$
Chip level OSSMIC	$P(5N_t{}^3G/6-N_t{}^2G+7N_tG/6+N_rG+N_tN_r{}^2G+N_rN_t{}^2G)$
Chip level OSSMIC / all user spr. seq.	$P(5N_t{}^3G/6-N_t{}^2G+7N_tG/6+N_rG+N_tN_r{}^2G+N_rN_t{}^2G)$
Operations	**Multiplications**
Symbol level OSIC	$P(5(N_rG)^3/6+(N_rG)^2+N_rG/6+N_rN_t{}^2GN_u^2+N_tN_r{}^2N_uG^2)$
Chip level OSSMIC	$P(5N_t{}^3G/6+N_t{}^2G-5N_tG/6+N_rG+N_tN_r{}^2G+N_rN_t{}^2G)$
Chip level OSSMIC / all user spr. seq.	$P(5N_t{}^3G/6+N_t{}^2G-5N_tG/6+N_rG+N_tN_r{}^2G+N_rN_t{}^2G)$
Despreading	
Operations	**Additions**
Chip level OSSMIC	PG
Chip level OSSMIC / all user spr. seq.	PN_uG
Operations	**Multiplications**
Chip level OSSMIC	PG
Chip level OSSMIC / all user spr. seq.	PN_uG
Respreading & Interference Calculation	
Operations	**Additions**
Chip level OSSMIC	$2PG$
Operations	**Multiplications**
Chip level OSSMIC	PG
Additional Noise Calculation	
Operations	**Additions**
Chip level OSSMIC	$P(2N_rG+4G)$
Operations	**Multiplications**
Chip level OSSMIC	$P(2N_rG+2G)$
Total number of operations per frame	
Symbol level OSIC	$P(5(N_rG)^3/3+7N_rG/3+2N_rN_t{}^2GN_u^2+2N_tN_r{}^2N_uG^2)$
Chip level OSSMIC	$P(5(N_t)^3G/3+N_tG/3+6N_rG+11G+2N_tN_r{}^2G+2N_rN_t{}^2G)$
Chip level OSSMIC / all user spr. seq.	$P(5(N_t)^3G/3+N_tG/3+2N_rG+2N_uG+2N_tN_r{}^2G+2N_rN_t{}^2G)$

Table 4.1: Computational Complexity for chip and symbol level MIMO MC-CDMA receivers: Total number of operations per frame

OSSMIC receiver, only the channel matrix inversion is required which produces a complexity in the order of $O(G(N_t)^3)$.

The complexity of symbol level OSIC detector is much higher than the chip level OSSMIC receiver therefore, it is not included in the simulation results. Figure 4.2 depicts a practical example for the complexity evaluation of OSSMIC detectors. If all the other users spreading sequences are known, the computational

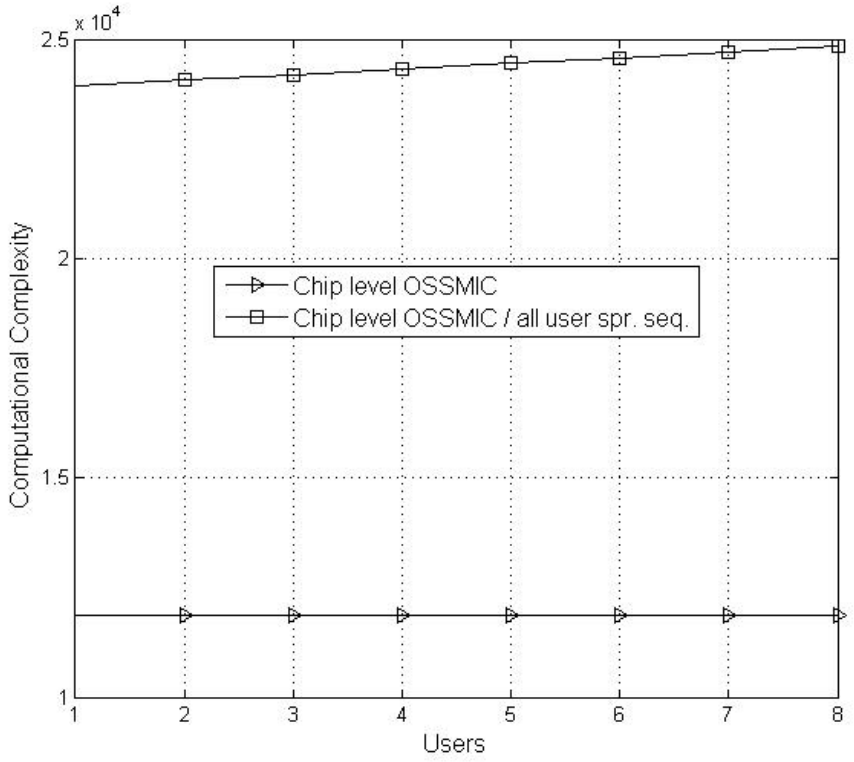

Figure 4.2: Complexity evaluation for chip level MIMO MC-CDMA systems.

complexity of the OSSMIC receiver is doubled for $N_u = 1$. This complexity increases with the increasing number of users. This is because the spreading matrix of all users is used to perform the despreading operation, and hence increases the complexity.

4.6 Simulation Results & Discussions

In this section, the performance of the proposed coded ZF / MMSE OSSMIC receiver with chip level block interleaving for downlink MC-CDMA systems is evaluated through Monte Carlo simulations. Furthermore, the performance of other detectors for MIMO MC-CDMA are evaluated for comparison. As multiple antennas are used for all systems, the word "MIMO" is omitted to ease the

comparative discussion in this chapter. For the simulation results, consider the same system parameters and assumptions as in Section 3.3.1.

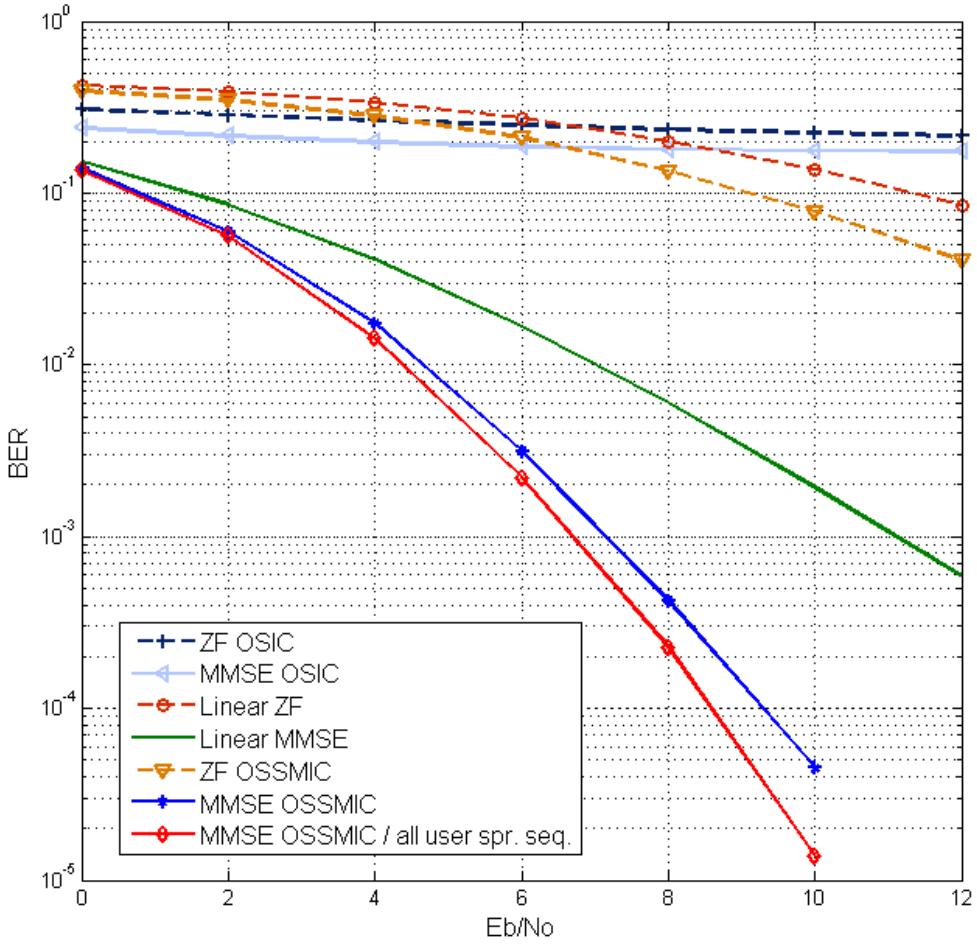

Figure 4.3: BER performance of proposed OSSMIC and linear detectors at half load for downlink MIMO MC-CDMA system.

4.6.1 OSSMIC vs Linear & OSIC detectors

Figures 4.3 and 4.4 demonstrate the BER performance with respect to different E_b/N_0 for the linear chip level ZF and MMSE detectors [2], the chip level OSIC detectors [1] and our proposed ZF and MMSE OSSMIC detectors for the

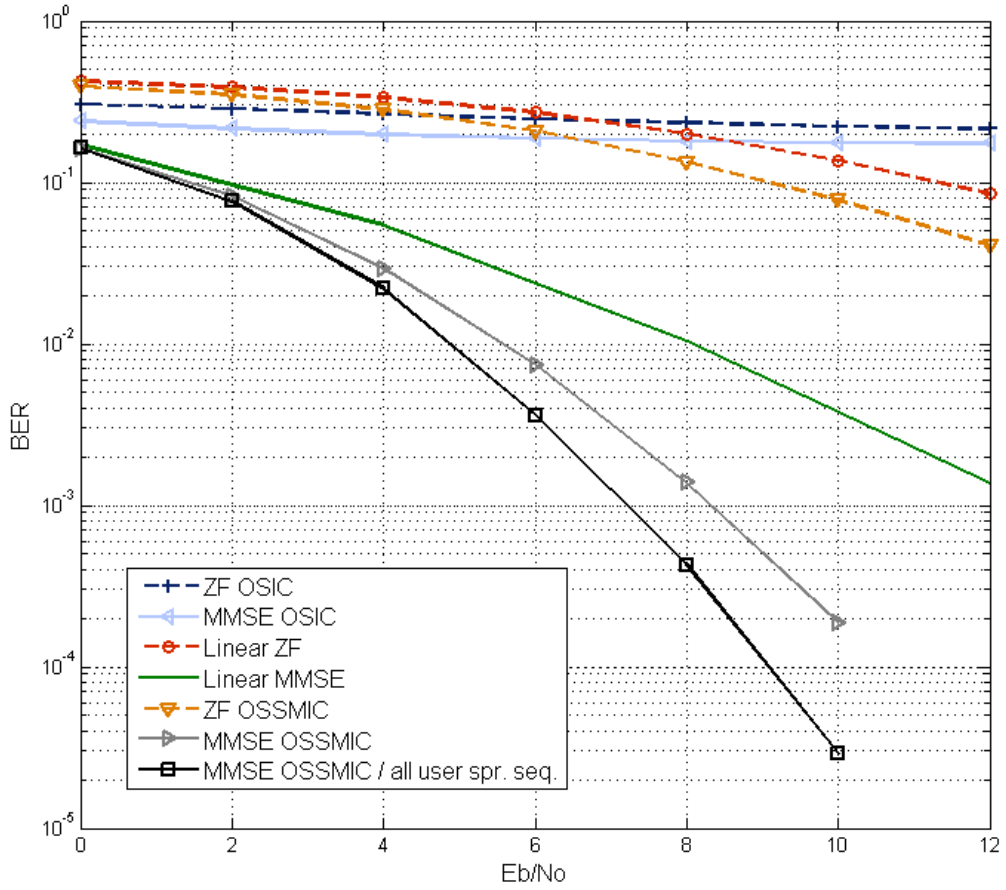

Figure 4.4: BER performance of proposed OSSMIC and linear detectors at full load for downlink MIMO MC-CDMA system.

half loaded four user ($N_u = 4$) case and the full loaded eight user ($N_u = 8$) case. The performance of ZF and MMSE OSIC detectors illustrate significant error floors in the higher SNR region due to MAI and error propagation as discussed in Section 4.2. From our results, it is evident that the proposed OSSMIC receiver overcomes the problem of MAI resulting in a superior performance over the OSIC detectors. Comparing to the linear detectors in half load case, the MMSE OSSMIC detector shows 4.2 dB improvement at BER = 10^{-3} over linear MMSE detector. In addition, if the other users' spreading sequences are known,

the MMSE OSSMIC receiver shows further 0.5 dB improvement at BER = 10^{-4}. It can also be observed that the MMSE OSSMIC significantly outperforms the ZF counterpart. This is because the MMSE filter will not amplify the noise as in ZF filter, and hence a reduced error rate occurs.

In the full load case, the performance improvement by MMSE OSSMIC with all users' spreading sequence knowledge over MMSE OSSMIC is increased to 1.5 dB at BER = 10^{-4}. This is because the noise enhancement in (4.14) increases with the increasing number of users and hence the performance improvement of MMSE OSSMIC is reduced.

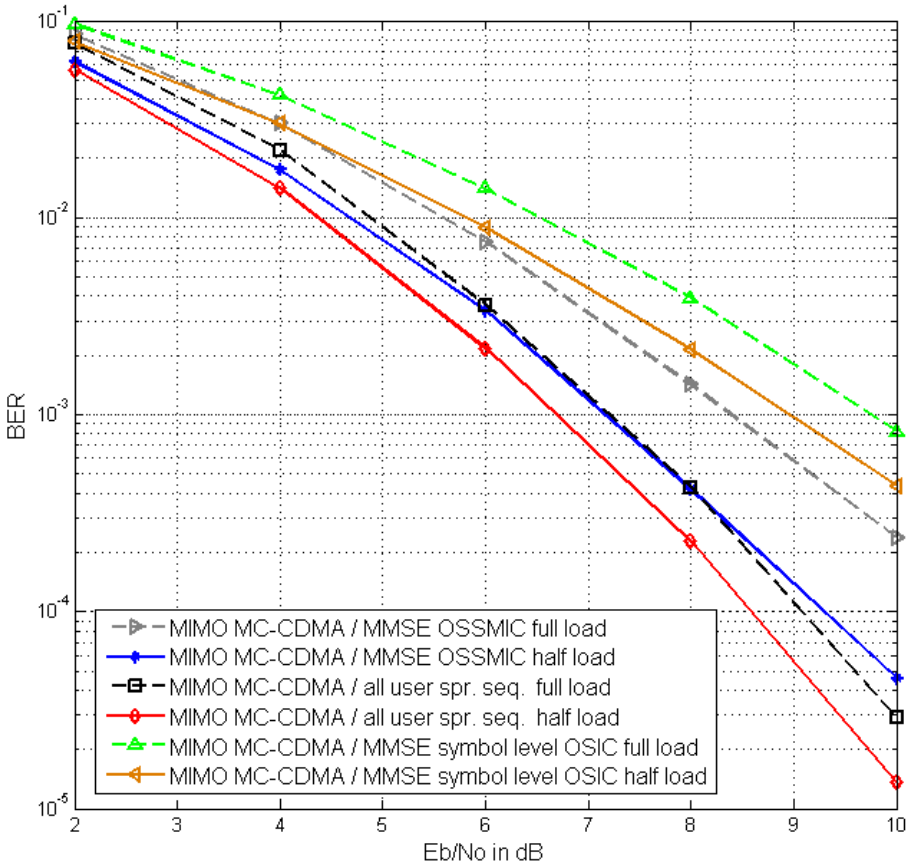

Figure 4.5: BER performance of chip and symbol level MIMO MC-CDMA at half and full load.

4.6.2 Chip vs Symbol level MIMO MC-CDMA

In [25], it is shown that symbol level OSIC detectors perform better than the chip level OSIC detectors. In order to invalidate this perception, the chip level OSSMIC detector is compared with the symbol level OSIC detector in this subsection.

In Figure 4.5 we consider the BER performance for the chip and symbol level MMSE MC-CDMA for the half loaded and the full loaded cases. For half-load case, OSSMIC and symbol level OSIC perform 1.3 dB and 1 dB better respectively than their corresponding full-load cases at BER = 10^{-3}. More importantly, for half-load case, OSSMIC performs 1.8 dB better than the symbol level MMSE MC-CDMA system at the same BER. In addition, if the other users' spreading sequences are known in the OSSMIC detector, OSSMIC achieves a further 1.2 dB improvement for both half and full load cases respectively.

Chapter 5

Performance Analysis & Comparisons

In this chapter, we compare the error rate performance between the proposed MIMO MC-CDMA with OSSMIC receiver, the symbol level MIMO MC-CDMA with OSIC receiver and the MIMO OFDMA system. The performance comparisons between these systems are justified by deriving and analysing their pairwise error probability (PEP).

5.1 Chip level MIMO MC-CDMA with OSSMIC

To formulate the general PEP equation, the codeword $\mathbf{d}$ is being transmitted but the erroneous sequence $\mathbf{e}$ is detected. The PEP conditioned on a fixed set of channel impulse responses can be calculated by [35]

$$P\left(\mathbf{d} \rightarrow \mathbf{e}|\mathbf{h}\right) = Q\left(\sqrt{\frac{d_E^2(\mathbf{d},\mathbf{e})}{2N_0}}\right) \tag{5.1}$$

where $Q(.)$ is the complementary Gaussian cumulative distribution function, $\mathbf{h}$ denotes the channel impulse response vector, N_0 the noise spectral density and $d_E^2(\mathbf{d},\mathbf{e})$ the squared Euclidean distance between codewords $\mathbf{d}$ and $\mathbf{e}$. To derive the error bound for chip level MIMO MC-CDMA, the MMSE filtered received signal in (4.7) is despread and shown to be

$$\begin{aligned} z_{n_u,p}^{n_t} &= \overbrace{\sum_{g=1}^{G} c_{n_u,g} y_{n_u,i(p,g)}^{n_t}}^{\text{desired}} = \overbrace{\sum_{g=1}^{G} c_{n_u,g} \left[\mathbf{H}_{i(p,g)}^{MMSE}\right]_{n_t} \mathbf{h}_{i(p,g)}^{n_t} s_{n_u,i(p,g)}^{n_t}} \\ &+ \overbrace{\sum_{n_t' \neq n_t}^{N_t} \sum_{g=1}^{G} c_{n_u,g} \left[\mathbf{H}_{i(p,g)}^{MMSE}\right]_{n_t} \mathbf{h}_{i(p,g)}^{n_t'} s_{n_u,i(p,g)}^{n_t'}}^{\text{CAI}} \\ &+ \overbrace{\sum_{n_u' \neq n_u}^{N_u} \sum_{g=1}^{G} c_{n_u,g} \left[\mathbf{H}_{i(p,g)}^{MMSE}\right]_{n_t} \mathbf{h}_{i(p,g)}^{n_t} s_{n_u',i(p,g)}^{n_t}}^{\text{MAI 1}} \\ &+ \overbrace{\sum_{n_u' \neq n_u}^{N_u} \sum_{n_t' \neq n_t}^{N_t} \sum_{g=1}^{G} c_{n_u,g} \left[\mathbf{H}_{i(p,g)}^{MMSE}\right]_{n_t} \mathbf{h}_{i(p,g)}^{n_t'} s_{n_u',i(p,g)}^{n_t'}}^{\text{MAI 2}} \\ &+ \sum_{g=1}^{G} c_{n_u,g} \left[\mathbf{H}_{i(p,g)}^{MMSE}\right]_{n_t} \mathbf{n}_{i(p,g)}. \end{aligned} \tag{5.2}$$

According to (5.2), the conditional variance on the channel for the Gaussian noise term is derived as follows

$$\begin{aligned} \sigma_{\tilde{n},p}^2 &= E\left[\left|\sum_{g=1}^{G} c_{n_u,g} \left[\mathbf{H}_{i(p,g)}^{MMSE}\right]_{n_t} \mathbf{n}_{i(p,g)}\right|^2\right] \\ &= \frac{N_0}{G} \sum_{g=1}^{G} \left\| \left[\mathbf{H}_{i(p,g)}^{MMSE}\right]_{n_t} \right\|_F^2 \end{aligned} \tag{5.3}$$

The conditional variance on the channel for the additional noise term (4.14) after MMSE filtering and despreading is given by

$$\begin{aligned}\sigma^2_{\overline{n},p} &= \frac{N_0}{G}\sum_{g=1}^{G}\left[\left\|\left[\widehat{\mathbf{H}}^{MMSE}_{i(p,g)}\right]_{n_t}\mathbf{h}^{n_t}_{i(p,g)}\right\|^2_F\right. \\ &\times \left.\left(\left\|\left[\mathbf{H}^{MMSE}_{i(p,g)}\right]_{n_t}\right\|^2_F\left(1-\frac{2}{G}\right)+\frac{1}{G^2}\sum_{g'=1}^{G}\left\|\left[\mathbf{H}^{MMSE}_{i(p,g')}\right]_{n_t}\right\|^2_F\right)\right]. \quad (5.4)\end{aligned}$$

In a similar way as with (5.3), the conditional variances on the channel for the CAI and the multiuser MAI 1 and MAI 2 in (5.2) can be approximated by the Gaussian random variables respectively as

$$\begin{aligned}\sigma^2_{CAI,p} &= E\left[\left|\sum_{n'_t\neq n_t}^{N_t}\sum_{g=1}^{G}c_{n_u,g}\left[\mathbf{H}^{MMSE}_{i(p,g)}\right]_{n_t}\mathbf{h}^{n'_t}_{i(p,g)}c_{n_u,g}d^{n'_t}_{n_u,p}\right|^2\right] \\ &= \frac{E_bR_c}{G^2}\sum_{n'_t\neq n_t}^{N_t}\left[\sum_{g=1}^{G}\left[\mathbf{H}^{MMSE}_{i(p,g)}\right]_{n_t}\mathbf{h}^{n'_t}_{i(p,g)}\right]^2 \quad (5.5)\end{aligned}$$

$$\begin{aligned}\sigma^2_{MAI1,p} &= E\left[\left|\sum_{n'_u\neq n_u}^{N_u}\sum_{g=1}^{G}c_{n_u,g}\left[\mathbf{H}^{MMSE}_{i(p,g)}\right]_{n_t}\mathbf{h}^{n_t}_{i(p,g)}c_{n'_u,g}d^{n_t}_{n'_u,p}\right|^2\right] \\ &= E_bR_c\sum_{n'_u\neq n_u}^{N_u}\left[\sum_{g=1}^{G}\left[\mathbf{H}^{MMSE}_{i(p,g)}\right]_{n_t}\mathbf{h}^{n_t}_{i(p,g)}c_{n'_u,g}c_{n_u,g}\right]^2 \quad (5.6)\end{aligned}$$

$$\begin{aligned}\sigma^2_{MAI2,p} &= E\left[\left|\sum_{n'_u\neq n_u}^{N_u}\sum_{n'_t\neq n_t}^{N_t}\sum_{g=1}^{G}c_{n_u,g}\left[\mathbf{H}^{MMSE}_{i(p,g)}\right]_{n_t}\mathbf{h}^{n'_t}_{i(p,g)}c_{n'_u,g}d^{n'_t}_{n'_u,p}\right|^2\right] \\ &= E_bR_c\sum_{n'_u\neq n_u}^{N_u}\sum_{n'_t\neq n_t}^{N_t}\left[\sum_{g=1}^{G}\left[\mathbf{H}^{MMSE}_{i(p,g)}\right]_{n_t}\mathbf{h}^{n'_t}_{i(p,g)}c_{n'_u,g}c_{n_u,g}\right]^2 \quad (5.7)\end{aligned}$$

where E_b refers to the bit energy and R_c denotes the ECC rate. Without loss of generality we assume that the first d_H (Hamming distance) symbols are in error which relates to the channel subcarriers $i \in \{1, \ldots, d_H\}$. Under this assumption, the squared Euclidean distance between two QPSK modulated and convolutionally encoded codewords separated by d_H can be represented as

$$\begin{aligned} d_E^2 &= \sum_{p=1}^{d_H} \left[\sum_{g=1}^{G} c_{n_u,g} \left[\mathbf{H}_{i(p,g)}^{MMSE} \right]_{n_t} \mathbf{h}_{i(p,g)}^{n_t} c_{n_u,g} \right]^2 \left| d_{n_u,p}^{n_t} - \tilde{d}_{n_u,p}^{n_t} \right|^2 \\ &= \frac{4E_b R_c}{G^2} \sum_{p=1}^{d_H} \left[\sum_{g=1}^{G} \left[\mathbf{H}_{i(p,g)}^{MMSE} \right]_{n_t} \mathbf{h}_{i(p,g)}^{n_t} \right]^2 \end{aligned} \tag{5.8}$$

where $\tilde{d}_{n_u,p}^{n_t}$ denotes the erroneous detected symbol. By substituting (5.8) into (5.1) and including (5.4)−(5.7), the average PEP of MIMO MC-CDMA with OSSMIC for the n_t-th substream under no error propagation is defined as

$$P\left(\mathbf{d} \rightarrow \mathbf{e}\right) = E\left[Q\left(\sqrt{ 2E_b R_c \sum_{p=1}^{d_H} \frac{\frac{1}{G^2} \left[\sum_{g=1}^{G} \left[\mathbf{H}_{i(p,g)}^{MMSE} \right]_{n_t} \mathbf{h}_{i(p,g)}^{n_t} \right]^2}{\left(\sigma_{\tilde{n},p}^2 + \sigma_{\overline{n},p}^2 + \sigma_{CAI,p}^2 + \sigma_{MAI1,p}^2 + \sigma_{MAI2,p}^2 \right)} } \right) \right] \tag{5.9}$$

where $E\left[.\right]$ refers to the expectation operator over the channel gains. The lower bound of (5.9) can be calculated by replacing d_H with the minimum Hamming distance $d_{H_{min}}$ of the ECC. It must be said that the closed form solution of (5.9) is not derived because it's very difficult to derive the probability distribution for $\left[\mathbf{H}_{i(p,g)}^{MMSE} \right]_{n_t}$. For this reason simulation results in Section 5.4 evaluate the PEP performance. The PEP analysis based on MMSE filtering can be easily extended to the ZF case when $\mathbf{H}_{i(p,g)}^{MMSE}$ is replaced by $\mathbf{H}_{i(p,g)}^{+}$. In the ZF case, the interference terms in equations (5.5), (5.6) and (5.7) become zero and $d_E^2 = 4E_b R_c$. Hence

the argument of the Q function in (5.9) becomes

$$\sqrt{\sum_{p=1}^{d_H} \frac{2E_bR_c}{\left(\sigma_{\tilde{n},p}^2 + \sigma_{\bar{n},p}^2\right)}} = \sqrt{\sum_{p=1}^{d_H} \frac{2E_bR_c}{N_0\left(\frac{1}{G}\sum_{g=1}^{G}\left\|\left[\mathbf{H}_{i(p,g)}^{+}\right]_{n_t}\right\|_F^2 + \frac{\sigma_{\bar{n},p}^2}{N_0}\right)}}. \tag{5.10}$$

If the other users' spreading sequences are known at the receiver, then the MAI 1 term can be eliminated without noise amplification. Assuming perfect detection on the other users' signal, the average PEP of MIMO MC-CDMA with OSSMIC for the n_t-th substream is simplified to

$$P\left(\mathbf{d} \rightarrow \mathbf{e}\right) = E\left[Q\left(\sqrt{2E_bR_c\sum_{p=1}^{d_H}\frac{\frac{1}{G^2}\left[\sum_{g=1}^{G}\left[\mathbf{H}_{i(p,g)}^{MMSE}\right]_{n_t}\mathbf{h}_{i(p,g)}^{n_t}\right]^2}{\left(\sigma_{\tilde{n},p}^2 + \sigma_{CAI,p}^2 + \sigma_{MAI2,p}^2\right)}}\right)\right]. \tag{5.11}$$

Similarly, the PEP analysis with ZF filtering can be formed when not only (5.5), (5.6) and (5.7) but also (5.4) become zero and hence the argument of the Q function in (5.11) becomes

$$\sqrt{\sum_{p=1}^{d_H} \frac{2E_bR_c}{\frac{N_0}{G}\sum_{g=1}^{G}\left\|\left[\mathbf{H}_{i(p,g)}^{+}\right]_{n_t}\right\|_F^2}}. \tag{5.12}$$

5.2 Symbol level MIMO MC-CDMA with OSIC

In order to justify the use of chip level detection for OSSMIC, comparison is made to the symbol level MMSE with SIC detector [2]. For fairer comparison, the PEP analysis of a modified symbol level detector with OSIC based on the detection ordering in Section 4.3 is presented here.

5.2.1 PEP bound for symbol level MIMO MC-CDMA

Following a similar procedure as for chip level MIMO MC-CDMA, the PEP for the symbol level MIMO MC-CDMA based on (3.21) is formed as

$$P\left(\mathbf{d}\rightarrow\mathbf{e}\right)=E\left[Q\left(\sqrt{2E_bR_c\sum_{p=1}^{d_H}\frac{\left(\left[\mathbf{W}_p^{MMSE}\right]_{n_t}\mathbf{w}_{n_u,p}^{n_t}\right)^2}{\left(\sigma_{\tilde{n},p}^2+\sigma_{CAI,p}^2+\sigma_{MAI1,p}^2+\sigma_{MAI2,p}^2\right)}}\right)\right] \tag{5.13}$$

where the conditional variance for the Gaussian noise, the CAI and the multiuser interference are represented respectively by

$$\sigma_{\tilde{n},p}^2=N_0\left\|\left[\mathbf{W}_p^{MMSE}\right]_{n_t}\right\|_F^2 \tag{5.14}$$

$$\sigma_{CAI,p}^2=E_bR_c\sum_{n_t'\neq n_t}^{N_t}\left(\left[\mathbf{W}_p^{MMSE}\right]_{n_t}\mathbf{w}_{n_u,p}^{n_t'}\right)^2 \tag{5.15}$$

$$\sigma_{MAI1,p}^2=E_bR_c\sum_{n_u'\neq n_u}^{N_u}\left(\left[\mathbf{W}_p^{MMSE}\right]_{n_t}\mathbf{w}_{n_u',p}^{n_t}\right)^2 \tag{5.16}$$

$$\sigma_{MAI2,p}^2=E_bR_c\sum_{n_u'\neq n_u}^{N_u}\sum_{n_t'\neq n_t}^{N_t}\left(\left[\mathbf{W}_p^{MMSE}\right]_{n_t}\mathbf{w}_{n_u',p}^{n_t'}\right)^2 \tag{5.17}$$

and the squared Euclidean distance between two codewords separated by d_H is denoted as

$$d_E^2=4E_bR_c\sum_{p=1}^{d_H}\left(\left[\mathbf{W}_p^{MMSE}\right]_{n_t}\mathbf{w}_{n_u,p}^{n_t}\right)^2. \tag{5.18}$$

To extend the PEP analysis with MMSE filtering into the ZF case, $\mathbf{W}_p^{MMSE}$ has to be replaced by $\mathbf{W}_p^{+}$. In the ZF case (5.15), (5.16) and (5.17) become zero and hence the argument of the Q function in (5.13) becomes

$$\sqrt{\sum_{p=1}^{d_H}\frac{2E_bR_c}{N_0\left\|\left[\mathbf{W}_p^{+}\right]_{n_t}\right\|_F^2}}. \tag{5.19}$$

5.3 MIMO OFDMA

Due to the lack of proper receiver structure for downlink chip level MIMO MC-CDMA, its error rate performance comparison with MIMO OFDMA has not clearly been conducted yet in existing literature. With our proposed OSSMIC receiver, a fair error rate performance comparison can be accomplished. In this section we first present the system model of MIMO OFDMA with OSIC detection and then we derive the PEP equation. Similar to the previous derivations, a non-interleaved system is considered. However, in practice interleaving should be used in order to improve performance.

5.3.1 System Model

The downlink MIMO OFDMA system with N_u users is considered. It has to be noted that the transmitter of MIMO OFDMA is similar to the SISO OFDMA case presented in Section 2.2.4. The information data are grouped into N_t substreams and then each substream is convolutionally encoded and QPSK modulated to P symbols. The received signal at the i-th subcarrier, after the FFT operation can be written as

$$\mathbf{r}_i = \overbrace{\mathbf{h}_i^{n_t} d_i^{n_t}}^{\text{desired}} + \overbrace{\sum_{n_t' \neq n_t}^{N_t} \mathbf{h}_i^{n_t'} d_i^{n_t'}}^{\text{CAI}} + \mathbf{n}_i. \tag{5.20}$$

Considering the received signal passing through a linear MMSE filter, the estimate for the n_t-th substream at the i-th subcarrier is expressed as

$$y_i^{n_t} = \overbrace{\left[\mathbf{H}_i^{MMSE}\right]_{n_t} \mathbf{h}_i^{n_t} d_i^{n_t}}^{\text{desired}} + \overbrace{\sum_{n_t' \neq n_t}^{N_t} \left[\mathbf{H}_i^{MMSE}\right]_{n_t} \mathbf{h}_i^{n_t'} d_i^{n_t'}}^{\text{CAI}} + \left[\mathbf{H}_i^{MMSE}\right]_{n_t} \mathbf{n}_i. \tag{5.21}$$

Symbol detection is then performed to obtain $\hat{d}_i^{n_t}$. The cancellation procedure

can be characterised by

$$\mathbf{r}_i' = \mathbf{r}_i - \left(\mathbf{h}_i^{n_t} \hat{d}_i^{n_t}\right) \tag{5.22}$$

where the modified received signal contains the undetected substreams and noise for the next detection layer. The above stated steps are repeated in order to detect all the remaining substreams.

5.3.2 PEP bound for MIMO OFDMA

The PEP for MIMO OFDMA can be derived in a similar way as for MIMO MC-CDMA. Considering the detector output for MIMO OFDMA at the *i-th* subcarrier in (5.21), the conditional variance for the Gaussian noise and the CAI term are represented respectively by

$$\sigma_{\tilde{n},i}^2 = N_0 \left\| \left[\mathbf{H}_i^{MMSE}\right]_{n_t} \right\|_F^2 \tag{5.23}$$

$$\sigma_{CAI,i}^2 = E_b R_c \sum_{n_t' \neq n_t}^{N_t} \left(\left[\mathbf{H}_i^{MMSE}\right]_{n_t} \mathbf{h}_i^{n_t'} \right)^2 . \tag{5.24}$$

The squared Euclidean distance between two codewords separated by Hamming distance d_H can be represented as

$$d_E^2 = 4 E_b R_c \sum_{i=1}^{d_H} \left(\left[\mathbf{H}_i^{MMSE}\right]_{n_t} \mathbf{h}_i^{n_t} \right)^2 . \tag{5.25}$$

The average PEP of MIMO OFDMA can be obtained by substituting (5.25) into (5.1) and including (5.23) and (5.24) as

$$P\left(\mathbf{d} \rightarrow \mathbf{e}\right) = E\left[Q\left(\sqrt{2 E_b R_c \sum_{i=1}^{d_H} \frac{\left(\left[\mathbf{H}_i^{MMSE}\right]_{n_t} \mathbf{h}_i^{n_t} \right)^2}{\left(\sigma_{\tilde{n},i}^2 + \sigma_{CAI,i}^2\right)}} \right) \right]. \tag{5.26}$$

Following a similar approach to the MIMO MC-CDMA system, the PEP analysis for MMSE MIMO OFDMA can be extended to the ZF case where (5.24) becomes zero and the argument of the Q function in (5.26) is given by

$$\sqrt{\sum_{i=1}^{d_H} \frac{2E_b R_c}{N_0 \left\| \left[\mathbf{H}_i^{+}\right]_{n_t} \right\|_F^2}}. \tag{5.27}$$

5.4 Simulation Results & Discussions

In this section, the FER and PEP performance of the proposed chip level MMSE OSSMIC and the symbol level MMSE OSIC receiver are compared through Monte Carlo simulations. Next we compare the BER, FER and PEP performance of the chip level MMSE MC-CDMA system with OSSMIC receiver and the MMSE OFDMA system with OSIC receiver. Finally, the BER performance of different systems is evaluated with respect to different number of users. Because of the use of multiple antennas by all the systems, the word "MIMO" is omitted to ease the comparative discussion in this section.

5.4.1 Chip vs Symbol level MIMO MC-CDMA

The simulated FER and PEP performance of the previous systems with eight users (full-load) are presented in Figure 5.1. It can be noted that the asymptotic slope for FER and PEP results is similar. The results show that both MMSE OFDMA and MMSE OSSMIC receivers outperform the symbol level MMSE OSIC receiver. Since the size of $\left[\mathbf{W}_p^{MMSE}\right]_{n_t}$ is much larger than the size of the MMSE filter matrix for OFDMA and chip level MC-CDMA, the noise and interference terms in (5.13) are larger and hence the system performance is

worst. Therefore, this supports the use of chip level detection for MIMO MC-CDMA over symbol level detection.

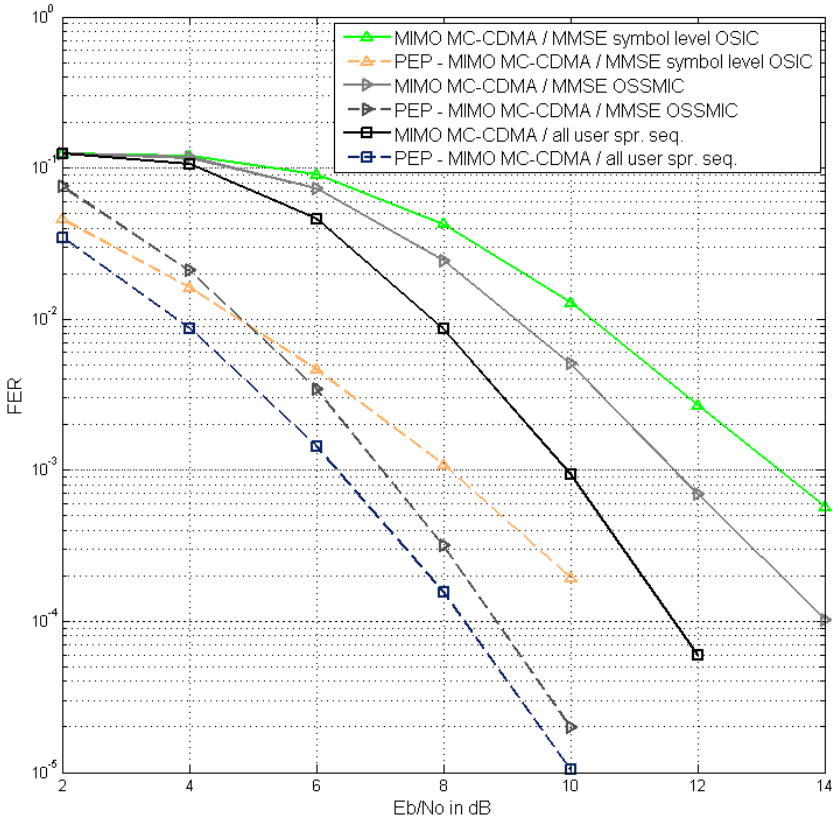

Figure 5.1: FER and PEP performance of chip and symbol level MIMO MC-CDMA at full load.

5.4.2 MIMO MC-CDMA vs MIMO OFDMA

Following the same system parameters for MIMO MC-CDMA as in Section 4.6, the number of chips in an encoded frame for MC-CDMA and the number of symbols per frame for OFDMA is 128. The size of the FFT is considered to be the same as the number of subcarriers, and is thus $N_s = 128$. The block interleaver has a size of $P \times K$ for OFDMA and $G \times P$ for MC-CDMA.

In Figure 5.2 we consider the BER performance for the chip level MC-CDMA and OFDMA systems for the half loaded and full loaded case. The results show a better BER performance of ZF OFDMA over ZF OSSMIC. This is because when

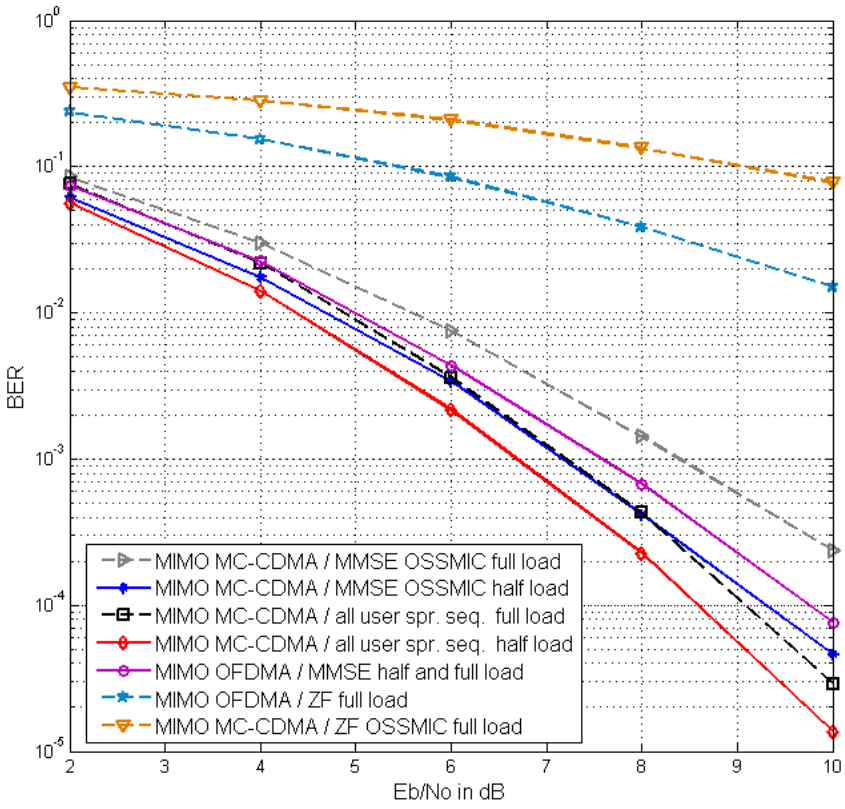

Figure 5.2: BER performance of chip level MIMO MC-CDMA and MIMO OFDMA at half and full load.

block interleaving is applied to OFDMA, consecutive symbols will be transmitted at interleaved subcarriers, which have more diverse channel gains. These channel gains affect the SNR for each symbol as in (5.27). With ECC, this diversity can be exploited to correct errors. However for MC-CDMA, the effects of these diverse channel gains are averaged for each symbol as in (5.10). Hence while diversity is achieved for each symbol, the instantaneous symbol SNR will be similar for all symbols and thus the effect of ECC will be reduced. Another reason is that

the noise in the ZF OSSMIC receiver is amplified by the presence of $\sigma^2_{\tilde{n},p}$ as shown in (5.10). Further observations illustrate that the system performance of MMSE OFDMA is independent of the number of users. This can be explained from the PEP analysis in Section 5.3.2, where the argument in the Q function of (5.26) is independent of the number of user N_u. However, the performance for the OSSMIC receiver depends on the number of active users. For half-load case, OSSMIC performs 0.5 dB better than the MMSE OFDMA at BER = 10^{-3}. In addition, if the other users' spreading sequences are known, OSSMIC achieves a further 0.5 dB and 1 dB improvement for both half and full load cases respectively.

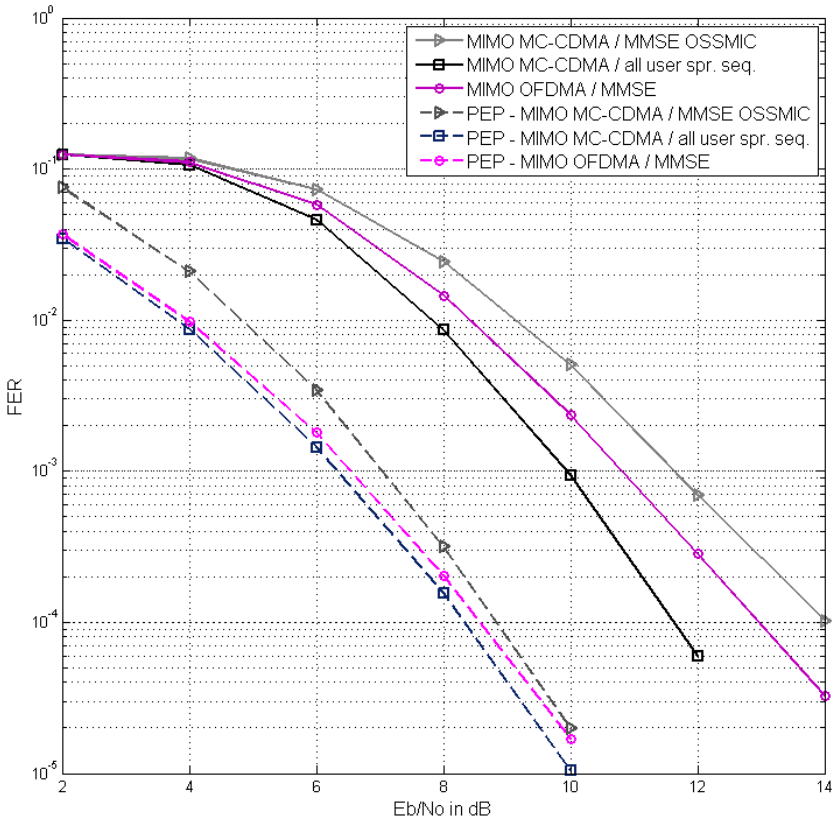

Figure 5.3: FER and PEP performance of chip level MIMO MC-CDMA and MIMO OFDMA at full load.

The simulated FER and PEP performance of MIMO MC-CDMA and MIMO

OFDMA systems with eight users (full-load) are presented in Figure 5.3. It can be observed that the asymptotic slope for FER and PEP results are similar.

The BER performances of different systems are also evaluated over different number of users at $E_b/N_0 = 8$ dB, and are shown in Figure 5.4. It is also observed that at low system load, the performance of MMSE OSSMIC is better than MMSE OFDMA. However the performance of OSSMIC deteriorates as the number of user increases towards the full load case. It performs worse than OFDMA when there are 5 or more users. This can also be explained from the

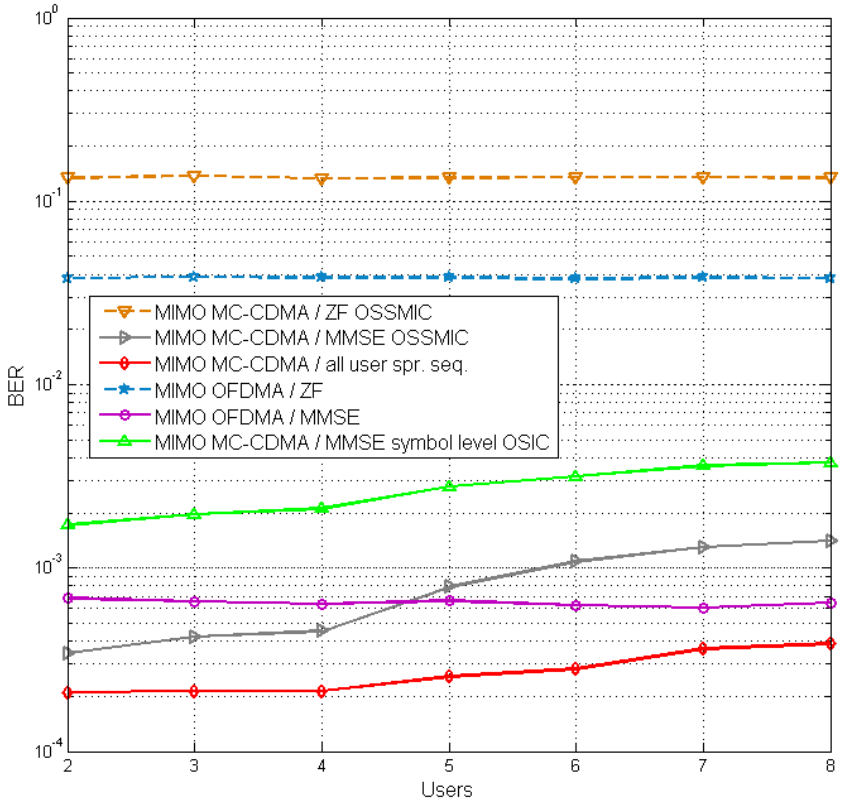

Figure 5.4: BER performance of MIMO MC-CDMA and MIMO OFDMA for different number of users.

PEP analysis. When the system load is low, the multiple access interference terms in (5.9) for MC-CDMA remain small. On the other hand as more subcarriers

contribute to the Euclidean distance for MC-CDMA in (5.8), frequency diversity is better exploited and it outperforms OFDMA. However as the number of user increases towards the full load case, the multiple access interference becomes higher which causes MC-CDMA to perform worse than OFDMA. It should be noted that if the other users' spreading sequences are known in the OSSMIC detector as in [25], the OSSMIC receiver outperforms OFDMA both in low and high system loads. This is because both (5.6) and (5.4) equal to zero such that the interference terms in (5.9) is smaller. Hence this result differs from the one in SISO MC-CDMA where OFDMA has better performance in higher loaded system [71]. However, this receiver requires the knowledge of all users spreading sequence, which might not be feasible in practice as well as an increased computational complexity.

Chapter 6

Resource Allocation for Power Minimisation

6.1 Introduction

In the past years, resource allocation has been investigated for MC-CDMA systems in order to improve the quality-of-service (QoS) and system performance. In [72], the authors consider power allocation among the sub-carriers of each user to improve each users BER performance in a single cell MC-CDMA system. In [73], the optimal transmit power allocation is developed to improve the BER performance of a multicarrier system with receive antenna diversity. Furthermore, a novel power allocation algorithm is proposed in [74] to minimise the average BER of all the users in MIMO MC-CDMA systems with two dimensional spreading. Also, subcarrier and power allocation is developed in [75] to reduce the MAI and enhance BER in MC-CDMA systems. Existing work so far on resource allocation for MC-CDMA is mostly focused in minimising the BER or maximising the total capacity [30, 76–78].

On the other hand, resource allocation is also used for energy reduction in

MC-CDMA. Saving energy will not only reduce operating cost but also reduces greenhouse gas emissions which is important for combating climate change. For this reason, reducing the power consumption to a minimum level is vital for the future wireless systems. Especially when using resource allocation to minimise the total transmitted power in MC-CDMA, the energy efficiency of the system can be improved significantly. In [29], rate, sub-carrier and power allocations are proposed for a multi-rate uplink MC-CDMA system with linear minimum mean square error (LMMSE) multiuser detection (MUD) to minimise total transmitted power based on different users' data rate and BER requirements. Also in [30], a joint precoding and power allocation method is proposed for downlink MISO MC-CDMA systems which minimises the total transmitted power of the system under a constraint on the signal-to-interference and noise ratio (SINR) of each user.

Although some research has been done for power minimisation in MC-CDMA systems, resource allocation with user grouping has not been considered for power minimisation in grouped MC-CDMA systems. Hence, the work in this chapter focuses on resource allocation for grouped MC-CDMA and STBC MC-CDMA systems. The idea of user and subcarrier grouping [31] allows different users in a group to share the same set of subcarriers while using their distinct spreading codes. In this way multiuser interference in each group is small and does not affect users in the rest of the groups. Hence multiuser detectors for different groups are practically feasible. In [79], Huang et al. proposed a suboptimal user grouping and subcarrier allocation algorithm to maximise the total system throughput in grouped MC-CDMA. Also the optimal power allocation for maximising the overall capacity in grouped MC-CDMA is given in [80]. Existing work on resource allocation in grouped MC-CDMA focuses on the maximisation of the total capacity. For this reason in this work we consider resource allocation with

user grouping to minimise the total transmitted power in grouped MC-CDMA and STBC MC-CDMA systems.

6.2 Power Minimisation in MC-CDMA systems

In this section, we study the minimisation of the total transmitted power in downlink MC-CDMA under a BER constraint for each user. This is achieved by performing power control according to an efficient user grouping algorithm which will be discussed in Section 6.4. It has to be said that perfect channel information of the users are assumed both at the transmitter and the receiver. First, the signal model of grouped MC-CDMA is presented. Next, we formulate the minimisation problem without fairness criteria.

6.2.1 Grouped MC-CDMA Signal Model

Consider the downlink MC-CDMA system with N_u users and Rayleigh fading channel. The channel is divided into N_s subcarriers which are further grouped consecutively into K groups. Each group uses a set of Walsh-Hadamard spreading sequences, with length $G = N_s/K$. Assuming multicode transmission is not used, each user in a group can only transmit one symbol over G subcarriers. Thus the maximum number of users per group U, equals to the spreading code length G. The total number of allocatable resource units is therefore $K \times G$ which equals to N_s. The same set of spreading sequence is used in all other groups. Hence in any one group the signature sequence of user u in that group (u = 1,2,...,U) is expressed as

$$\mathbf{c}_u = \begin{bmatrix} c_{u,1} & c_{u,2} & \cdots & c_{u,G} \end{bmatrix}^T \in C^{G\times 1}. \tag{6.1}$$

To illustrate the concept of grouped MC-CDMA systems we consider a system

with six users ($N_u = 6$). The channel consists of 16 subcarriers ($N_s = 16$) which are grouped consecutively into four groups ($K = 4$). Each group uses a set of Walsh-Hadamard spreading sequences, with length of four ($G = 4$). Each user in a group can only transmit one symbol over four subcarriers. Thus the maximum number of users per group, equals to four ($U = 4$). Figure 6.1 demonstrates an example of how the six users can be allocated in different groups. It has to be noted that a user can only be assigned in a group once, but could be allocated in another group (e.g. User 1 is allocated once in group 1, 2 & 4).

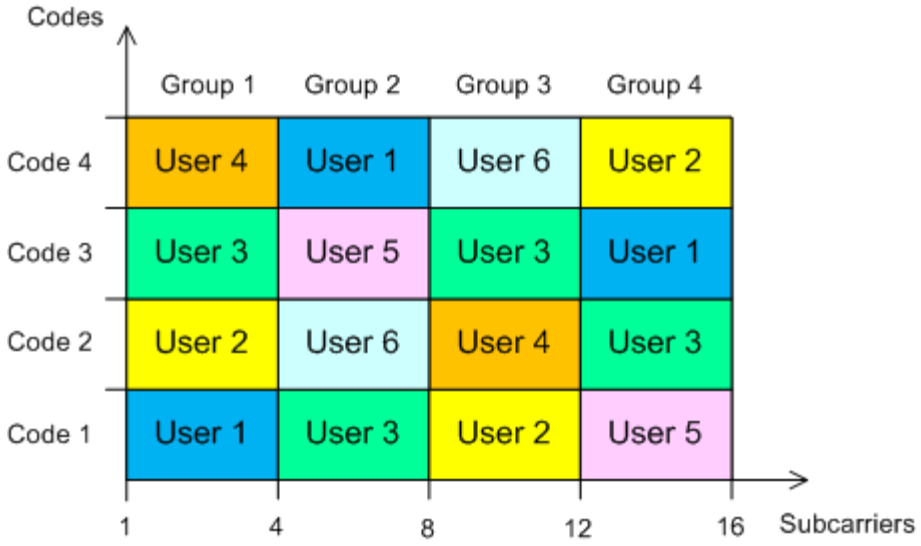

Figure 6.1: Illustration of codes vs subcarriers in grouped MC-CDMA.

The received signal model at the *u-th* user terminal of the *k-th* group (k = 1,2,...,K) can be characterised as

$$\mathbf{r}_u^k = \mathbf{H}_u^k \mathbf{C} \sqrt{\mathbf{P}^k} \mathbf{d}^k + \mathbf{n}_u^k \tag{6.2}$$

where the users' symbol vector and AWGN vector with power N_0 are represented respectively by

$$\mathbf{d}^k = \begin{bmatrix} d_1^k & d_2^k & \cdots & d_U^k \end{bmatrix}^T \in \mathbb{C}^{U \times 1} \tag{6.3}$$

and

$$\mathbf{n}_u^k = \begin{bmatrix} n_{u,1}^k & n_{u,2}^k & \cdots & n_{u,G}^k \end{bmatrix}^T \in \mathbb{C}^{G\times 1}. \tag{6.4}$$

The transmit power and spreading code matrices are given respectively by

$$\mathbf{P}^k = \text{diag}(\rho_1^k, \rho_2^k, ..., \rho_U^k) \in \mathbb{C}^{U\times U} \tag{6.5}$$

and

$$\mathbf{C} = \begin{bmatrix} \mathbf{c}_1 & \mathbf{c}_2 & \cdots & \mathbf{c}_U \end{bmatrix} \in \mathbb{C}^{G\times U}. \tag{6.6}$$

The channel response matrix at the *u-th* user terminal of the *k-th* group is denoted as

$$\mathbf{H}_u^k = \text{diag}(h_{u,1}^k, h_{u,2}^k, ..., h_{u,G}^k) \in \mathbb{C}^{G\times G} \tag{6.7}$$

where $h_{u,g}^k$ represents the channel gain of the *u-th* user in the *k-th* group at the *g-th* subcarrier (g = 1,2,...,G). The received signal vector can be symbolised as

$$\mathbf{r}_u^k = \begin{bmatrix} r_{u,1}^k & r_{u,2}^k & \cdots & r_{u,G}^k \end{bmatrix}^T \tag{6.8}$$

in which $r_{u,g}^k$ is the received signal of the *u-th* user in the *k-th* group at the *g-th* subcarrier and it can be expressed as

$$r_{u,g}^k = h_{u,g}^k \sum_{u'=1}^{U} c_{u',g}\sqrt{\rho_{u'}^k} d_{u'}^k + n_{u,g}^k. \tag{6.9}$$

When the signal in (6.9) passess through a linear ZF filter, the estimates of the

u-th user in the *k-th* group at the *g-th* subcarrier can be represented as

$$\begin{aligned} y_{u,g}^{k} &= \left(h_{u,g}^{k}\right)^{-1} r_{u,g}^{k} \\ &= c_{u,g}\sqrt{\rho_{u}^{k}}d_{u}^{k} + \sum_{u'=1,u'\neq u}^{U} c_{u',g}\sqrt{\rho_{u'}^{k}}d_{u'}^{k} + \tilde{n}_{u,g}^{k}. \end{aligned} \tag{6.10}$$

where $\tilde{n}_{u,g}^{k} = (h_{u,g}^{k})^{-1} n_{u,g}^{k}$. The *u-th* user's symbol decision statistic is obtained when the chip estimates in (6.10) are despread by the corresponding spreading sequence, given by

$$z_{u}^{k} = \sum_{g=1}^{G} c_{u,g} y_{u,g}^{k} = \sqrt{\rho_{u}^{k}}d_{u}^{k} + \sum_{g=1}^{G} c_{u,g}\tilde{n}_{u,g}^{k}. \tag{6.11}$$

According to (6.11), it is obvious that MAI from other users in the group is cancelled by despreading. Thus power allocation for the *u-th* user can be performed by requiring only the *u-th* user's power information ρ_{u}^{k}. From (6.11), the received SINR for the *u-th* user of the *k-th* group is calculated by

$$\begin{aligned} \mathrm{SINR}_{u}^{k} &= \frac{\rho_{u}^{k} E_{d}}{\sum_{g=1}^{G} E_{h}\left[c_{u,g}(h_{u,g}^{k})^{-1} n_{u,g}^{k} n_{u,g}^{k^{*}} (h_{u,g}^{k})^{-1^{*}} c_{u,g}^{*}\right]} \\ &= \frac{G\rho_{u}^{k} E_{d}}{N_{0}\sum_{g=1}^{G}\left[(h_{u,g}^{k})^{-1}(h_{u,g}^{k})^{-1^{*}}\right]} \end{aligned} \tag{6.12}$$

where $E_{h}[.]$ and $(.)^{*}$ refer to the conditional expectation on the channel gain h and the complex conjugate operators respectively, and E_{d} refers to the symbol energy. Hence if there is a certain target SINR, denoted as γ_{u}^{k}, the transmitted power for the *u-th* user of the *k-th* group is expressed as

$$\rho_{u}^{k} = \frac{\gamma_{u}^{k} N_{0}}{E_{d} G}\sum_{g=1}^{G}\left[(h_{u,g}^{k})^{-1}(h_{u,g}^{k})^{-1^{*}}\right]. \tag{6.13}$$

6.2.2 Problem Formulation in MC-CDMA

In this section we consider the minimisation of system's total transmitted power under a BER constraint by performing user grouping and power control. The minimisation problem is formulated with and without fairness criteria. Fairness is applied to ensure some bandwidth is allocated to each user. The total transmitted power of the system can be expressed as

$$P_T = \sum_{k=1}^{K} \sum_{u=1}^{U} \rho_u^k = \sum_{k=1}^{K} \sum_{u=1}^{U} \frac{\gamma_u^k N_0}{E_d G} \omega_u^k \tag{6.14}$$

where ω_u^k represents a channel related factor of the $u\text{-}th$ user in the $k\text{-}th$ group given by

$$\omega_u^k = \sum_{g=1}^{G} \left[(h_{u,g}^k)^{-1} (h_{u,g}^k)^{-1^*} \right]. \tag{6.15}$$

To group users for power minimisation, the following channel related factor for all system users ($n_u = 1, ..., N_u$) has to be considered,

$$\overline{\omega}_{n_u}^k = \sum_{g=1}^{G} \left[(h_{n_u,g}^k)^{-1} (h_{n_u,g}^k)^{-1^*} \right]. \tag{6.16}$$

Using the probability of error for BPSK modulation in [81], the target SINR can be represented with respect to a target BER as

$$\gamma_u^k = 1/2 \left[Q^{-1} \left(\mathrm{BER}_u^k / 2 \right) \right]^2. \tag{6.17}$$

Hence the optimization problem without any fairness criteria can be formulated mathematically as

$$\min_{\xi_{n_u}^k} \sum_{k=1}^{K} \sum_{n_u=1}^{N_u} \frac{N_0 \left[Q^{-1} \left(\mathrm{BER}_u^k / 2 \right) \right]^2}{2 E_d G} \overline{\omega}_{n_u}^k \xi_{n_u}^k \tag{6.18}$$

$$s.t. \qquad \mathrm{BER}_u^k \leq \overline{\mathrm{BER}} \tag{6.19}$$

$$\sum_{n_u=1}^{N_u} \xi_{n_u}^k = G \qquad \forall k = 1, 2, ..., K. \tag{6.20}$$

in which $\xi_{n_u}^k \in \{0, 1\}$ is an indicator function with '1' denoting user n_u being allocated to group k and '0' otherwise. Constraint (6.19) requires that the instantaneous BER for the *u-th* user of the *k-th* group is equal to or smaller than the minimum BER value $\overline{\mathrm{BER}}$, whereas constraint (6.20) ensures that each group consists of G users.

6.3 Power Minimisation in STBC MC-CDMA systems

To further exploit both spatial diversity and channel coding in MIMO systems and with low complexity receiver implementation, STBC has been combined with MC-CDMA systems in the past years [82–87]. In this section we follow similar approach as for MC-CDMA to study the minimisation of the total transmitted power in downlink STBC MC-CDMA under a BER constraint for each user.

6.3.1 Grouped STBC MC-CDMA Signal Model

Consider a downlink MIMO MC-CDMA system based on Alamouti's STBC with $N_t = 2$ transmit and N_r receive antennas. The system consists of N_u users and each user experiences a Rayleigh fading channel. The available bandwidth is divided into groups in the same way as in the analysis for the MC-CDMA system. Each group uses the same spreading sequences as above. Furthermore, no multicode transmission is assumed, and hence each user in a group can only transmit one symbol over G subcarriers. Thus the maximum number of users per

group U equals to the spreading code length G. The total number of allocatable resource units is therefore $K \times G$ which equals to N_s.

During the Alamouti's transmission scheme, the u-th user transmits two symbols d_u^0 and d_u^1 over two consecutive transmissions. During the first transmission, d_u^0 and d_u^1 are transmitted simultaneously at time t from the two transmit antennas. During the second transmission, $-d_u^{1*}$ and d_u^{0*} are transmitted at time $t+T_d$ from the two transmit antennas where T_d denotes the OFDM symbol duration. The received signal model at the u-th user terminal of the k-th group for the n_r-th antenna (n_r = 1,2,...,N_r) can be expressed as

$$\underbrace{\begin{bmatrix} \mathbf{r}_{u,k}^{n_r}(1) \\ \mathbf{r}_{u,k}^{n_r H}(2) \end{bmatrix}}_{\mathbf{R}_{u,k}^{n_r}} = \underbrace{\begin{bmatrix} \mathbf{H}_{u,k}^{1,n_r} & \mathbf{H}_{u,k}^{2,n_r} \\ \mathbf{H}_{u,k}^{2,n_r *} & -\mathbf{H}_{u,k}^{1,n_r *} \end{bmatrix}}_{\mathcal{H}_{u,k}^{n_r}} \underbrace{\begin{bmatrix} \mathbf{C} & 0 \\ 0 & \mathbf{C} \end{bmatrix}}_{\mathcal{C}} \underbrace{\begin{bmatrix} \boldsymbol{\rho}_k & 0 \\ 0 & \boldsymbol{\rho}_k \end{bmatrix}}_{\mathbf{P}_k} \underbrace{\begin{bmatrix} \mathbf{d}_k^0 \\ \mathbf{d}_k^1 \end{bmatrix}}_{\mathbf{D}_k} + \underbrace{\begin{bmatrix} \mathbf{n}_{u,k}^{n_r}(1) \\ \mathbf{n}_{u,k}^{n_r H}(2) \end{bmatrix}}_{\mathbf{N}_{u,k}^{n_r}} \tag{6.21}$$

where the received signal vector after the i-th transmission is expressed as

$$\mathbf{r}_{u,k}^{n_r}(i) = \begin{bmatrix} r_{u,k,1}^{n_r}(i) & r_{u,k,2}^{n_r}(i) & \cdots & r_{u,k,G}^{n_r}(i) \end{bmatrix}^T \in \mathbb{C}^{G\times 1} \tag{6.22}$$

in which $r_{u,k,g}^{n_r}(i)$ symbolizes the received signal of the u-th user in the k-th group at the g-th subcarrier for the n_r-th antenna that is received after the i-th transmission. The channel response matrix of the u-th user terminal in the k-th group at the n_t-th transmit and n_r-th receive antenna is denoted as

$$\mathbf{H}_{u,k}^{n_t,n_r} = \mathrm{diag}(h_{u,k,1}^{n_t,n_r}, h_{u,k,2}^{n_t,n_r}, ..., h_{u,k,G}^{n_t,n_r}) \in \mathbb{C}^{G\times G} \tag{6.23}$$

where $h_{u,k,g}^{n_t,n_r}$ represents the channel gain of the u-th user in the k-th group for the g-th subcarrier at the n_t-th transmit and n_r-th receive antennas. The users' symbol vector is represented by

$$\mathbf{d}_k^j = \left[\begin{array}{cccc} d_{1,k}^j & d_{2,k}^j & \cdots & d_{U,k}^j \end{array} \right]^T \in \mathbb{C}^{U\times 1} \tag{6.24}$$

and the AWGN vector with power N_0 is represented by

$$\mathbf{n}_{u,k}^{n_r}(i) = \left[\begin{array}{cccc} n_{u,k,1}^{n_r}(i) & n_{u,k,2}^{n_r}(i) & \cdots & n_{u,k,G}^{n_r}(i) \end{array} \right]^T \in \mathbb{C}^{G\times 1}. \tag{6.25}$$

The transmit power vector and spreading code matrix are given respectively by

$$\boldsymbol{\rho}_k = \left[\begin{array}{cccc} \sqrt{\rho_{1,k}/2} & \sqrt{\rho_{2,k}/2} & \cdots & \sqrt{\rho_{U,k}/2} \end{array} \right] \in \mathbb{C}^{1\times U} \tag{6.26}$$

and

$$\mathbf{C} = \left[\begin{array}{cccc} \mathbf{c}_1 & \mathbf{c}_2 & \cdots & \mathbf{c}_U \end{array} \right] \in \mathbb{C}^{G\times U}. \tag{6.27}$$

When the signal in (6.21) passess through a space-time filter, the output signal can be expressed by

$$\begin{aligned} \underbrace{\left[\begin{array}{c} \mathbf{y}_{u,k}^{n_r}(1) \\ \mathbf{y}_{u,k}^{n_r}(2) \end{array} \right]}_{\mathbf{Y}_{u,k}^{n_r}} = & \underbrace{\overbrace{\left[\begin{array}{cc} \mathbf{H}_{u,k}^{1,n_r*} & \mathbf{H}_{u,k}^{2,n_r} \\ \mathbf{H}_{u,k}^{2,n_r*} & -\mathbf{H}_{u,k}^{1,n_r} \end{array} \right]}^{\mathcal{G}_{u,k}^{n_r}} \left[\begin{array}{cc} \mathbf{H}_{u,k}^{1,n_r} & \mathbf{H}_{u,k}^{2,n_r} \\ \mathbf{H}_{u,k}^{2,n_r*} & -\mathbf{H}_{u,k}^{1,n_r*} \end{array} \right]}_{\left(\left|\mathbf{H}_{u,k}^{1,n_r}\right|^2+\left|\mathbf{H}_{u,k}^{2,n_r}\right|^2\right)\mathbf{I}_2} \left[\begin{array}{cc} \mathbf{C} & 0 \\ 0 & \mathbf{C} \end{array} \right] \\ & \times \left[\begin{array}{cc} \boldsymbol{\rho}_k & 0 \\ 0 & \boldsymbol{\rho}_k \end{array} \right] \left[\begin{array}{c} \mathbf{d}_k^0 \\ \mathbf{d}_k^1 \end{array} \right] + \overbrace{\left[\begin{array}{cc} \mathbf{H}_{u,k}^{1,n_r*} & \mathbf{H}_{u,k}^{2,n_r} \\ \mathbf{H}_{u,k}^{2,n_r*} & -\mathbf{H}_{u,k}^{1,n_r} \end{array} \right]}^{\mathcal{G}_{u,k}^{n_r}} \left[\begin{array}{c} \mathbf{n}_{u,k}^{n_r}(1) \\ \mathbf{n}_{u,k}^{n_r H}(2) \end{array} \right] \end{aligned} \tag{6.28}$$

where the equalised signal of the u-th user in the k-th group at the n_r-th antenna is given by

$$\mathbf{y}_{u,k}^{n_r}(i) = \left[\begin{array}{cccc} \mathbf{y}_{u,k,1}^{n_r}(i) & \mathbf{y}_{u,k,2}^{n_r}(i) & \cdots & \mathbf{y}_{u,k,G}^{n_r}(i) \end{array} \right]^T \in \mathbb{C}^{G\times 1}. \tag{6.29}$$

The u-th user's symbols decision statistic is obtained when the two successive equalised signals in (6.28) are space-time combined and despread by the corresponding spreading sequence. This is represented by

$$\begin{aligned} \mathbf{z}_{u,k} &= \left(\mathbf{I}_2 \otimes \mathbf{c}_u^T\right) \sum_{n_r=1}^{N_r} \mathbf{Y}_{u,k}^{n_r} \\ &= \sqrt{\frac{\rho_{u,k}}{2}} \left[\sum_{g=1}^{G} \sum_{n_r=1}^{N_r} \left|h_{u,k,g}^{1,n_r}\right|^2 + \left|h_{u,k,g}^{2,n_r}\right|^2 \right] \left[\begin{array}{c} d_{u,k}^0 \\ d_{u,k}^1 \end{array} \right] \\ &+ \left(\mathbf{I}_2 \otimes \mathbf{c}_u^T\right) \sum_{n_r=1}^{N_r} \mathcal{G}_{u,k}^{n_r} \mathbf{N}_{u,k}^{n_r} \end{aligned} \tag{6.30}$$

where $\mathbf{z}_{u,k} = \left[\begin{array}{cc} z_{u,k}(1) & z_{u,k}(2) \end{array} \right]^T \in \mathbb{C}^{2\times 1}$. According to (6.30), MAI from other users in the group is cancelled by despreading. The power allocation for the u-th user can be performed by requiring only the u-th user's power information $\rho_{u,k}$. From (6.30) we calculate the received SINR for the u-th user of the k-th group as shown by

$$\begin{aligned} \mathrm{SINR}_u^k &= \frac{\frac{\rho_{u,k}}{2} E_d \left[\sum_{g=1}^{G} \sum_{n_r=1}^{N_r} \left|h_{u,k,g}^{1,n_r}\right|^2 + \left|h_{u,k,g}^{2,n_r}\right|^2 \right]^2}{\frac{N_0}{G} \sum_{g=1}^{G} \sum_{n_r=1}^{N_r} \left|h_{u,k,g}^{1,n_r}\right|^2 + \left|h_{u,k,g}^{2,n_r}\right|^2} \\ &= \frac{\rho_{u,k} G E_d}{2N_0} \sum_{g=1}^{G} \sum_{n_r=1}^{N_r} \left|h_{u,k,g}^{1,n_r}\right|^2 + \left|h_{u,k,g}^{2,n_r}\right|^2 \\ &= \frac{\rho_{u,k} G E_d}{2N_0} \sum_{g=1}^{G} tr\left(\overline{\mathbf{H}}_{u,k,g}^H \overline{\mathbf{H}}_{u,k,g}\right) \end{aligned} \tag{6.31}$$

where

$$\overline{\mathbf{H}}_{u,k,g} = \begin{bmatrix} h_{u,k,g}^{1,1} & h_{u,k,g}^{2,1} \\ h_{u,k,g}^{1,2} & h_{u,k,g}^{2,2} \\ \vdots & \vdots \\ h_{u,k,g}^{1,n_r} & h_{u,k,g}^{2,n_r} \end{bmatrix}. \tag{6.32}$$

and $tr(\mathbf{A})$ denotes the trace of matrix $\mathbf{A}$. Hence if there is a certain target SINR, denoted as γ_u^k, the transmitted power for the u-th user of the k-th group is expressed as

$$\rho_{u,k} = \frac{2\gamma_u^k N_0}{GE_d \sum_{g=1}^{G} tr\left(\overline{\mathbf{H}}_{u,k,g}^H \overline{\mathbf{H}}_{u,k,g}\right)}. \tag{6.33}$$

6.3.2 Problem Formulation in STBC MC-CDMA

In this section, the power minimisation problem for STBC MC-CDMA is formulated in a similar way as for MC-CDMA. By performing user grouping and power control we consider the minimisation of system's total transmitted power under a BER constraint. The total transmitted power of the system can be characterised as

$$P_T = \sum_{k=1}^{K} \sum_{u=1}^{U} \rho_{u,k} = \sum_{k=1}^{K} \sum_{u=1}^{U} \frac{2\gamma_u^k N_0}{GE_d} \omega_u^k \tag{6.34}$$

where ω_u^k is denoted by

$$\omega_u^k = \frac{1}{\sum_{g=1}^{G} tr\left(\overline{\mathbf{H}}_{u,k,g}^H \overline{\mathbf{H}}_{u,k,g}\right)} \tag{6.35}$$

The channel related factor for all system users can be expressed as

$$\overline{\omega}_{n_u}^k = \frac{1}{\sum_{g=1}^{G} tr\left(\overline{\mathbf{H}}_{n_u,k,g}^H \overline{\mathbf{H}}_{n_u,k,g}\right)}. \tag{6.36}$$

Similar to the MC-CDMA analysis, the optimisation problem without any

fairness criteria can be formulated mathematically as

$$\min_{\xi_{n_u}^k} \sum_{k=1}^{K} \sum_{n_u=1}^{N_u} \frac{N_0 \left[Q^{-1}\left(\mathrm{BER}_u^k/2\right)\right]^2}{GE_d} \overline{\omega}_{n_u}^k \xi_{n_u}^k \tag{6.37}$$

$$s.t. \qquad \mathrm{BER}_u^k \leq \overline{\mathrm{BER}} \tag{6.38}$$

$$\sum_{n_u=1}^{N_u} \xi_{n_u}^k = G \qquad \forall k = 1, 2, ..., K. \tag{6.39}$$

in which $\xi_{n_u}^k$ and the two constraints are the same as in the problem formulation for MC-CDMA.

6.4 Optimisation Problem

Having formulated the problem for MC-CDMA and STBC MC-CDMA in the previous sections, we propose several power minimising user grouping algorithms in this section. First, the optimal algorithm based on Greedy approach is proposed when there is no fairness criterion in the data rate. However when fairness is applied, the optimal solution requires high computational complexity and is not favourable for practical applications. Therefore, we propose two complexity reduced suboptimal allocation algorithms. The performance of these algorithms are evaluated in Section 6.5.

6.4.1 Greedy Allocation

The optimal solution to the minimisation problem with no fairness criterion is first presented. Consider an example of a MC-CDMA system with five users ($N_u = 5$). The channel is divided into eight subcarriers ($N_s = 8$) which are further grouped consecutively into two groups ($K = 2$). Each group uses a set

of Walsh-Hadamard spreading sequences, with length of four ($G = 4$). Assuming multicode transmission is not used, each user in a group can only transmit one symbol over four subcarriers. Furthermore, the maximum number of users per group is four ($U = 4$). Figure 6.2 shows the instantaneous channel gains for each of the N_u users over the whole bandwidth. The respective $\overline{\omega}_{n_u}^k$ of these users at

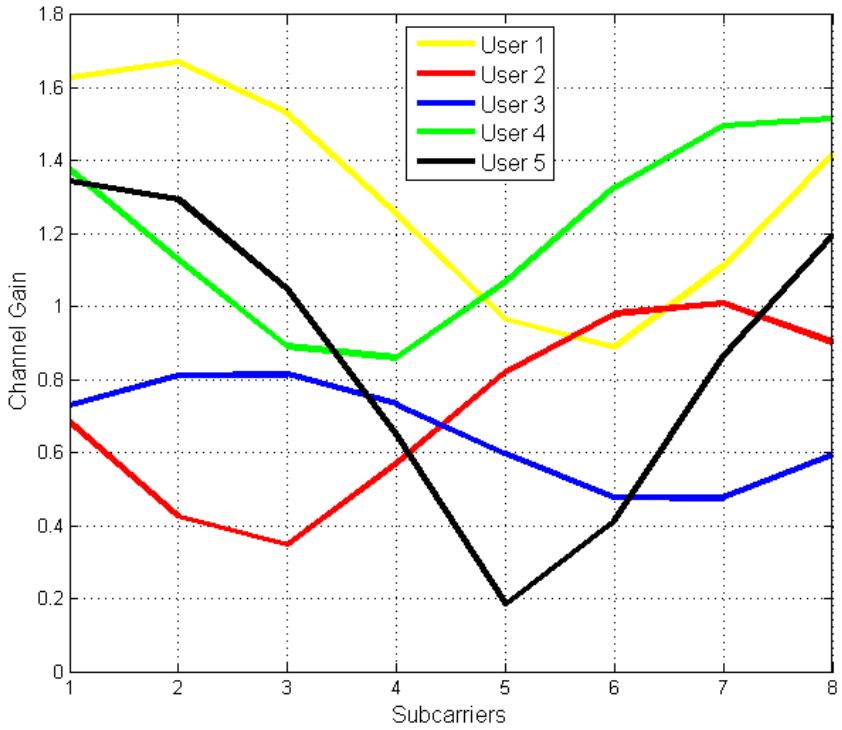

Figure 6.2: An example of channel gains for 5 users.

each group is depicted in Figure 6.3. Since we assume that users can be allocated to more than one group of subcarriers, the optimum solution to the minimisation problem in (6.18) or (6.37) would be to allocate users with the smallest $\overline{\omega}_{n_u}^k$ to the corresponding *k-th* group. Hence the total transmitted power can be minimised if we only allow users with the largest channel gains to use the available subcarriers. From Figure 6.3, it is evident that the Greedy algorithm will not assign user 2 in the first group and user 5 in the second group. The Greedy algorithm can be

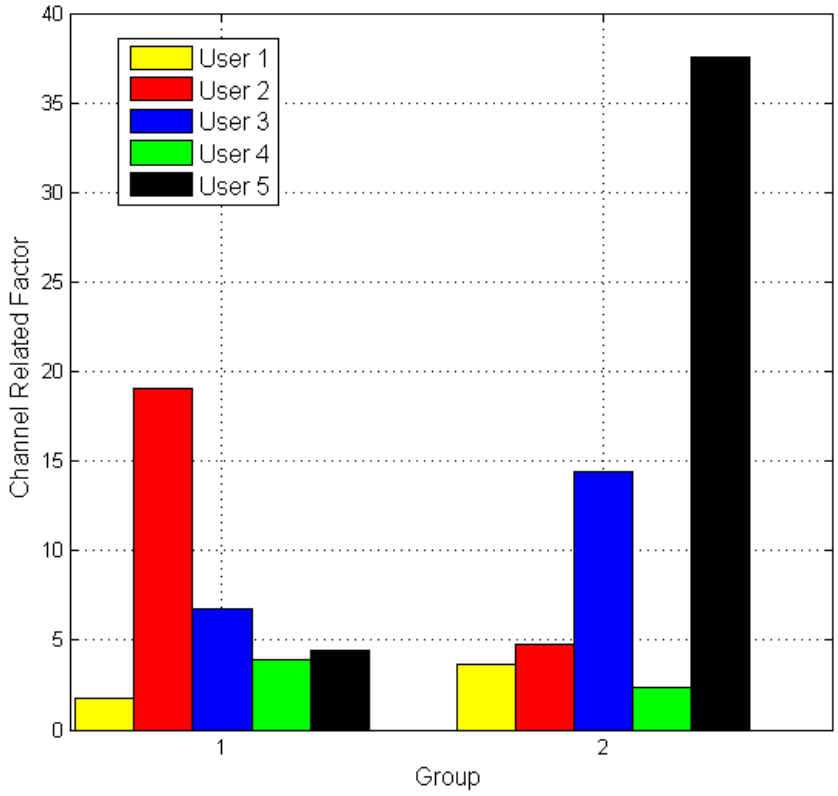

Figure 6.3: $\overline{\omega}_{n_u}^k$ for 5 users in 2 groups.

described as follows.

Greedy

Step 1: Divide the available bandwidth into $K = N_s/G$ groups. Each group consists of $U = G$ available positions for user assignment.

Step 2: For all K groups, calculate $\overline{\omega}_{n_u}^k$ for every n_u-th user according to (6.16) for MC-CDMA and (6.36) for STBC MC-CDMA.

Step 3: Allocate the U users with the smallest $\overline{\omega}_{n_u}^k$ in the k-th group.

Step 4: Repeat Step 3 until all groups are assigned with U users.

Step 5: Calculate the total transmitted power according to (6.14) for MC-CDMA and (6.34) for STBC MC-CDMA by setting $\text{BER}_u^k = \overline{\text{BER}}$.

By selecting users with the lowest $\varpi_{n_u}^k$, it is evident from (6.14) and (6.34) that the total transmitted power for every group and hence for the system will be minimised. This satisfies both minimisation problems in (6.18) and (6.37) with the constraints in (6.19), (6.20) and (6.38), (6.39) respectively.

6.4.2 Allocation with Fairness Criterion

When there is no fairness requirement, users with low channel gains, i.e. weaker users in the system, may not be allocated to any group and hence not be able to transmit their data. For this reason the fairness criterion is considered such that each user has to be assigned to a group at least once, i.e. each user can transmit using at least one resource unit before the Greedy allocation is applied. In this way it is possible for all users to transmit their data. The fairness constraint for the problem in MC-CDMA or STBC MC-CDMA can be imposed as

$$\sum_{k=1}^{K} \xi_{n_u}^k \geq 1 \qquad \forall n_u = 1, 2, ..., N_u. \tag{6.40}$$

The optimal solution to the minimisation problem with this additional fairness constraint is given by calculating the total transmitted power for all possible combinations of user allocations, and choosing the one that gives the minimum total power. However this method requires very high computational complexity. Hence we propose a simple suboptimal algorithm that requires less complexity and we call this Fairness A algorithm.

Fairness A

Step 1: Follow Steps 1 and 2 in Greedy algorithm.

Step 2: Set up the list $\mathcal{L} \in \{1, ..., N_u\}$ that contains unallocated users.

Step 3: Allocate the user with the smallest $\varpi_{n_u}^k$ from $\mathcal{L}$, in the k-th group.

Remove this allocated user from $\mathcal{L}$.

Step 4: Repeat Step 3 until each user is assigned in a group once, i.e. until $\mathcal{L}$ becomes a null set. If a group has already been allocated with U users, this group is filled and will not be allocated anymore users.

Step 5: If not all groups are assigned with U users, follow Steps 3 and 4 of the Greedy algorithm.

Step 6: Calculate the total transmitted power as in Step 5 of the Greedy algorithm.

The Fairness A algorithm is a simple and low complexity solution. However, as will be shown in Section 6.5, it has poor performance when the number of users approaches the maximum supportable by the system, i.e., $N_u \rightarrow KG$. This is because this algorithm first allocates users with large channel gains to the group containing their best subcarriers. When a group is filled, the remaining users will be allocated to other groups, even though their best subcarriers may lie in this group. Thus these remaining users could be allocated with poorer subcarriers, and this requires a larger transmission power. As the number of users increases, the groups will be filled more quickly and hence this situation occurs more often. Therefore, the total system transmission power will be significantly increased.

To overcome this problem, we propose a second suboptimal algorithm (Fairness B) that considers the amount of channel variation over the entire bandwidth. Consider a scenario in Figure 6.4 where two users have their best subcarriers in the same group, but there is only one resource unit left in that group. User 1 has a larger but relatively flatter channel gain over the entire bandwidth, while User 2 has a smaller gain but with larger channel variation. Their corresponding $\overline{\omega}_{n_u}^k$ are shown in Figure 6.5. The Fairness A algorithm will assign User 1 to this group due to its larger gain. User 2 will then be allocated to another group,

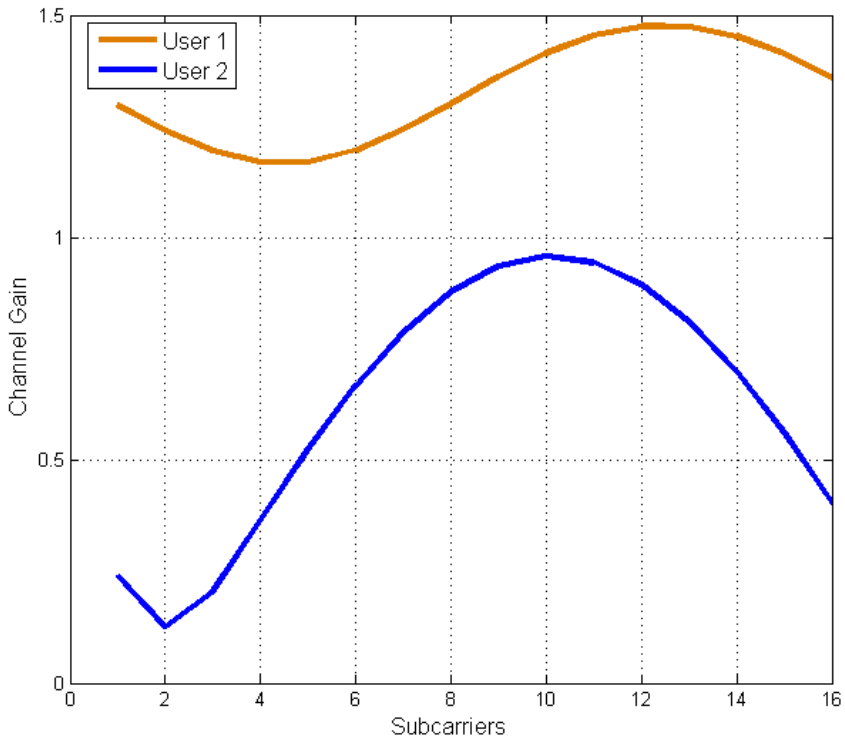

Figure 6.4: An example of channel gains for 2 users.

which might have a much lower channel gain due to the large channel variation. On the contrary if User 2 was allocated to this group, User 1 will be allocated to another group having a similarly large channel gain due to its relatively flat channel response. Hence, both users will be allocated to good channels, and the total transmission power can be significantly reduced. Therefore, it is important to group users with large channel variation first, such that their best subcarriers are used. Users with flatter channel responses should be allocated later as the difference between the subcarriers is not significant. The proposed Fairness B algorithm measures channel variation by the standard deviation of the channel related factor $\overline{\omega}_{n_u}^k$ for each user, and is detailed below.

Fairness B

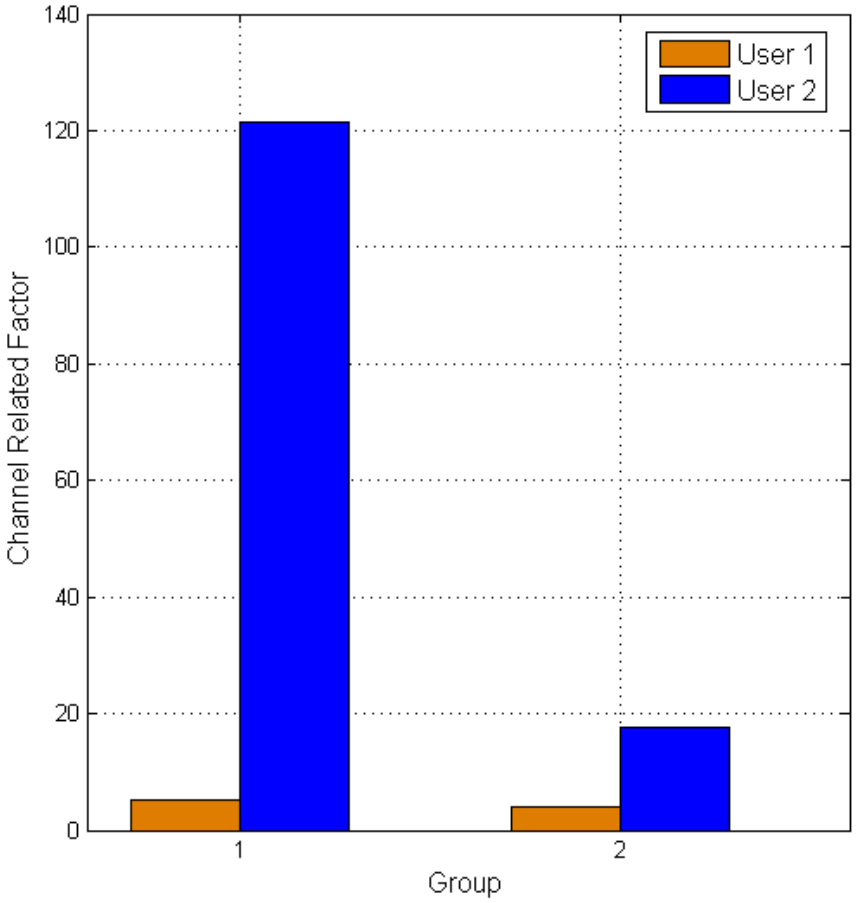

Figure 6.5: $\overline{\omega}_{n_u}^k$ for 2 users in 2 groups.

Step 1: Same as Step 1 & 2 in Greedy algorithm.

Step 2: For each user, calculate the standard deviation of $\overline{\omega}_{n_u}^k$ over the K groups. Rank the users in a descending order of this standard deviation.

Step 3: Follow the ranking order to allocate the next user to the group with its lowest $\overline{\omega}_{n_u}^k$. Remove this allocated user from the ranking list.

Step 4: Repeat Step 3 until each user is assigned one resource unit. If a group is filled, no more users can be assigned to that group.

Step 5: Same as Step 5 in Greedy algorithm.

6.5 Performance Evaluation and Discussions

In this section, the performance of the proposed algorithms are evaluated through Monte Carlo simulations. Consider a SISO MC-CDMA system, and a 2×1 and 2×2 antenna configuration for the STBC MC-CDMA system. Each of the spreading sequences is assumed to comprise eight chips ($G = 8$) and Walsh-Hadamard spreading sequences are used for each user. The FFT size is considered to be the same as the number of subcarriers and is set to be 64 ($N_s = 64$). Thus the available bandwidth is divided into eight groups ($K = 8$), each consisting of eight users ($U = 8$) and eight subcarriers. The channel is assumed to be a typical urban area propagation model specified in [55], with 6 taps and the parameters are listed in Table 2.1 in Section 2.2.3.2. It is also assumed that the maximum delay spread is shorter than the duration of the cyclic prefix. Hence, ISI is avoided and each chip experiences flat fading. As power minimisation is the aim of the proposed schemes, the performance measure is chosen to be the total transmit power over the noise level (P_T/N_0) in dB.

6.5.1 Power Consumption in MC-CDMA

Figure 6.6 demonstrates the P_T/N_0 with respect to different number of users for our proposed algorithms and the random user grouping algorithm in MC-CDMA systems. For these results we assume a target BER value of 10^{-4} ($\overline{\text{BER}} = 10^{-4}$). The results show that Fairness A & B significantly outperform the random allocation algorithm. Further power reduction can be obtained when the Greedy algorithm is performed. Hence when there is no fairness requirement in the user selection process, more power can be saved since we only assign subcarriers to

the stronger users. However weaker users in the system will not be able to send their data. Furthermore the results for Greedy algorithm depict that the total transmitted power decreases as the number of users increases. This is because with more users in the system, there will be higher multiuser diversity. Thus, it is more likely to assign users onto better subcarriers and hence the total power becomes smaller.

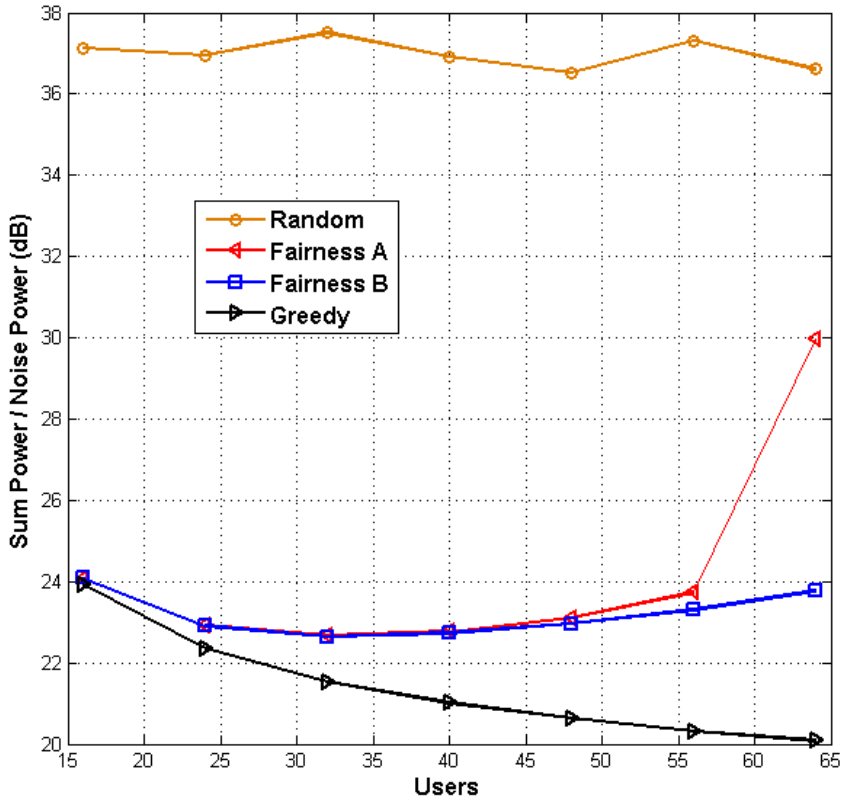

Figure 6.6: Total system transmitted power for different number of users.

When the total number of users increases towards the total number of subcarriers, a significant increase in power consumption is observed for Fairness A algorithm. As explained in Section 6.4.2, the assignment of weaker users into groups with deep faded subcarriers increases the total power consumption. With the use of Fairness B algorithm, this increase in power is avoided. This is because

Fairness B first allocates the users with higher standard deviation with respect to $\overline{\omega}_{n_u}^k$, i.e. the users with larger channel variation. Hence these users are allocated to the group where they will require less power. Users with lower channel variation are subsequently assigned, which do not require significantly different transmission power. The results validated the proposed approach for Fairness B algorithm.

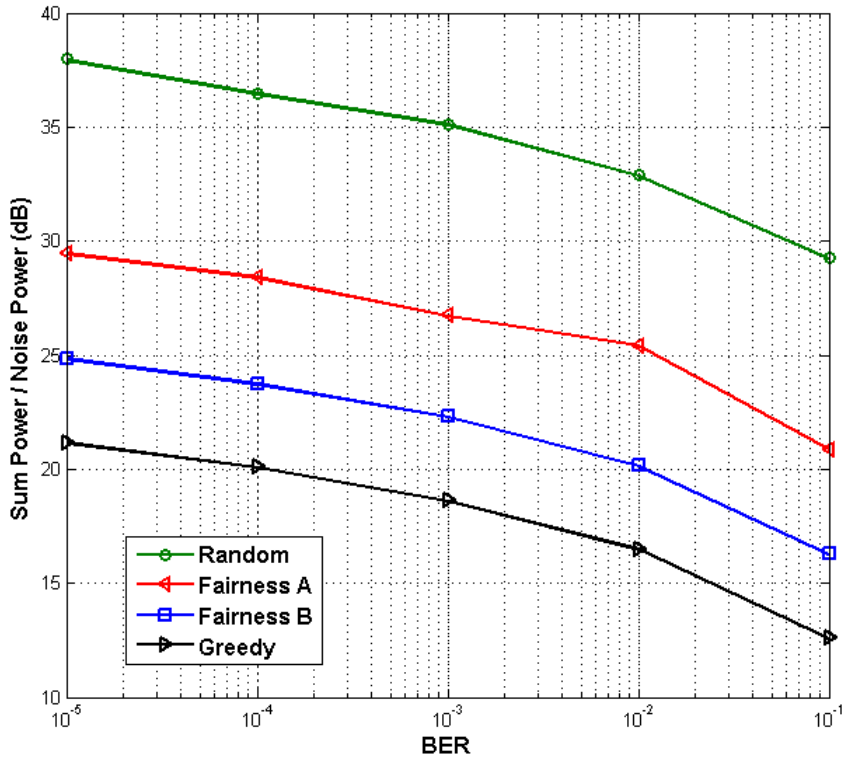

Figure 6.7: Total system transmitted power for different BERs.

In Figure 6.7, we evaluate the total transmitted power ratio for our proposed algorithms with respect to different target BER values. We also compare our results with the random user grouping algorithm. For these results we assume a full load system of $N_u = 64$. It can be observed that at a target BER of 10^{-4}, Fairness A can save 9 dB of transmission power in comparison to the Random

allocation. A further 4 dB of power reduction can be obtained when Fairness B is utilised. Further observations show that if no fairness constraint is considered and the Greedy algorithm is used, a 4 dB decrement in power is achieved in comparison to the Fairness B algorithm. Thus the Fairness B algorithm achieves good performance even though the fairness criterion is considered.

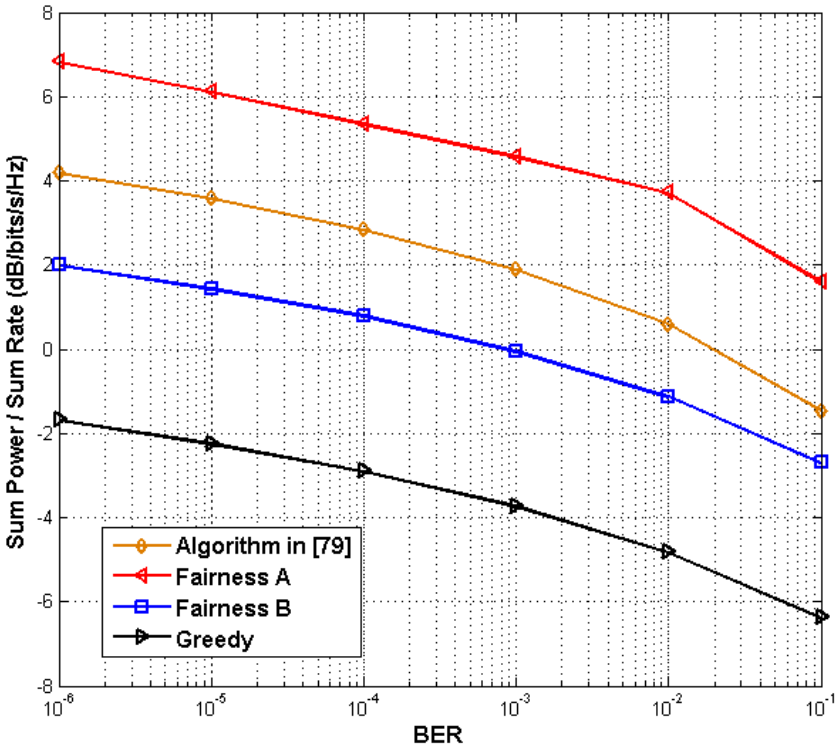

Figure 6.8: Total system transmitted power over total sum rate for different BERs.

Since no previous work has been done on user grouping for power minimisation in MC-CDMA, we compare our proposed algorithms with the user and subcarrier grouping algorithm proposed in [79]. This algorithm maximises the total system sum rate in MC-CDMA for different received SINR values. Thus to obtain a fair comparison between the proposed power minimisation problem and the sum rate maximisation problem [79], the performance measure is chosen to be the total

transmitted power ratio over the total sum rate for different BER values and the results are presented in Figure 6.8. This performance measure is important as it shows how much power should be invested in the system per b/s/Hz. In [79], the total system sum rate is maximised assuming equal transmitted power allocation for each user. Hence the total system transmitted power can be calculated when the received SINR is known. For our proposed algorithms, the total transmitted power is minimised under an equal target SINR for each user. Thus the sum rate for each user remains fixed and the total system sum rate can be calculated. Assuming a system with $N_u = 64$, observations at a BER of 10^{-4} illustrate that the algorithm in [79] outperforms Fairness A by 2 dB/b/s/Hz. However when Fairness B is considered, 4 dB of less power per b/s/Hz are obtained in comparison with the algorithm in [79]. Furthermore, 4 dB reduction in power per b/s/Hz is observed when the Greedy algorithm is used. Thus, the proposed Fairness B & Greedy algorithms are more power efficient.

6.5.2 Power Consumption in STBC MC-CDMA

Figure 6.9 demonstrates the P_T/N_0 with respect to different number of users when the proposed algorithms and the random user grouping algorithm are applied in STBC MC-CDMA systems. The results show that when multiple transmit and multiple receive antennas are applied in MC-CDMA systems, the use of STBC can exploit spatial diversity to significantly reduce power consumption. Further observations show that Fairness A & B outperform the random allocation algorithm. Also when Greedy algorithm is performed, further power reduction can be obtained. Similar to the MC-CDMA system, the results for Greedy algorithm depict that the total transmitted power decreases as the number of users increases.

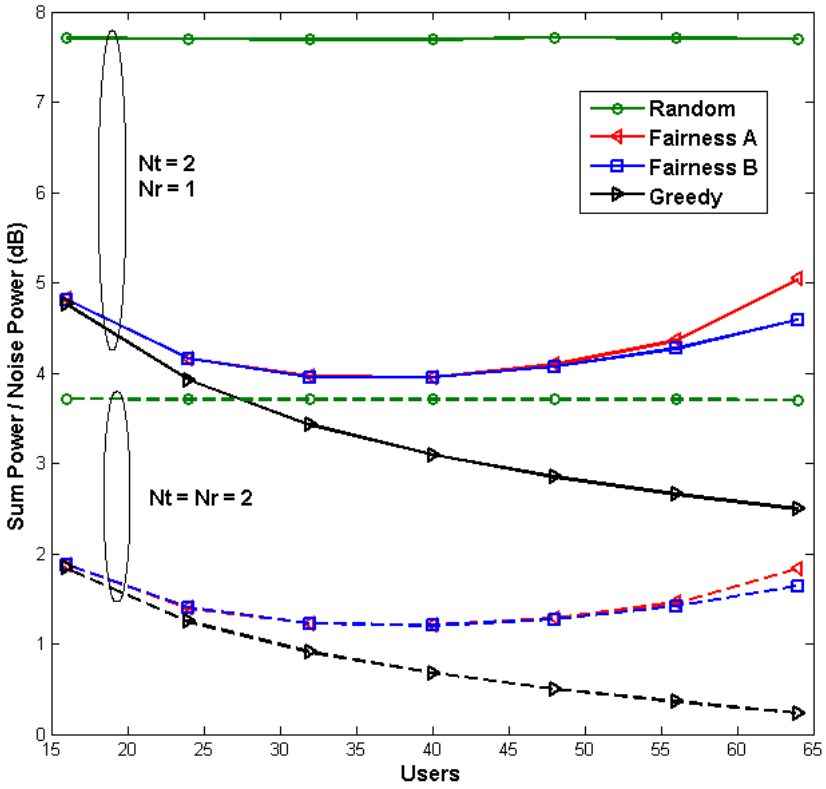

Figure 6.9: Total system transmitted power for different number of users.

When the number of receive antennas increases to 2, a decrease in power consumption is observed for all the algorithms. This is because with more receiving antennas there will be higher spatial diversity. Thus $\overline{\omega}_{n_u}^k$ in (6.36) gets smaller and the total power consumption is decreased.

In Figure 6.10, we evaluate the total transmitted power ratio for our proposed algorithms with respect to different target BER values. We also compare our results with the random user grouping algorithm. For these results we assume a full load system of $N_u = 64$. It can be observed that at a target BER of 10^{-4} and when $N_r = 1$, Fairness A can save 4 dB of transmission power in comparison to the Random allocation. A further 0.5 dB of power reduction can be obtained when Fairness B is utilised. Further observations show that if no fairness constraint

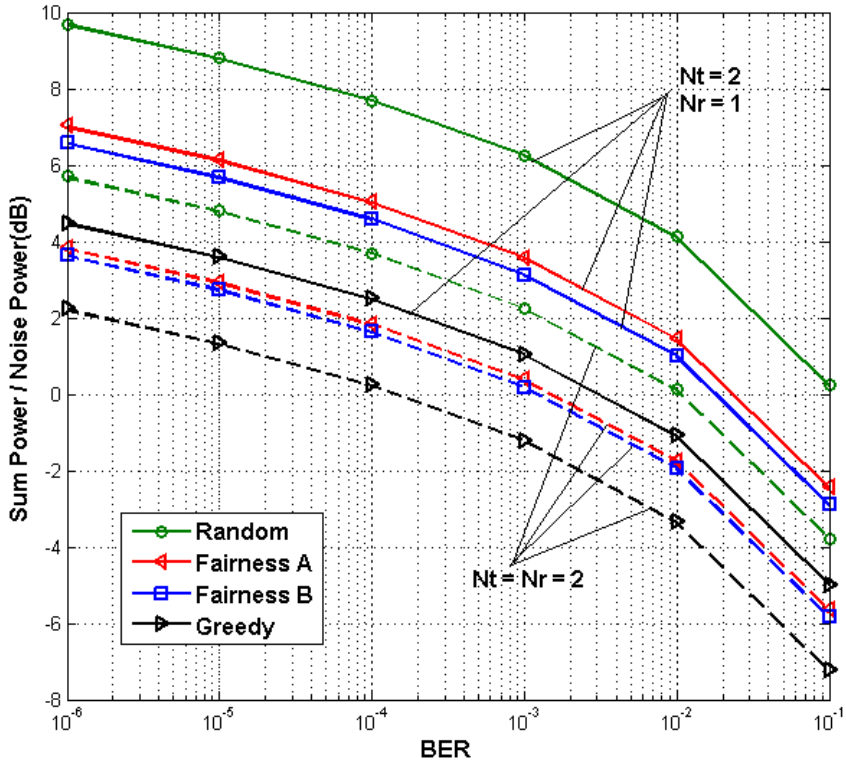

Figure 6.10: Total system transmitted power for different SINRs.

is considered and the Greedy algorithm is used, a 2 dB decrement in power is achieved in comparison to the Fairness B algorithm. It has to be noticed that as the number of receive antennas increases, the power reduction between the different algorithms decreases.

Chapter 7

MC-CDMA in Underlay Cognitive Radio

7.1 Introduction to Cognitive Radio

The increasing number of high data rate wireless applications and users tend to limit the available spectrum and increase spectrum congestion. Recent studies suggest that these problems are mainly caused by inefficient spectrum usage [88, 89]. Cognitive Radio (CR) [32] is a new emerging technique that can reduce spectrum crowding and improve spectrum efficiency. It is believed that CR will enable users in a network to: (1) determine which portions of the spectrum are available and detect the presence of licensed users when a user operates in a licensed band (spectrum sensing), (2) select the best available channel (spectrum management), (3) coordinate access to this channel with other users (spectrum sharing), and (4) vacate the channel when a licensed user is detected (spectrum mobility). Spectrum sharing is further categorised into two sections: (i) Overlay and (ii) Underlay techniques [90]. With overlay spectrum sharing, the cognitive radio users access the white spectral regions i.e. the portion of spectrum that

is not used by the licensed users. On the other hand, for underlay spectrum sharing, the cognitive radio users are allowed to share the same frequency bands (gray spectral regions) for transmission with the licensed users as long as their transmit power can be regarded as noise by the licensed users [33].

Multi-carrier modulations such as OFDM and MC-CDMA are promising candidates [91, 92] for overlay CR networks. In [93], OFDM has been exploited for implementing a spectrum pooling method to enhance spectrum efficiency in overlay CR. Spectrum pooling uses a vector of zeros and ones for the bins of the IFFT block at the OFDM transmitter to null desired portions of the band and mitigate interference. Also, in [94] the proposed non-contiguous OFDM (NC-OFDM) system deactivates fixed-bandwidth subcarriers to mitigate interference with the primary user bands. Further work in [95–97] has considered other physical layer parameters in NC-OFDM such as power, modulation and coding to optimize the overlay CR physical layer. A comparison of NC-OFDM and non-contiguous MC-CDMA (NC MC-CDMA) has been investigated in [98]. It is shown that as the number of deactivated sub-bands increases, the BER performance degradation of NC MC-CDMA becomes more than NC-OFDM approach. However, even after sub-band deactivation in NC-OFDM, there is a possibility of leaked interference from the active subbands into the nulled sub-bands. Instead of deactivating the fixed-bandwidth sub-bands, a cognitive MC-CDMA is proposed in [99] which can adaptively change its transmission parameters according to the interference pattern in that sub-band.

The majority of early research is focused on OFDM modulation as a suitable candidate for overlay CR networks. However, OFDM suffers from interference leakage problems [94] which can degrade the network performance. Moreover, although suitable for overlay CR, OFDM will have poor performance in the underlay approach. In this chapter we investigate the performance of MC-CDMA

and OFDM in underlay CR networks. As MC-CDMA spreads the cognitive user signal over a wider bandwidth, it is expected to cause lower interference to the primary system compared to OFDM. Furthermore, MC-CDMA has good interference rejection from the primary system.

7.2 Signal Model & Power Control

Consider the scenario in Figure 7.1 where the primary radio (PR) transmitter (T_P) transmits the modulated symbols using OFDM modulation. The primary receiver (R_P) is situated at a distance l_{pr} from T_P. Similarly, the secondary transmitter (cognitive transmitter, T_C) transmits the data to the cognitive receiver (R_C) over a distance l_{cr}. The goal in this work is to justify that MC-CDMA is

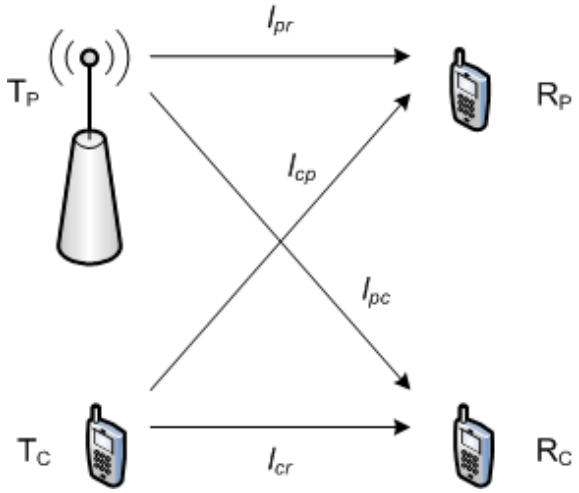

Figure 7.1: Cognitive Radio system.

more suitable for underlay CR networks than OFDM. Hence both schemes are considered for the CR system. It must be noted that since underlay spectrum sharing is assumed, the same frequency bands are used for both communication links. Therefore the signal coming from T_C must be low enough such that it can be regarded as noise at the primary receiver. Also at the cognitive receiver, the

signal coming from T_P is considered as narrowband interference. Furthermore, T_C has to be kept at a certain distance from R_P (also the same for T_P and R_C) so as to keep low interference level and maintain good communication links for both systems.

The received signal model at R_P for the *i-th* subcarrier is characterised as

$$r_{pr}^{i} = \frac{1}{\sqrt{PL_{pr}}} H_{pr}^{i} d_{pr}^{i} + \frac{1}{\sqrt{PL_{cp}}} H_{cr}^{i} d_{cr}^{i} + n^{i} \tag{7.1}$$

where H_{pr}^{i}, H_{cr}^{i}, d_{pr}^{i} and d_{pr}^{i} denote the channel and the symbol at the *i-th* subcarrier for the primary and cognitive radio respectivelly. The AWGN signal at the *i-th* subcarrier is represented by n^{i}. Furthermore, the interference power of the signal coming from the cognitive user is given by

$$\frac{I^{cr}}{N_0} = \frac{P_T^{cr}}{PL_{cp} N_0} \tag{7.2}$$

and PL_{pr} and PL_{cp} denote the path loss at distances l_{pr} and l_{cp} respectively. The path loss at distance l_x is calculated by [34]

$$PL_x = \frac{(4\pi)^2}{G_t G_r \lambda^2} (l_x)^{\alpha} \tag{7.3}$$

where G_t and G_r denote the transmitting and receiving antenna gains respectively, λ is the wavelength of the transmission and α represents the path loss exponent. Furthermore, the transmitted power at T_C is represented by

$$\frac{P_T^{cr}}{N_0} = SNR_{cr} PL_{cr} \tag{7.4}$$

where SNR_{cr} and PL_{cr} denote the SNR and path loss over the distance l_{cr} at the cognitive receiver respectively. Next, the symbol estimates for the primary

user are obtained by performing ZF equalisation on each subcarrier. Finally the detection of the estimated symbols is performed.

A similar procedure is followed to calculate the received signal model at R_C which is represented by

$$r_{cr}^{i} = \frac{1}{\sqrt{PL_{pc}}} H_{pr}^{i} d_{pr}^{i} + \frac{1}{\sqrt{PL_{cr}}} H_{cr}^{i} d_{cr}^{i} + n^{i} \tag{7.5}$$

where the interference power of the signal from the primary user is given by

$$\frac{I^{pr}}{N_0} = \frac{P_T^{pr}}{PL_{pc} N_0} \tag{7.6}$$

and PL_{cr} and PL_{pc} denote the path loss over distances l_{cr} and l_{pc} respectively. The transmitted power at T_P is represented by

$$\frac{P_T^{pr}}{N_0} = SNR_{pr} PL_{pr} \tag{7.7}$$

where SNR_{pr} and PL_{pr} represent the SNR and path loss over the distance l_{pr} at the primary receiver respectively.

7.3 Simulation Results & Discussions

In this section, the performance of MC-CDMA and OFDM techniques are evaluated in underlay CR networks under frequency selective fading. In this section CR MC-CDMA and CR OFDM refer to cognitive radio MC-CDMA and OFDM systems respectively. The transmitted frame is assumed to consist 64 QPSK modulated symbols. The FFT size for OFDM or CR OFDM is considered to be the same as the number of subcarriers and is set to be 64. The channel is assumed to be the typical urban area propagation model specified in [55], with 6 taps and the

parameters are listed in Table 2.1 in Section 2.2.3.2. It is also assumed that the maximum delay spread is shorter than the duration of the cyclic prefix. Hence,

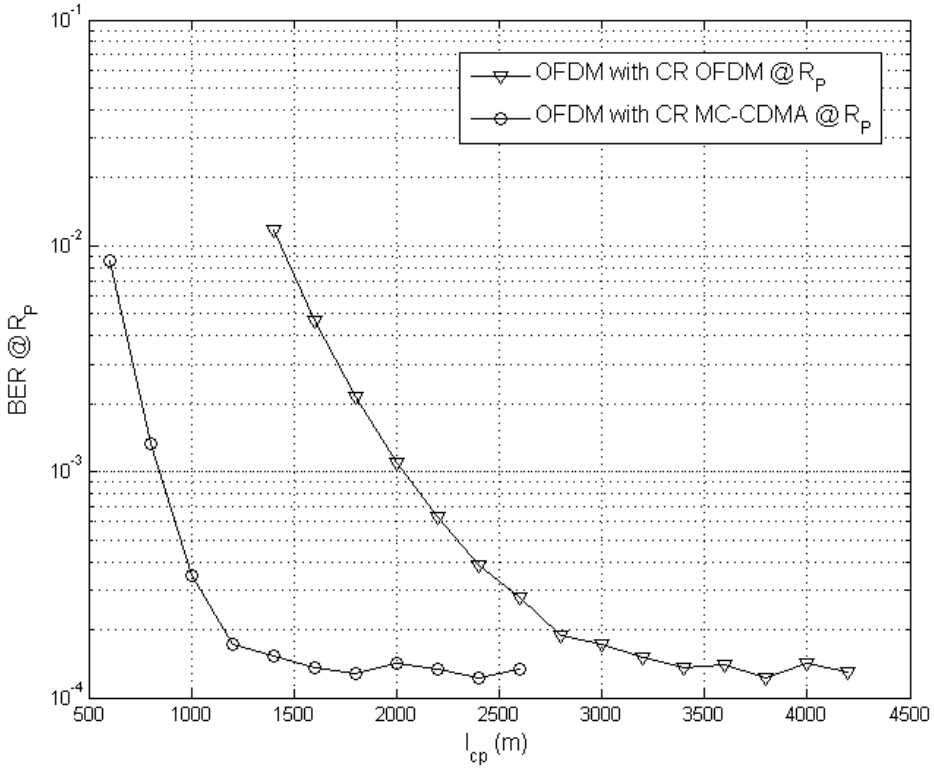

Figure 7.2: BER vs l_{cp} distance when SNR_{pr} is fixed at 30 dB.

ISI is avoided and each symbol experiences flat fading. Furthermore the CR MC-CDMA system spreads the data using the Walsh-Hadamard spreading sequence of length 512 chips ($G = 512$). The FFT size for CR MC-CDMA is considered to be the same as the code length and this is 512. It must be noted that in order to test the performance of CR MC-CDMA, the same portion of bandwidth as with OFDM is used. The path loss exponent for an urban cellular network is assumed to be 3.5, and the transmitting and receiving antenna gains are 10 dBi and 5 dBi respectively ($G_t = 10$ / $G_r = 5$). Also, the system operates at a frequency of 2.5 GHz.

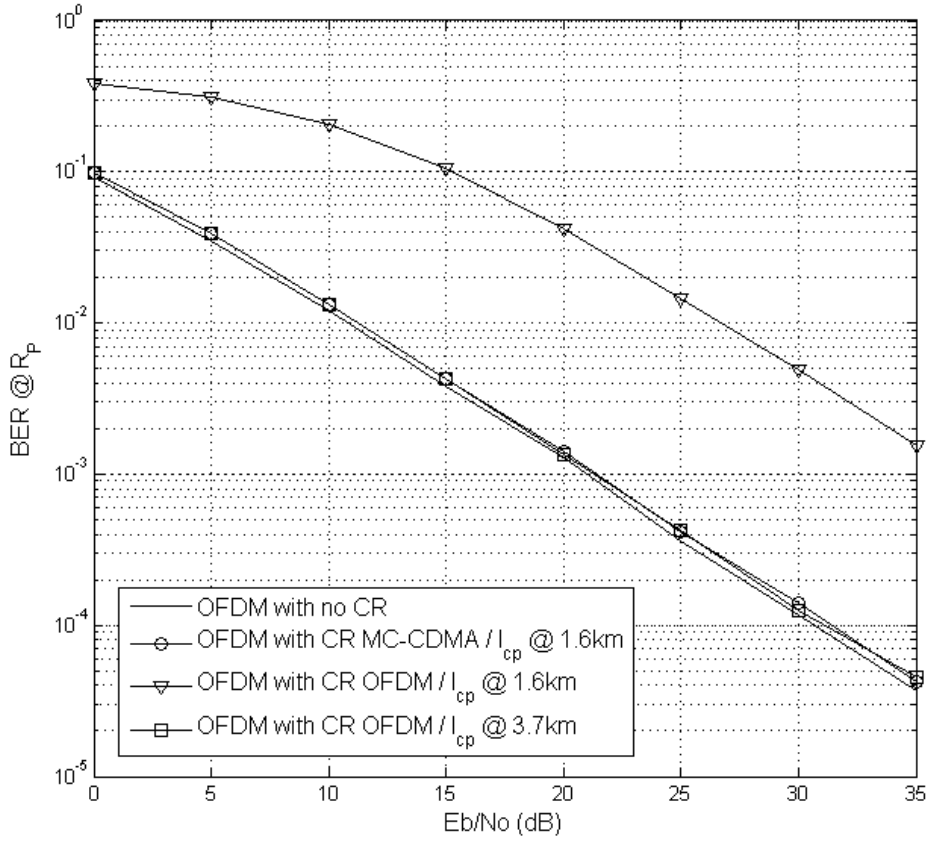

Figure 7.3: BER at R_P for CR OFDM and CR MC-CDMA.

The SNR for the desired signal at the primary and cognitive systems is assumed to be 30 dB and l_{pr} and l_{cr} are kept at 1 km. On the other hand, the distance l_{cp} is varied (hence this varies the SINR of the primary system). Figure 7.2 demonstrates the BER performance at R_P with respect to different distances of l_{cp} for the primary system. The results for CR MC-CDMA illustrate that at $l_{cp} = 1.6$ km the BER starts to become flat. This means that if T_C is greater or equal to 1.6 km from R_P, the interference caused by the cognitive system remains low and hence the performance of the primary system will not degrade. Similarly for CR OFDM, performance degradation of the primary system is avoided if $l_{cp} \geq 3.7$ km. These results show that at the same distance from R_P, CR

MC-CDMA causes much lower interference to the PR network than CR OFDM.

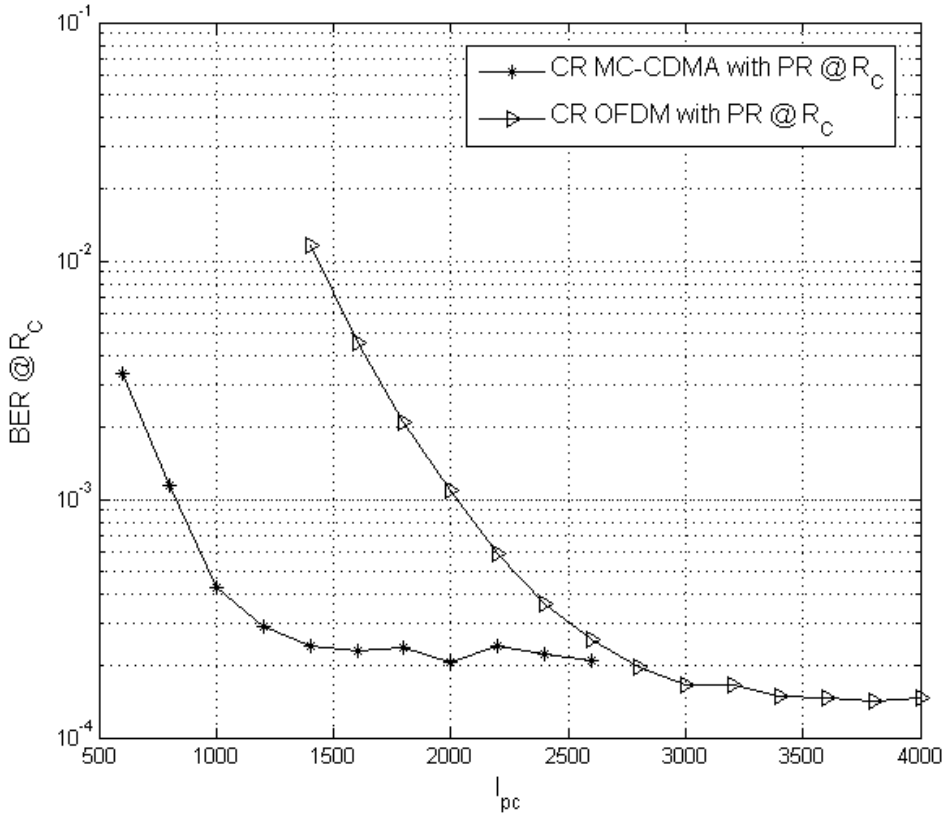

Figure 7.4: BER vs l_{pc} distance when SNR_{cr} is fixed at 30 dB.

Figure 7.3 demonstrates the BER performance with respect to different E_b/N_0 for the primary system. From the results it is evident that when $l_{cp} = 1.6$ km CR MC-CDMA outperforms CR OFDM by 16 dB at BER $= 10^{-3}$. Furthermore, the results illustrate that with CR MC-CDMA, the performance of the primary system is almost the same as that with no CR. This ensures that the communication link at the primary system is maintained and the CR interference can be regarded as noise.

In order to test the performance of the CR MC-CDMA and CR OFDM systems, the BER at R_C is measured for different distances of l_{pc}. In Figure 7.4, it is observed that at $l_{pc} = 1.6$ km the BER for CR MC-CDMA starts to become

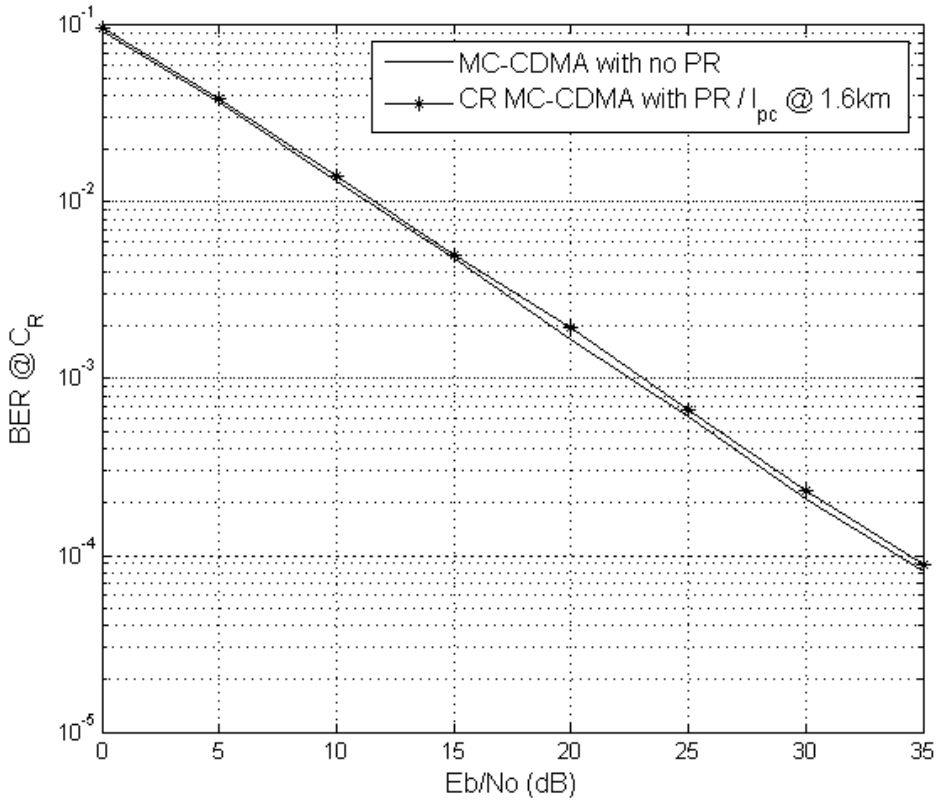

Figure 7.5: BER at R_C for CR MC-CDMA.

flat. Thus at this distance, the interference from the primary system remains low. Instead, for CR OFDM the interference becomes low and the BER starts to become flat at $l_{pc} = 3.5$ km. Finally, Figure 7.5 verifies that the communication at CR MC-CDMA is successfull if $l_{pc} \geq 1.6$ km.

Overall, the results in this work justify that MC-CDMA is much more favourable than OFDM for underlay CR networks.

Chapter 8

Conclusions & Future work

8.1 Conclusions & Discussions

This thesis studies the combination of MC-CDMA systems with MIMO technology. It is known that in multiuser downlink MIMO MC-CDMA systems with OSIC receivers, significant error floor appears in the higher SNR region because the system suffers from MAI and error propagation. Therefore, this research develops downlink MIMO MC-CDMA systems that can overcome multi-user and multi-antenna interference, and outperform existing techniques in terms of system performance and complexity.

A chip level coded OSSMIC receiver architecture with ZF or MMSE filtering is proposed for downlink MIMO MC-CDMA systems. The proposed scheme cancels both CAI and MAI that arise within the system during multiuser transmission. Furthermore, the proposed receiver is able to operate with only the desired user's signature sequence during the detection process. Simulation results demonstrate that the proposed OSSMIC receiver significantly outperforms the OSIC receiver which suffers from high residual MAI. It is also shown that with the enhanced

noise estimation, the MMSE OSSMIC significantly outperforms its ZF counterpart. The use of chip level detection in favour of symbol level detection is justified by the significant performance and complexity difference between the proposed OSSMIC receiver and the modified symbol level OSIC detector. On the other hand, when comparing to MIMO OFDMA system, the proposed MMSE OSSMIC receiver shows better performance in low system load. When the system load is increased, multiple access interference causes the performance of MIMO MC-CDMA to deteriorate. If all other users spreading sequences are available at the receiver, the impact of MAI is minimised and MIMO MC-CDMA performs better than MIMO OFDMA even in high system load. However in this case the computational complexity of the OSSMIC receiver increases with the increasing number of users.

In addition to this work, expressions of the PEP bounds for all the systems are derived and justified that the system performance depends on the type of filtering and the number of users. Thus the proposed receiver permits layered space-time processing with good performance for spatially multiplexed MC-CDMA systems, which could outperform its OFDMA counterpart.

In the second part of this work, low complexity user grouping algorithms for power minimisation are proposed for grouped MC-CDMA and grouped STBC MC-CDMA systems. The optimal solution for minimising the total transmitted power with respect to a target BER is proposed when no fairness requirement on the data rate is needed. When a fairness requirement is considered in the user grouping process, we propose two suboptimal algorithms for the optimisation problem. The first algorithm is a simple approach based on the subcarrier channel gains, while the second algorithm is based on the channel variation. Simulation results justify that our proposed algorithms provide a significant reduction in power consumption when compared with the random user allocation algorithm

and the algorithm in [79].

To briefly summarise, a chip level coded OSSMIC receiver with ZF/MMSE filtering is proposed for downlink MIMO MC-CDMA systems. The proposed receiver permits layered space-time processing with good performance for spatially multiplexed MC-CDMA systems, which could outperform its OFDMA counterpart. Furthermore, low complexity user grouping algorithms are proposed for grouped MC-CDMA and STBC MC-CDMA systems which can significantly reduce power consumption.

8.2 Future work

From this research, we conclude that MC-CDMA can provide a significant performance improvement when combined with MIMO systems. This is quite promising for future developments. Furthermore, the proposed user grouping algorithms have shown a significant reducton in power consumption. Saving energy is vital nowadays and hence this work could be further extended to achieve power minimisation in scenarios with more requirements. Therefore, several new ideas are listed below and indicate how to extend this work in the future.

1. A future goal would be to extend the current single-cell MIMO MC-CDMA system with OSSMIC receiver into a multi-cell environment. This will require to take into account inter-cell interference which arises to the system from neighbouring cells. Furthermore, the performance of MIMO MC-CDMA with OSSMIC in multi-cell scenario could be compared with the MIMO OFDMA system with OSIC. Without perfect knowledge of the interference at the base station, MC-CDMA would be more robust to interference than OFDMA due to its interference rejection capability.

2. Power minimisation for grouped MC-CDMA and STBC MC-CDMA systems could be extended in a scenario where adaptive modulation is considered in order to satisfy fixed rate requirements for each user. In this scenario, multi-code could be used to allow users to be assigned in the same group more times.

3. Chapter 7 demonstrated that MC-CDMA is a potential candidate for underlay cognitive radio networks. This work could be extended to test the performance of CR MC-CDMA with an OFDMA primary radio network i.e. include a multi-user scenario for the primary system. Furthermore, other multicarrier modulations such as MC-CDMA with carrier interferometry codes (CI/MC-CDMA) [100] and transform-domain communication system (TDCS) [101] could be tested for underlay CR and compared with CR MC-CDMA. A future goal would also be to apply multiple antennas in CR MC-CDMA to test the performance of MIMO MC-CDMA in underlay CR networks.

References

[1] L. Zhongding, P. Xiaoming, and C. Francois, "V-BLAST receivers for downlink MC-CDMA systems," in *Proc. IEEE VTC fall*, Sep. 2003, pp. 866–870.

[2] M. Vehkapera, D. Tujkovic, Z. Li, and M. Juntti, "Receiver design for spatially layered downlink MC-CDMA system," *IEEE Transactions on Vehicular Technology*, vol. 54, no. 3, pp. 1042–1055, May 2005.

[3] E. Biglieri, R. Calderbank, A. Constantinides, A. Goldsmith, A. Paulraj, and H. Poor, *MIMO Wireless Communications*. Cambridge University Press, 2007.

[4] V. Kuhn, *Wireless Communications over MIMO Channels*. John Wiley & Sons Ltd, 2006.

[5] S. Glisic, *Advanced Wireless Communications*. John Wiley & Sons Ltd, 2004.

[6] D. Tse and P. Viswanath, *Fundamentals of Wireless Communications*. Cambridge University Press, 2005.

[7] G. J. Foschini and M. J. Gan, "On the limits of wireless communications in a fading environment when using multiple antennas," *Wireless Personal Communications*, vol. 6, no. 3, pp. 311–335, 1998.

[8] G. J. Foschini, "Layered space-time architecture for wireless communication in a fading environment when using multiple antennas," *Bell Laboratories Technical Journal*, vol. 1, no. 2, pp. 41–59, 1996.

[9] P. Wolniansky, G. Foschini, G. Golden, and R. Valenzuela, "V-BLAST: An architecture for realizing very high data rates over the rich-scattering wireless channel," in *Proc. IEEE ISSSE*, Sep. 1998, pp. 295–300.

[10] G. Foschini, G. Golden, R. Valenzuela, and P. Wolniansky, "Simplified processing for high spectral efficiency wireless communication employing multi-element arrays," vol. 17, pp. 1841–1852, Nov. 1999.

[11] N. Yee, J. Linnartz, and G. Fettweis, "Multicarrier CDMA in indoor wireless radio networks," in *Proc. IEEE PIMRC*, Sep. 1993, pp. 109–113.

[12] K. Fazel and S. Kaizer, *Multi-Carrier and Spread Spectrum Systems.* John Wiley & Sons Ltd., 2003.

[13] A. Chouly, A. Brajal, and S. Jourdan, "Orthogonal multicarrier techniques applied to direct sequence spread spectrum CDMA systems," in *Proc. IEEE GLOBECOM*, pp. 1723–1728.

[14] S. Hara and R. Prasad, "Overview of multi-carrier CDMA," *IEEE Communications Magazine*, vol. 35, no. 12, pp. 126–133, Dec. 1997.

[15] ——, "Design and performance of multicarrier CDMA system in frequency-selective rayleigh fading channels," *IEEE Transactions on Vehicular Technology*, vol. 48, no. 5, pp. 1584–1595, Sep. 1999.

[16] R. Prasad and S. Hara, "An overview of multi-carrier CDMA," in *Proc. IEEE ISSSTA*, vol. 1, Sep. 1996, pp. 107–114.

[17] H. Schulze and C. Luders, *Theory and Applications of OFDM and CDMA Wideband Wireless Communications*. John Wiley & Sons Ltd, 2005.

[18] L. Hanzo, M. Munster, B. Choi, and T. Keller, *OFDM and MC-CDMA for Broadband Multi-User Communications, WLANS and Broadcasting*. John Wiley & Sons Ltd., 2003.

[19] R. V. Nee and R. Prasad, *OFDM for Wireless Multimedia Communications*. Artech House Publishers, 2000.

[20] S. Verdu, *Multiuser Detection*. Cambridge University Press, 1998.

[21] A. J. Viterbi, *CDMA - Principles of Spread Spectrum Communication*. Addison Wesley, 1995.

[22] M. Juntti, M. Vehkapera, J. Leinonen, Z. Li, D. Tujkovic, S. Tsumura, and S. Hara, "MIMO MC-CDMA communications for future cellular systems," *IEEE Communications Magazine*, vol. 43, no. 2, pp. 118–124, Feb. 2005.

[23] M. Vehkapera, D. Tujkovic, Z. Li, and M. Juntti, "Combined spatial multiplexing and diversity techniques for coded MC-CDMA systems with suboptimal MMSE-based receivers," in *Proc. IEEE VTC spring*, vol. 1, May 2005, pp. 280–284.

[24] M. Vehkapera, D. Tujkovic, M. Juntti, and Z. Li, "Layered space-frequency coding and receiver design for MIMO MC-CDMA," in *Proc. IEEE ICC*, vol. 5, Jun. 2004, pp. 3005–3009.

[25] Y. Lee and H. Park, "Low-complexity detections for downlink MIMO MC-CDMA systems," in *Proc. IEEE PIMRC*, Sep. 2006, pp. 1–5.

[26] K. Kyeongyeon, H. Jaesang, L. Chungyong, and S. Seijoon, "Asymptotic analysis of downlink MIMO multicarrier CDMA systems with a minimum mean square error receiver," in *Proc. IEEE VTC spring*, vol. 3, May 2006, pp. 1501–1505.

[27] K. Kyeongyeon, H. Jaesang, L. Chungyong, and H. Daesik, "Performance analysis of a downlink MIMO MC-CDMA system with turbo coding and channel interleaving," in *Proc. IEEE VTC fall*, vol. 2, Sep. 2004, pp. 1439–1442.

[28] J. Hu, K. Kim, S. Shim, M. Kim, and C. Lee, "An MMSE-nulling partial-PIC receiver for multiuser downlink MIMO MC-CDMA systems," *IEICE Transactions on Communications*, vol. E88-B, no. 4, pp. 1725–1729, Apr. 2005.

[29] P. Fu and K. Chen, "Rate, sub-carrier, and power allocations for multi-carrier CDMA with LMMSE multiuser detection," *IEEE Transactions on Wireless Communications*, vol. 6, no. 5, pp. 1574–1580, May 2007.

[30] N. Benvenuto, P. Bisaglia, and F. Boccardi, "Joint optimum linear precoding and power control strategies for downlink MC-CDMA systems," *IEEE Transactions on Communications*, vol. 56, no. 5, pp. 769–777, May 2008.

[31] X. Cai, S. Zhou, and G. Giannakis, "Group-orthogonal multicarrier CDMA," *IEEE Transactions on Communications*, vol. 52, no. 1, pp. 90–99, Jan. 2004.

[32] J. Mitola, "Cognitive radio: An integrated agent architecture for software defined radio," Ph.D. thesis, Royal Institute of Technology (KTH), Stocholm, Sweden, 2000.

[33] I. F. Akyildiz and et. al., "Next generation/dynamic spectrum access/cognitive radio wireless networks: A survey," *Computer Networks: The International Journal of Computer and Telecommunications Networking*, vol. 50, no. 13, pp. 2127–2159, 2006.

[34] T. S. Rappaport, *Wireless Communications*. Prentice Hall, 2002.

[35] M. K. Simon and M. S. Alouini, *Digital Communications over Fading Channels*. John Wiley & Sons Inc., 2005.

[36] G. L. T. et al., "A statistical model of urban multipath propagation," *IEEE Transactions on Vehicular Technology*, vol. 21, pp. 1–9, Feb. 1972.

[37] C. Nassar, B. Natarajan, Z. Wu, D. Wiegandt, S. Zekavat, and S. Shattil, *Multi-carrier Technologies for Wireless Communications*. Kluwer Academic Publishers, 2002.

[38] A. Jamalipour, T. Wada, and T. Yamazato, "A tutorial on Multiple Access technologies for beyond 3G mobile networks," *IEEE Communications Magazine*, vol. 43, no. 2, pp. 110–117, Feb. 2005.

[39] S. Haykin and M. Moher, *Modern Wireless Communications*. Pearson Prentice Hall, 2005.

[40] R. W. Chang, "Synthesis of band-limited orthogonal signals for multichannel data transmission," *Bell Systems Technical Journal*, vol. 46, pp. 1775–1796, 1966.

[41] L. J. Cimini, "Analysis and simulation of a digital mobile channel using orthogonal frequency division multiplexing," *IEEE Transactions on Communications*, vol. 33, pp. 665–675, 1985.

[42] *Radio broadcast systems: digital audio broadcasting (DAB) to mobile, portable and fixed receivers*, European Telecommunication Standard pr ETS 300 401, Nov. 1994.

[43] U. H. Reimers, "DVB-the family of international standards for digital video broadcasting," *Proceedings of the IEEE*, vol. 94, no. 1, pp. 173–182, 2006.

[44] W. Y. Chen and D. L. Waring, "Applicability of ADSL to support video dial tone in the copper loop," *IEEE Comm. Mag.*, vol. 32, pp. 102–109, May 1994.

[45] J. Heiskala and J. Terry, *OFDM Wireless LANs: A Theoretical and Practical Guide*. Sams Indianapolis, 2001.

[46] Y. Wu and W. Zou, "Orthogonal frequency division multiplexing: a multi-carrier modulation scheme," *IEEE Transactions on Consumer Electronics*, vol. 41, no. 3, pp. 392–399, Aug. 1995.

[47] A. Molisch, *Wireless Communications*. John Wiley & Sons Ltd, 2005.

[48] D. So and R. Cheng, "Performance evaluation of space-time coding over frequency selective fading channel," in *Proc. IEEE VTC*, May 2002, pp. 635–639.

[49] D. Koulakiotis and A. H. Aghvami, "Data detection techniques for DS-CDMA mobile systems: a review," *IEEE Personal Communications*, vol. 7, no. 3, pp. 24–34, Jun. 2000.

[50] S. Moshavi, "Multi-user detection for DS/CDMA communications," *IEEE Communications Magazine*, vol. 34, no. 10, pp. 124–136, Oct. 1996.

[51] P. Patel and J. Holtzman, "Analysis of a simple successive interference cancellation scheme in a DS/CDMA system," *IEEE Journal on Select Areas in Communications*, vol. 12, no. 5, pp. 796–807, Jun. 1994.

[52] K. Fazel and L. Papke, "On the performance of convolutionally coded CDMA-OFDM for mobile communication system," in *Proc. IEEE PIMRC*, Sep. 1993, pp. 468–472.

[53] S. Kaiser, "Multi-carrier CDMA mobile radio systems - analysis and optimization of detection, decoding, and channel estimation," Ph.D. thesis, VDI-Verlag, Dusseldorf, Germany, 1998.

[54] A. Goldsmith, *Wireless Communications*. Cambridge University Press, 2005.

[55] *3rd Generation Partnership Project (3GPP); Technical specification group radio access network; Radio transmission and reception (Release 7).*

[56] Y. Hujun and S. Alamouti, "OFDMA: A broadband wireless access technology," in *IEEE Sarnoff Symposium*, Mar. 2006, pp. 1–4.

[57] Y. W. Cheong, R. Cheng, K. Lataief, and R. D. Murch, "Multiuser OFDM with adaptive subcarrier, bit, and power allocation," *IEEE Journal on Selected Areas in Communications*, vol. 17, no. 10, pp. 1747–1758, Oct. 1999.

[58] H. Sari, Y. Levy, and G. Karam, "An analysis of orthogonal frequency division multiple access," in *Proc. IEEE GLOBECOM*, vol. 3, Nov. 1997, pp. 1635–1642.

[59] H. Yaghoobi, "Scalable OFDMA physical layer in ieee 802.16 wirelessMAN," *Intel Technology J.*, vol. 8, pp. 201–212, Aug. 2004.

[60] D. Gesbert, M. Shafi, S. Da-shan, P. Smith, and A. Naguib, "From theory to practice: an overview of MIMO space-time coded wireless systems," *IEEE Journal on Selected Areas in Communications*, vol. 21, no. 3, pp. 281–302, Apr. 2003.

[61] Q. H. Spencer, C. B. Peel, A. L. Swindlehurst, and M. Haardt, "An introduction to the multi-user MIMO downlink communications," *IEEE Communications Magazine*, vol. 42, no. 10, pp. 60–67, Oct. 2004.

[62] V. L. Nir, M. Helard, and L. G. Rodolphe, "Spatial multiplexing applied to turbo coded multicarrier CDMA," in *Proc. IEEE ISSSTA*, Aug. 2004, pp. 565–569.

[63] A. Gershman and N. Sidiropoulos, *Space-Time Processing for MIMO Communications*. John Wiley & Sons, 2005.

[64] V. Tarokh, N. Seshadri, and A. R. Calderbank, "Space-time codes for high data rate wireless communication: performance criteria and code construction," *IEEE Transactions on Information Theory*, vol. 44, no. 2, pp. 744–765, Mar. 1998.

[65] A. Naguib, V. Tarokh, N. Seshadri, and A. R. Calderbank, "A space-time coding modem for high-data-rate wireless communications," *IEEE Journal on Select Areas in Communications*, vol. 16, no. 8, pp. 1459–1478, October 1998.

[66] V. Tarokh, A. Naguib, N. Seshadri, and A. R. Calderbank, "Space-time codes for high data rate wireless communication: performance criteria in the presense of channel estimation errors, mobility, and multiple paths," *IEEE Transactions on Communications*, vol. 47, no. 2, pp. 199–207, Feb. 1999.

[67] Z. Chen, J. Yuan, and B. Vucetic, "Improved spacetime trellis coded modulation scheme on slow fading channels," in *Proc. IEEE ICC*, Jun. 2001, pp. 1110–1116.

[68] E. G. Larsson and P. Stoica, *Space-Time Block Coding for Wireless Communications*. Cambridge University Press, 2003.

[69] S. M. Alamouti, "A simple transmit diversity technique for wireless communications," *IEEE Journal on Select Areas in Communications*, vol. 16, no. 8, pp. 1451–1458, Oct. 1998.

[70] V. Tarokh, H. Jafarkhani, and A. R. Calderbank, "Space-time block codes from orthogonal designs," *IEEE Transactions on Information Theory*, vol. 45, pp. 1456–1467, Jul. 1999.

[71] C. Ibars and Y. Bar-Nes, "Comparing the performance of coded multiuser OFDM and coded MC-CDMA over fading channels," in *Proc. IEEE GLOBECOM*, vol. 2, Nov. 2001, pp. 881–885.

[72] J. Zhu and Y. Bar-Ness, "Power allocation algorithm in MC-CDMA," in *Proc. IEEE ICC*, vol. 2, 2002, pp. 931–935.

[73] C. S. Park and K. B. Lee, "Transmit power allocation for BER performance improvement in multicarrier systems," *IEEE Transactions on Communications*, vol. 52, no. 10, pp. 1658–1663, Oct. 2004.

[74] W. Bocquet, K. Harashi, and H. Sakai, "Power allocation scheme for MIMO MC-CDMA with two dimensional spreading," in *Proc. IEEE VTC spring*, 2007, pp. 3145–3149.

[75] P. K. Sampath, H. Cam, and A. Natarajan, "Power and subcarrier allocation for multirate MC-CDMA system," in *Proc. IEEE VTC fall*, vol. 3, 2003, pp. 1900–1902.

[76] E. Lo, P. Chan, V. Lau, R. Cheng, K. Letaief, R. Murch, and W. Mow, "Adaptive resource allocation and capacity comparison of downlink multiuser MIMO-MC-CDMA and MIMO-OFDMA," *IEEE Transactions on Wireless Commununications*, vol. 6, no. 2, pp. 1083–1093, Mar. 2007.

[77] E. Costa, H. Haas, E. Schulz, and A. Filippi, "Capacity optimisation in MC-CDMA systems," *European Transactions on Telecommunications*, vol. 13, no. 5, pp. 455–463, Sep. 2002.

[78] C. Li and X. Wang, "Adaptive subchannel allocation in multiuser MC-CDMA systems," in *Proc. IEEE GLOBECOM*, Dec. 2004, pp. 2503–2507.

[79] J. Huang and J. Niu, "A fairness-based and adaptive user grouping and subcarrier allocation algorithm for grouped MC-CDMA systems," in *Proc. IEEE GLOBECOM*, Nov. 2006, pp. 1–5.

[80] Y. Wang, J. Shen, P. Zhang, S. Liu, and Y. Liu, "Optimized power control and resource allocation in grouped MC-CDMA systems," in *Proc. IEEE ICC*, May 2008, pp. 4785–4789.

[81] G. J. Proakis, *Digital Communications*. McGraw Hill, 2001.

[82] Z. Yang, B. Lu, and X. Wang, "Bayesian monte carlo multiuser receiver for spacetime coded multicarrier CDMA systems," *IEEE Journal on Selected Areas in Communications*, vol. 19, no. 8, pp. 1625–1637, Aug. 2001.

[83] H. Zhihua and V. Dubey, "Performance analysis for downlink MC-CDMA

systems with space-time block codes in frequency-selective rayleigh fading channels," in *Proc. ICICS-PMC*, Dec. 2003, pp. 658–662.

[84] F. Portier, J. Baudais, and J. Helard, "Performance of STBC MC-CDMA systems over outdoor realistic MIMO channels," in *Proc. IEEE VTC fall*, Sep. 2004, pp. 2409–2413.

[85] F. Portier, J. Helard, J. Auffray, and J. Baudais, "STBC MC-CDMA systems for indoor and outdoor scenarios," in *Proc. IEEE ISSSTA*, Sep. 2004, pp. 555–559.

[86] A. Nallanathan and P. Meng, "On the performance of MC-CDMA with transmit diversity over fast frequency selective fading channels," in *Proc. IEEE VTC spring*, vol. 3, May 2004, pp. 1361–1365.

[87] V. L. Nir, M. Helard, and R. L. Gouable, "Space-time block coding applied to turbo coded multicarrier CDMA," in *Proc. IEEE VTC spring*, Apr. 2003, pp. 577–581.

[88] S. Haykin, "Cognitive radio: Brain-empowered wireless communications," *IEEE Journal on Selected Areas in Communications*, vol. 23, no. 2, pp. 201–220, 2005.

[89] Q. Zhao and B. M. Sadler, "A survey of dynamic spectrum access," *IEEE Signal Processing Magazine*, vol. 24, no. 3, pp. 79–89, May 2007.

[90] V. Chakravarthy and et. al., "Novel overlay/underlay cognitive radio waveforms using SD-SMSE framework to enhance spectrum efficiencypart i: Theoretical framework and analysis in AWGN channel," *IEEE Transactions on Communications*, vol. 57, no. 12, pp. 3794–3804, Dec. 2009.

[91] H. Tang, "Some physical layer issues of wide-band cognitive radio systems," in *Proc. IEEE Dynamic Spectrum Access Networks*, Nov. 2005, pp. 151–159.

[92] B. F. Boroujeny and R. Kempter, "Multicarrier communication techniques for spectrum sensing and communications in cognitive radio," *IEEE Communications Magazine*, vol. 46, no. 4, pp. 80–85, Apr. 2008.

[93] T. A. Weiss and F. K. Jondral, "Spectrum pooling: an innovative strategy for the enhancement of spectrum efficieny," *IEEE Communications Magazine*, vol. 42, no. 3, pp. S8–S14, Mar. 2004.

[94] J. D. Poston and W. D. Horne, "Discontigous ofdm considerations for dynamic spectrum access in idle tv channels," in *Proc. IEEE Dynamic Spectrum Access Networks*, Nov. 2005, pp. 607–610.

[95] A. M. Wyglinski, "Effects of bit allocation on non-contiguous multicarrier-based cognitive radio transceivers," in *Proc. IEEE VTC fall*, Sep. 2006, pp. 1–5.

[96] Q. Qu, L. B. Milstein, and D. R. Vaman, "Cognitive radio based multiuser resource allocation in mobile ad hoc networks using multi-carrier CDMA modulations," *IEEE Journal on Selected Areas in Communications*, vol. 26, no. 1, pp. 70–82, Jan. 2008.

[97] M. B. Pursley and T. C. R. IV, "Low-complexity adaptive transmission for cognitive radio in dynamic spectrum access networks," *IEEE Journal on Selected Areas in Communications*, vol. 26, no. 1, pp. 83–94, Jan. 2008.

[98] R. Rajbanshi, Q. Chen, A. Wyglinski, G. Milden, and J. Evans, "Quantitative comparision of agile modulation technique for cognitive radio tranceivers," in *Proc. IEEE CCNC*, Jan. 2007, pp. 1144–1148.

[99] A. Attar, M. R. Nakhai., and A. H. Aghvami, "Cognitive radio transmission based on direct sequence MC-CDMA," *IEEE Transactions on Wireless Communications*, vol. 7, no. 4, pp. 1157–1162, Apr. 2008.

[100] B. Natarajan, C. Nassar, S. Shattil, and Z. Wu, "High-performance MC-CDMA via carrier interferometry codes," *IEEE Transactions on Vehicular Technology*, vol. 50, pp. 1344–1353, Nov. 2001.

[101] V. Chakravarthy, A. Shaw, M. Temple, and A. Nunez, "TDCS, OFDM and MC-CDMA: a brief tutorial," *IEEE Communications Magazine*, vol. 43, pp. S11–S16, Sep. 2005.